Dressing an Atom in a Field of Many Colours

T. Rudolph

A thesis submitted to the Faculty of Graduate Studies
in partial fulfillment of the requirements for the degree of

Doctor of Philosophy

Graduate Program in Physics and Astronomy

York University

Toronto, Canada

June 1998

Dressing an Atom in a Field of Many Colours

by

Terry Rudolph

a dissertation submitted to the Faculty of Graduate Studies of York University in partial fulfillment of the requirements for the degree of

DOCTOR OF PHILOSOPHY

Abstract

This thesis examines the AC Stark effect from the perspective of the dressed atom model, specifically that associated with an atom driven by more than one laser field. Almost all calculations contained herein are analytical in nature, and are aimed at providing a physical understanding of the dynamics of a two level atom driven by two or three laser fields. All calculations agree completely with those obtained by numerically solving the optical Bloch equations for the system and, where available, with experimental observations.

When an atom already subject to a strong driving field is monitored by a strong probe beam, it is observed that the absorption and dispersion spectra display resonances at frequencies detuned from the atomic transition frequency ω_0 by integer fractions of the Rabi frequency 2Ω of the first field. However, a "strong probe" is an intense field which itself alters the characteristics of the system it is supposed to be probing. Based on this observation, we have considered the system from the point of view that both fields "dress" the atom, and calculated the energy levels and spectra of the "doubly-dressed" atom. We find a new physical phenomenon: The second field couples to multiphoton resonances between dressed states of the first field, and their energy levels are split due to this n-photon coupling, *i.e.* this represents an n-photon AC Stark effect. The resulting fluorescence and near-resonance and Autler-Townes absorption and dispersion spectra are extremely rich in detail, containing multiplets at the subharmonic as well as harmonic resonance frequencies with an intricate dependence on the order n of the resonance and on the relative Rabi frequencies of the two fields. An outstanding problem associated with the subharmonic resonances has been the observation that they do not occur at detunings from ω_0 exactly equal to $2\Omega/n$, but rather for detun-

ings slightly shifted from these values. In this thesis we interpret these shifts as arising from the coupling via the rotating terms of the interaction Hamiltonian V_2 between non-resonant doublets belonging to the doubly-dressed atom, thus having the physical interpretation of a dynamic Stark shift. We demonstrate that at precisely these shifted resonance frequencies the fluorescence by the atom vanishes identically at the central frequency ω_0, and that the splitting of the features within the spectral multiplets is a minimum.

We have also calculated the dressed states and spectra of a two-level atom driven by an intense amplitude-modulated field of modulation frequency δ, for both weak and strong modulation amplitudes. The spectra arising for a weak modulation are best described by comparison with those of the monochromatically driven atom: For the fluorescence and near-resonance absorption spectra, the central component of the Mollow triplet is unaffected, while the sideband lines are replaced by multiplets with spacing δ and an intensity dependent on the ratio of the modulation amplitude to its frequency. In the Autler-Townes spectrum, each line is similarly replaced by a multiplet. For strong modulation, we describe the spectra by comparison with those which arise for an equal amplitude bichromatic (AM with suppressed carrier) driving field: The central lines of the fluorescence and near-resonance absorption multiplets are split into triplet features, while all other lines, as well as those of the Autler-Townes spectra, are split into doublets, with doublet splitting proportional to the amplitude of the carrier frequency.

Acknowledgments

I would first like to express my gratitude to Zbyszek Ficek, who guided me into Quantum Optics as a field, and then proceeded to teach me how research was done. In addition, his rapid response to my frequent requests for numerical calculations has made performing this research much easier, and I am truly appreciative of our collaboration.

My office mates (so many of you I cannot count), I will always remember the fun and be appreciative of your tolerance. You know what I mean.

Thanks are in order too for my Canadian friends outside of physics, in particular Rob Simpson and Peter Cerny. We had many fun times together, only breaking the law when absolutely necessary. These times provided the balance to keep me (at least partially) sane.

To my wonderful Family, whose love and support I have enjoyed over so many years, despite my protracted abscences. I love you all very much.

To North York, Toronto, whose awesome grandeur and breath-taking beauty was an endless source of inspiration.

To God, who gave me the curiosity to attempt an understanding of His secrets. I know You still have a few - we'll see how far I get uncovering them.

Finally to my wonderful supervisor Helen Freedhoff, whose patience, tolerance and guidance I have appreciated so much. You have my deepest gratitude Helen for allowing me the freedom to develop as a physicist and for being much more than just a supervisor - for truly being my Jewish-Canadian Mother.

Table of Contents

List of Figures

1. Introduction

In the nearly 40 years since the development of the first working (optical) laser, our understanding of how light interacts with matter has grown at a rate which has made the underlying theory now one of the best understood in all of physics, and certainly one of the most applicable.

At the most fundamental level, our understanding of how light and matter interact is based upon the theory of Quantum Electrodynamics (QED). This is the field theory which is the relativistic version of single particle quantum mechanics, and is one of the best experimentally verified theories in any branch of science in all time. It describes the interaction of electrons (or other electrically charged particles) with photons to an incredible degree of accuracy. The agreement between theory and experiment is better than 1 part in 10^{14}, which is equivalent to the ratio between the diameter of an atom and the distance between Toronto and Vancouver.

Despite being a relativistic theory, QED contains lessons for those of us who practise physics at more moderate energies. To begin with, it teaches us to think of the vacuum as an important player in the dynamics of physical systems; in particular the vacuum can act as a probe field which causes an atom in an excited energy level to spontaneously emit a photon. The second major fact of importance to us is related to the quantisation of the radiation field. QED makes explicit for us the description of the electromagnetic field as a set of decoupled harmonic oscillators with definite numbers of energy quanta.

Unfortunately full QED calculations are best performed within the framework of scattering theory, wherein one can assume that the initial and final states for the system are solutions of the free Hamiltonian. For more complex systems for which this does not apply, the equations rapidly become prohibitive and furthermore contain a redundancy of information for our purposes, because we are concerned only with slow moving (*i.e.* non-relativistic) atomic systems. As such, a variety of theoretical techniques designed to focus on the essential "room temperature" physics have grown up over the years.

In 1974, a phenomenon known as the AC Stark effect was first observed [1], after having been predicted 5 years earlier by Mollow [2]. This is an effect which occurs when a strong laser is tuned close to the transition frequency between two atomic levels. The laser's oscillating electric field can cause a splitting of the observed spectral line, in analogy with the splitting caused by a static electric field. The resulting fluorescence spectrum is known as the Mollow triplet. Unfortunately the technique used by Mollow did not lead to good physical intuition, especially when applied to more complicated systems. It was a major breakthrough therefore, when Cohen-Tannoudji and Reynaud introduced a technique now known as the "dressed-atom model" that gives a clear and concise method for deriving the Mollow spectrum [3]. One of the most appealing features of the dressed-atom model is that once we have the dressed states we can automatically understand *why* the particular spectral features appear; moreover it is usually only a small amount of work from there to the expressions for the spectra. All we need essentially are the transition rates between dressed states. From these

the population and coherence equations follow easily, along with the associated linewidths.

This is the computer age however, and so the dressed-atom model now finds itself competing with numerical simulations, which for more complicated systems than just a single atom and one laser rapidly become computationally intensive, though certainly possible. However, these reveal very little about the underlying dynamics of the problem and as such do not increase our insight into the behaviour of these systems. With this in mind, it is perhaps useful to discuss why the calculation of strong field effects is difficult, and briefly describe the other major approaches to studying the interaction of atoms and laser fields.

If the laser intensity is low then we can perform perturbation calculations within a QED framework. However these rapidly become intractable as the intensity of the laser increases and a large number of intermediate processes have to be included in calculations of the scattering amplitudes. We are thus forced to other methods.

It is well known that when an atom is irradiated by an intense monochromatic field nearly resonant with the transition between an atomic ground state $|g\rangle$ and excited state $|e\rangle$, an oscillation of frequency 2Ω is induced between them. This frequency is known as the Rabi nutation frequency. When 2Ω is much larger than the spontaneous emission rate Γ of the upper level $|e\rangle$, then we certainly do not have an equilibrium situation. Rather we have a dynamic process wherein photons of the laser mode are continually being transferred to the vacuum modes. Our

approach to studying the system depends precisely upon the questions in which we are interested. In this thesis we will be mainly concerned with the *frequency* distribution of the fluorescence photons, as opposed to say transient effects or photon statistics associated with arrival times and so on. In experiments, which measure such frequency distributions, information regarding the order of photon emission is lost, and so for a given ensemble of photons one has to take into account interference in the amplitudes describing all possible ways such an ensemble can be created.

Dynamical theories of spontaneous emission were first presented by Weisskopf and Wigner [4], and these methods were later generalised by Heitler and Ma [5]. These formulations were very successful for many processes associated with weak driving fields, and allowed for detailed discussions of lineshapes and level shifts. They were limited however to problems involving *one* fluorescence photon only.

Another class of theories, known as "quantum statistical theories", grew up in the 1970's [6,7], and proved to have several advantages over the previous treatments. In particular they are easily generalised to cases of multiple atoms and/or atomic levels; they also allow for easier treatments of processes involving virtual levels, which are required for computations such as calculation of the Lamb shift. The quantum statistical theories encompass a broad class of approaches, including master and Bloch equation treatments, Fokker-Planck methods and quantum Langevin and associated stochastic methods. For an overview of all these methods see [8] and references therein. Different treatments are often better suited to specific problems. In particular the master equation approach has proved successful

in describing the AC Stark and associated effects. For most problems the master equation cannot be solved exactly, and so numerical techniques are used. This thesis will focus however on using the dressed atom model, which is also based on the master equation, to retrieve analytical results for a number of different situations involving the AC Stark effect.

In this thesis we will be concerned with analysing a system that consists of an atom driven simultaneously by two or three strong lasers. We will use a technique known as "doubly dressing" the atom [9], which has been developed to allow us to calculate analytic expressions for parameters of interest in this type of system. These analytic expressions give us much more intuition into the physics of the system, and allow us a better understanding of the effect changes in various parameters will have upon the dynamics.

The thesis is organised as follows. Chapter 2 is an introduction to the dressed atom model, focussing on the case of a single atom driven by a single laser. The reader familiar with this model may pass directly to Chapter 3, which is fully self contained with regard to notation and essential equations. In fact, at the risk of a small amount of repetition, every chapter has been written so as to be as fully self-contained in this regard as possible. Chapter 3 describes the application of the double dressing technique to explain a new phenomenon known as the "multi-photon AC Stark effect", which occurs when a single atom is driven by two lasers of unequal strength, where the weaker laser is detuned to an integer fraction $1/n$ of the Rabi frequency 2Ω of the stronger laser. This effect is the underlying cause of the "subharmonic resonances" which are observed when a strongly driven atom

is monitored by a strong probe. The next chapter provides an explanation of a phenomenon that was also first noticed experimentally: namely that the exact subharmonic resonance points are shifted from the exact values $2\Omega/n$. As well, we report that fluorescence at ω_0 is suppressed at these shifted points. In Chapter 5 we describe a system of an atom driven by three lasers, in particular by an amplitude modulated field, and show the dramatically different structures that arise. The work is summarised in Chapter 6.

Various sections of this thesis have already been published. The results of Chapter 3 are published in [10] and [11], while the results of Chapter 4 are published in [12].

References

[1] B.R. Mollow, Phys. Rev. **188**, 1969 (1969).

[2] F. Schuda, C.R. Stroud, Jr., and M. Hercher, J. Phys. B **7**, L198 (1974); F.Y. Wu, R.E. Grove and S. Ezekiel, Phys. Rev. Lett. **35**, 1426 (1975)

[3] C. Cohen-Tannoudji and S. Reynaud, J. Phys. B **10**, 345 (1977).

[4] V. Weisskopf, and E. Wigner, Z. Physik **63**, 54 (1930); ibid **65**, 18 (1931).

[5] W. Heitler and S.T. Ma, Proc. Roy. Irish Acad. **52**, 109 (1949).

[6] R. Lehmberg, Phys. Rev. A **2**, 883 (1970), *ibid* 889.

[7] G. S. Agarwal, *Springer Tracts in Modern Physics*, **70**.

[8] C. Cohen-Tannoudji, J. Dupont-Roc, and G. Grynberg *Atom-Photon Interactions* (Wiley, New York, 1992).

[9] Z.Ficek and H.S. Freedhoff, Phys. Rev. A **53**, 4275 (1996).

[10] T.G. Rudolph, Z. Ficek and H.S. Freedhoff, Opt. Comm. **147**, 78 (1998).

[11] T.G. Rudolph, H.S. Freedhoff and Z. Ficek, Phys. Rev. A (in press).

[12] T.G. Rudolph, H.S. Freedhoff and Z. Ficek, J. Opt. Soc. Am. B (in press).

2. The dressed atom model: monochromatic driving

2.1 Introduction

In this chapter the dressed atom model for describing the interaction between an atom and a single laser field is introduced. However, one cannot do justice to the model in such a short work as this; we are therefore introducing only those features essential to an understanding of the next three chapters. In addition to serving as an introduction to the model for the uninitiated, we will save many pages of calculations later on by performing the simple calculations of this chapter in a fairly detailed manner, thereby allowing a less explicit treatment later on. A comprehensive introduction to all aspects of atom-photon interactions, including the dressed atom model, can be found in [1].

To begin with, let me point out that in the blasé manner characteristic of theoreticians, we will discuss atoms here as if they possessed only two energy levels: a ground state $|g\rangle$ and an excited state $|e\rangle$ separated by an energy $E = \hbar\omega_0$, and connected by an atomic dipole moment $\vec{\mu}$. This is justified, because throughout this thesis we will consider atoms irradiated by lasers with frequencies that lie close to a single atomic transition frequency, and hence the effects on these two levels far outweigh those on any others. The energy E is assumed to be the *experimentally* measured transition energy, that is it incorporates the Lamb shifts and other effects due to the presence of other atomic levels.

2.2 An excited atom in the vacuum

Before we consider an atom driven by lasers however, let us consider an atom which has been excited by some unspecified process to the level $|e\rangle$, and is left sitting in the vacuum. If the atom is otherwise undisturbed, then we expect that after some characteristic average time (known as the radiative lifetime) t_R of the level, the atom will decay and emit a photon of energy E. However we realise that in fact the energy of the emitted photon must lie within some energy range, since the Heisenberg uncertainty principle prevents us from making an infinitely precise measurement of energy in a finite time (which is what this would constitute). Thus the process is intrinsically probabilistic, and the width of the resulting probability distribution of emitted energies (centred at $\hbar\omega_0$) is the emission rate $\Gamma \equiv 1/t_R$. The emission is most easily understood as the result of a "probing" by the vacuum, which can be viewed as the cumulative effect of the vacuum fluctuations around the electron. These vacuum fluctuations are characterised by a very short correlation time t_C. This is analagous to a process wherein a heavy particle moving through a fluid has its velocity changed over some (relatively) large timescale by repeated small but fast collisions with the microscopic particles of the fluid.

2.3 An undressed atom in a single laser field

When the atom is surrounded by laser photons, the dynamics become more complicated. In particular, if the field is strong (in a sense defined more precisely below) then large numbers of absorption and stimulated emission processes may

occur within the characteristic time t_R. These transitions occur with a characteristic time t_S much longer than t_C but shorter (for all situations considered in this thesis) than t_R ($t_R \gg t_S \gg t_C$). The inverse of t_S is known as the Rabi frequency (denoted by 2Ω), and is a crucial experimental parameter. If, for a moment, one thinks of the driving field as a classical oscillating electromagnetic field, then the Rabi frequency is directly proportional to the scalar product of the electron's dipole moment and the electric field vector. As such it measures the strength of the coupling between the atomic energy levels and the incident laser beam. In a picture in which we consider the laser field as fully quantised, the Rabi frequency is directly proportional to the mean number of photons and the atom-field coupling constant g, which characterises the interaction Hamiltonian.

The time evolution of the system may now be described, qualitatively at least, as follows. The atom starts in the ground state with N laser photons present, that is the initial state is $|g, N\rangle \equiv |g\rangle \otimes |N\rangle$ (throughout this thesis, modulo typographical errors, commas within kets denote tensor products). The atom may now absorb a photon and the system goes to the state $|e, N-1\rangle$, that is the number of photons in the laser mode has been reduced by one and the atom is excited. Another laser photon may now cause stimulated emission and the state returns to $|g, N\rangle$ (remembering the whole process is still probabilistic). This process may be repeated many times (since for our purposes $t_S < t_R$) before a spontaneous emission occurs. When a spontaneous emission does occur however, the system makes a transition from $|e, N-1\rangle$ to $|g, N-1\rangle$, since spontaneous emission doesn't affect the number of photons in the laser mode. The system can now "Rabi

oscillate" between $|g, N-1\rangle$ and $|e, N-2\rangle$, before another spontaneous emission occurs. The dynamics is rather complicated; the presence of three characteristic time scales should have warned us of this fact.

2.4 The dressed states

The dressed atom approach essentially consists of describing the system dynamics in a basis corresponding to eigenstates of the full Hamiltonian (including the atom-driving field interaction), rather than the "undressed" basis of the free Hamiltonian considered in 2.3.

The Hamiltonian of the system takes the form (from here on we set $\hbar = 1$)

$$H = H_a + H_L + V, \tag{2.1}$$

where

$$H_a = \omega_0 S^z$$

is the Hamiltonian of the atom, and

$$H_L = \omega_L a^\dagger a,$$

is the Hamiltonian of the driving field. Here $S^z = \frac{1}{2}(|e\rangle\langle e| - |g\rangle\langle g|)$ is the atomic inversion, and $a(a^\dagger)$ is the annihilation (creation) operator for the driving field mode. H_a and H_L describe the energy of the atom and laser mode respectively. The interaction V is given by

$$V = g(a^\dagger S^- + S^+ a), \tag{2.2}$$

where g is the atom-field coupling constant and describes the strength of the interaction between the laser mode and the atom. $S^+(S^-) = |e\rangle\langle g|(|g\rangle\langle e|)$ is the atomic raising (lowering) operator. The two terms of V describe the processes of stimulated emission and absorption respectively.

To understand the form of the interaction V, note that we are working within the dipole approximation, within which we expect the interaction part of the Hamiltonian to be proportional to the dot product of the atomic dipole moment $\vec{\mu}$, and the electric field at the position of the atom, $\vec{\varepsilon}$. Since the former is proportional to $S^+ + S^-$, while the latter is proportional to $a + a^\dagger$, it might at first glance appear as if two terms are missing from (2.2). However; the above Hamiltonian is correct within the rotating-wave approximation (RWA) [1], which assumes that non-resonant processes (which contain terms of the form $a^\dagger S^+$ and aS^-) are negligible when the laser beam is quasi-resonant, *i.e.* when $(\omega_L - \omega_0) \equiv \Delta \ll \omega_0$. In fact these terms do contribute shifts; however these are of order Γ/ω_0, and for atomic systems driven by optical frequencies are completely negligible.

Because the interaction term V only couples states in pairs, the total Hamiltonian H, in the undressed basis $|g, N\rangle, |e, N-1\rangle$, has a simple block diagonal matrix form,

$$H = \begin{pmatrix} \ddots & & & \\ \cdots & A_N & 0 & \cdots \\ \cdots & 0 & A_{N+1} & \cdots \\ & & & \ddots \end{pmatrix} \tag{2.3}$$

where

$$A_N = \begin{pmatrix} N\omega_L & g\sqrt{N} \\ g\sqrt{N} & N\omega_L - \Delta \end{pmatrix}.$$

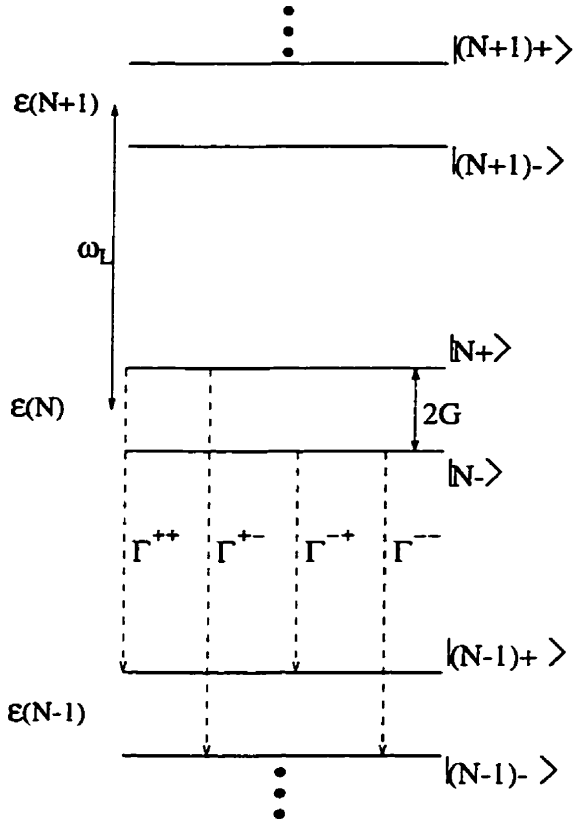

Figure 2.1 The dressed state energy level structure of the singly-dressed atom. The dressed states consist of an infinite number of doublets, with inter-doublet separation ω_L and intra-doublet separation $2G$. Transitions contributing to the spectra are shown in dashed arrows.

In this thesis we are primarily concerned with strong driving lasers, for which the (mean) number of photons in the laser mode is typically greater than 10^8. This allows us to approximate

$$g\sqrt{N} \approx g\sqrt{N+1} \approx \ldots \equiv 2\Omega,$$

where 2Ω is known as the (on resonance) Rabi frequency.

By diagonalising (2.3), we find that the eigenstates of H form an infinite set of energy manifolds separated by the laser frequency ω_L, each containing a single doublet with intra-doublet splitting $2G$, as depicted in Figure 2.1. These

eigenstates (the "dressed" states) are given by

$$\begin{aligned} |N+\rangle &= \sin\theta|g,N\rangle + \cos\theta|e,N-1\rangle \\ |N-\rangle &= \cos\theta|g,N\rangle - \sin\theta|e,N-1\rangle, \end{aligned} \tag{2.4}$$

where

$$\sin^2\theta = \frac{1}{2} + \frac{\Delta}{4G},$$

and the generalised Rabi frequency is given by

$$2G = \sqrt{4\Omega^2 + \Delta^2}.$$

2.5 Transition rates, populations and coherences

The dashed arrows in Figure 2.1 depict spontaneous transitions between the different energy manifolds, which occur with transition rates $\Gamma^{++}, \Gamma^{--}, \Gamma^{+-}$ and Γ^{-+} (defined more precisely below). The first two of these correspond to transitions at frequency ω_L, while the next two correspond to transitions at frequencies $\omega_L + 2G$ and $\omega_L - 2G$ respectively. Thus knowledge of the dressed states can already help us qualitatively understand the origin of the three components of the Mollow triplet. We wish to compute the linewidths and intensities of these transitions, and ultimately to obtain an expression for the spectrum of the light emitted by the dressed atom via spontaneous emission, or alternatively by the bare atom as resonance fluorescence. We will also consider other methods of observing the atomic dynamics, for example the weak probe absorption and dispersion spectra or the Autler-Townes spectra. All of these can be easily calculated within the dressed atom framework.

To analyse the time evolution of the system, we turn now to the Lehmberg-Agarwal master equation [2], which describes the evolution in terms of the reduced atomic density operator ρ.[†] In the Schrödinger picture, the master equation is given by

$$\frac{\partial \rho}{\partial t} = -i[H, \rho] - \frac{\Gamma}{2}(S^+S^-\rho + \rho S^+S^- - 2S^-\rho S^+). \tag{2.5}$$

We project (2.5) onto the dressed state basis (2.4), to obtain differential equations for the time evolution of the populations (the probabilities of occupation) of the dressed states, and for the coherences between the dressed states. However this will still result in an infinite set of coupled equations. We make a further approximation, known as the secular approximation, in which we ignore all coupling between density matrix elements which oscillate at different frequencies. This approximation is equivalent mathematically to neglecting terms of order Γ/Ω, and is valid because at the large Rabi frequencies we are considering, non-secular couplings are quickly "washed out", and consequently contribute little to the steady-state spectrum.

The populations $\pi_N^{\pm} \equiv \langle N\pm|\rho|N\pm\rangle$ are found from (2.5) to obey the equations of motion

$$\dot{\pi}_N^{\pm} = -(\Gamma^{\pm\pm} + \Gamma^{\pm\mp})\pi_N^{\pm} + \Gamma^{\mp\pm}\pi_{N+1}^{\mp} + \Gamma^{\pm\pm}\pi_{N+1}^{\pm} \tag{2.6}$$

[†] The reduced density operator is obtained from the more familar "full" density operator by taking a trace over the empty (*i.e.* vacuum) modes of the electromagnetic field. This corresponds to treating the vacuum as an infinite reservoir, and results in the damping term proportional to Γ in (2.5) which appears as if an addition to the Heisenberg equation of motion.

where the dot denotes differentiation with respect to time. Here the quantities $\Gamma^{\pm\pm}, \Gamma^{\pm\mp}$ are the transition rates between the dressed states. These are proportional to the modulus squared of the matrix elements (in the dressed state basis) $\mu^{\pm\pm} = \langle N \pm | S^+ | (N-1)\pm \rangle$ and $\mu^{\pm\mp} = \langle N \pm | S^+ | (N-1)\mp \rangle$ of the operator S^+. They are independent of N, and are given by

$$\Gamma^{\pm\pm} \equiv \Gamma \left| \mu^{\pm\pm} \right|^2 = \Gamma \cos^2\theta \sin^2\theta, \tag{2.7a}$$

$$\Gamma^{+-} \equiv \Gamma \left| \mu^{\pm\pm} \right|^2 = \Gamma \cos^4\theta, \tag{2.7b}$$

$$\Gamma^{-+} \equiv \Gamma \left| \mu^{\pm\pm} \right|^2 = \Gamma \sin^4\theta. \tag{2.7c}$$

The interpretation of the equations (2.6) should be clear. Consider just π_N^+, which is the population of the state $|N+\rangle$. Equation (2.6) indicates that this state decays via spontaneous emission to states $|(N-1)+\rangle$ with a rate Γ^{++} and $|(N-1)-\rangle$ with a rate Γ^{+-}. It is repopulated however from the state $|(N+1)-\rangle$ with a rate Γ^{-+}, and from the state $|(N+1)+\rangle$ with a rate Γ^{++}.

In fact equations (2.6) still constitute an infinite set of coupled equations, however we know that for large N the populations in adjacent manifolds will be almost identical, and so we approximate $\pi_N^{\pm} \approx \pi_{N+1}^{\pm} \approx \pi_{N+2}^{\pm} \approx \ldots$. We also realise that flux out from one manifold will be balanced by the influx from the manifold above (the detailed balance condition), and so we concentrate on the so-called "reduced populations", $\Pi^{\pm} \equiv \sum_N \pi_N^{\pm}$, which can easily be shown to satisfy the equations of motion

$$\dot{\Pi}^{\pm} = -\Gamma^{\pm\mp}\Pi^{\pm} + \Gamma^{\mp\pm}\Pi^{\mp}. \tag{2.8}$$

These equations have the steady state solutions

$$\Pi^{+}_{ss} = 1 - \Pi^{-}_{ss} = \frac{\sin^4\theta}{\Gamma_c}, \tag{2.9}$$

where $\Gamma_c = \Gamma^{+-} + \Gamma^{-+} = \cos^4\theta + \sin^4\theta$. We could also consider the density matrix element between two plus or two minus states on different manifolds, *e.g.* $\varrho^{\pm\pm} = \langle (N+1) \pm |\rho| N \pm \rangle$. It turns out that these off diagonal density matrix elements ("coherences") obey the same equations of motion as the populations (2.6) with the addition of a free evolution term at the transition frequency between the states (in this case ω_L).

We next consider the density matrix elements between a plus and a minus state (and vice versa). In the same way as we considered the reduced populations, we must consider the reduced coherences and find their equations of motion. The main reduced coherences of interest are $\varrho^{\pm\mp} \equiv \sum_N \langle N \pm |\rho| (N-1) \mp \rangle$, and they obey the equation of motion

$$\dot{\varrho}^{\pm\mp} = \left(i(\omega_L \pm 2G) - \Gamma_s\right) \varrho^{\pm\mp}, \tag{2.10}$$

where $\Gamma_s = \Gamma(\frac{1}{2} + \cos^2\theta \sin^2\theta)$. We see from (2.10) that the coherences obey uncoupled equations of motion, and will reach a (quasi-) steady state after a transient time of $1/\Gamma_s$. Other coherences, say between different pairs of manifolds or within one manifold, will obey an equation of motion similar to (2.10), with only a different free evolution frequency (first term in the right hand side of (2.10)).

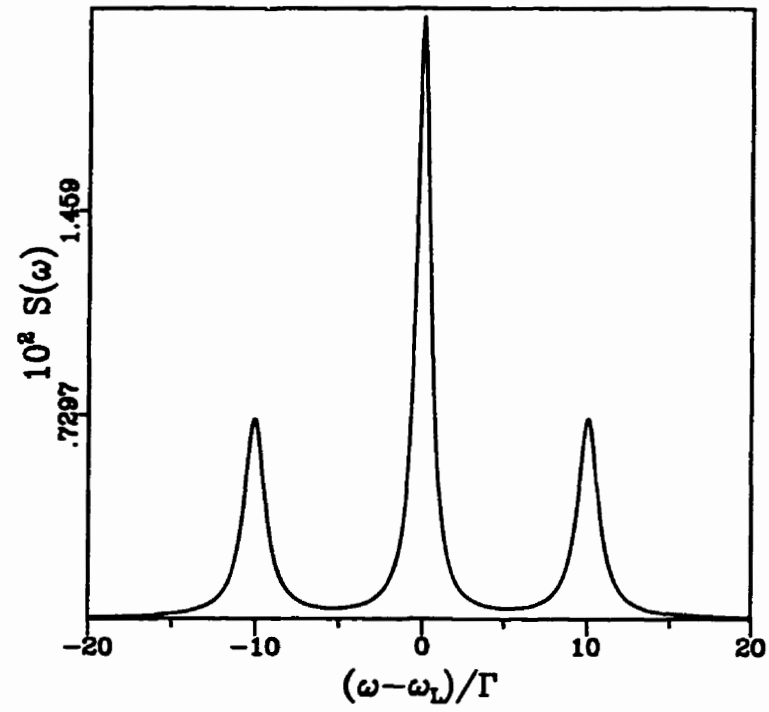

Figure 2.2 The Mollow fluorescence spectrum for $\Delta = \Gamma$, $2\Omega = 10\Gamma$ The ratio of the central peak intensity to that of the sidebands is (approximately) 3:1, the ratio of the sideband linewidths to that of the central component is (approximately) 3:2.

2.6 The fluorescence spectrum

The steady state fluorescence spectrum $S(\omega)$ of a strongly driven two-level atom was predicted by Mollow [3], and was subsequently verified experimentally [4]. It is well known to be given by the expression

$$S(\omega) = \mathcal{N}\Re \int_0^\infty d\tau\, e^{i\omega\tau} \lim_{t\to\infty} \langle S^+(t) S^-(t+\tau)\rangle \tag{2.11}$$

where $\Re$ denotes the real part of the integral. The normalisation $\mathcal{N}$ of (2.11) can be chosen such that the total intensity $I = \int d\omega\, S(\omega)$ corresponds to the total number of photons emitted per second. In general, however, we will not worry

about the normalisation of our spectra, and numerical values on the vertical axis should be considered useful only for comparing relative peak intensities.

Let us consider briefly how we may compute the fluorescence spectrum with our present knowledge of the dressed atom dynamics.

First let us formally expand the operator S^+ in the dressed state basis:

$$S^+ = S^+_{+-} + S^+_{-+} + S^+_{++} + S^+_{--} \tag{2.12}$$

where $S^+_{\epsilon\sigma} = \mu^{\epsilon\sigma} \sum_N |N\epsilon\rangle\langle(N-1)\sigma|$ with $\epsilon, \sigma \in \{+,-\}$. If we now consider the first term of (2.12), we can see that the average value of S^+_{+-} is given by

$$\langle S^+_{+-}\rangle = \mu^{+-} \sum_N \langle (N-1) + |\rho| N-\rangle = \mu^{+-} \varrho^{+-}. \tag{2.13}$$

Thus $\langle S^+_{+-}\rangle$ will obey the same equation of motion (2.10) as does ϱ^{+-}. Similarly the average value of the second term of (2.12) obeys the same equation of motion as ϱ^{-+}. The last two terms of (2.12) obey the same *coupled* equations of motion as $\varrho^{\pm\pm}$, which (as the comment under (2.9) indicates) are the same as the population equations (2.8) with the addition of a free evolution term of frequency ω_L.

Now why have we been concentrating on the evolution of $\langle S^+\rangle$, when the spectrum in (2.11) is given by the fourier transform of a *two time* correlation function? It turns out that we can apply a theorem known as the "quantum regression theorem"[2] which states that (within the approximations employed here) the two-time correlation function $\langle S^+(t+\tau)S^-(t)\rangle$ obeys the same equation of motion as the one-time correlation function $\langle S^+(\tau)\rangle$.

Thus if we use (2.12) in (2.11), we can see that the spectrum will break up into three distinct terms. The first two terms, which have decoupled equations of motion, evolve in time according to the equations

$$\langle S^+_{\pm\mp}(\tau)S^-(0)\rangle = \Gamma\langle S^+_{\pm\mp}(0)S^-(0)\rangle e^{[i(\omega_L \pm G)-\Gamma_s]\tau}. \tag{2.14}$$

When we substitute (2.14) into (2.11) we obtain contributions to the spectrum

$$\Gamma\langle S^+_{\pm\mp}(0)S^-(0)\rangle \frac{\Gamma_s}{(\omega-\omega_L \pm 2G)^2+\Gamma_s^2}, \tag{2.15}$$

which are two Lorentzians centred at $\omega_L \pm 2G$ of linewidth Γ_s, and thus correspond to the sidebands of the Mollow triplet. The intensities of these two lines depend on the initial values of the correlation functions $\Gamma\langle S^+_{\pm\mp}(0)S^-(0)\rangle$, which are still to be determined. Let us consider $\Gamma\langle S^+_{+-}(0)S^-(0)\rangle$. Using (2.13) we can deduce

$$\begin{aligned}
\Gamma\langle S^+_{+-}(0)S^-(0)\rangle &= \langle \mu^{+-}\sum_N |N+\rangle\langle (N-1)-|S^-(0)\rangle \\
&= \Gamma\mu^{+-}\mathrm{Tr}\{\sum_N |N+\rangle\langle (N-1)-|S^-\rho\} \\
&= \Gamma\mu^{+-}\sum_N \langle (N-1)-|S^-\rho|N+\rangle \\
&= \Gamma\mu^{+-}\sum_{N,N',\epsilon} \langle (N-1)-|S^-|N'\epsilon\rangle\langle N'\epsilon|\rho|N+\rangle.
\end{aligned}$$

Now $\langle (N-1)-|S^-|N'\epsilon\rangle$ is zero unless $N'=N$, and $\langle N'+|\rho|N+\rangle$ is zero in the steady state. Thus we see that the intensities of the sidebands are given by

$$\Gamma\langle S^+_{\pm\mp}(0)S^-(0)\rangle = \Gamma^{\pm\mp}\Pi^+_{ss}. \tag{2.16}$$

The analysis of the $S^+_{\pm\pm}$ terms, which contribute the central line of the spectrum at ω_L, is similar to that outlined above, though it is a little more complicated

due to the fact that their equations of motion are coupled. It should be pointed out however that the eigenfrequencies obtained when solving the pair of linear coupled equations are $i\omega_L$ and $i\omega_L - \Gamma_c$. From this second term we obtain the central line of the inelastic spectrum, which has a linewidth of Γ_c. It is left as a challenge for the curious reader to determine to what the first term corresponds.

The final expression for the (incoherent part of the) fluorescence spectrum is given by (normalising all quantities to Γ)

$$S(\omega) = \frac{\Gamma^{+-}\Pi^{+}_{ss}\Gamma_s}{(\omega - (\omega_L + 2G))^2 + \Gamma_s^2} + \frac{\Gamma^{-+}\Pi^{-}_{ss}\Gamma_s}{(\omega - (\omega_L - 2G))^2 + \Gamma_s^2} + \frac{(\Gamma^{++}\Pi^{+}_{ss} + \Gamma^{--}\Pi^{-}_{ss})\,\Gamma_c}{(\omega - \omega_L)^2 + \Gamma_c^2}. \tag{2.17}$$

An examination of (2.17) shows that the spectrum is what one should intuitively expect, given a knowledge of dressed state dynamics. The sidebands of the spectrum consist of lorentzians with frequencies determined from the allowed transitions between the dressed states. Their linewidths are determined by the damping rate Γ_s of the coherence which evolves at the same transition frequency, and their intensities are proportional to the product of the population of the dressed state and the transition rate out of the state. The central component of the spectrum has two contributions since both $|N+\rangle \rightarrow |(N-1)+\rangle$ and $|N-\rangle \rightarrow |(N-1)-\rangle$ transitions occur at frequency ω_L. It is the fact that this spectrum *is* so intuitive that makes the dressed atom model so appealing. In practice we can just write down the spectrum given a knowledge of the population and coherence equations. We will see that even with more laser fields and much

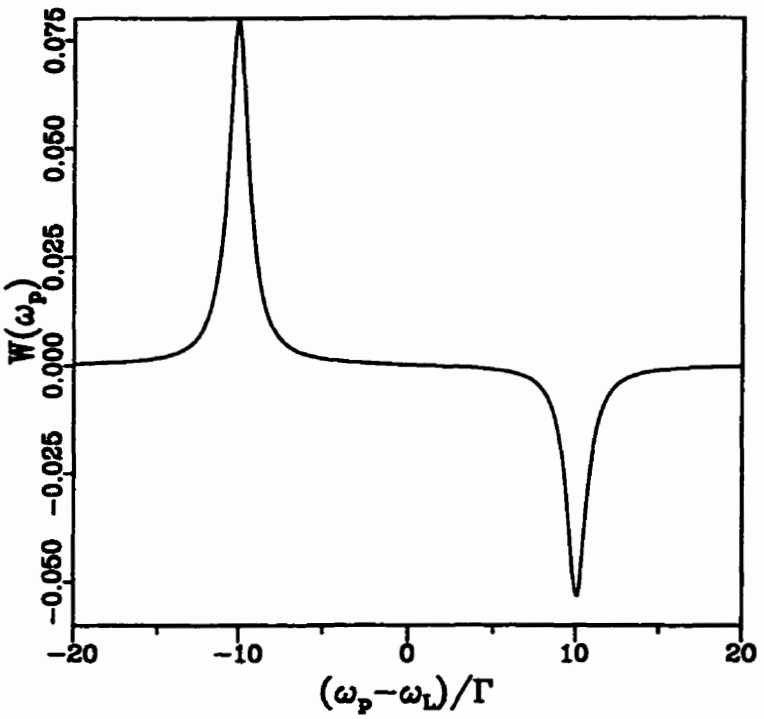

Figure 2.3 The weak probe absorption spectrum for the same parameters as in Figure 2.2. The positive y direction corresponds to absorption.

more complicated dressed states, all fluorescence spectra in this thesis will have the same general form as (2.17).

The spectrum (2.17) is known as the Mollow triplet, and is plotted in Figure 2.2 for $2\Omega = 10\Gamma$ and $\Delta = \Gamma$. All fluorescence spectra presented in the later chapters of this thesis should be compared to this spectrum, to understand the differences that an extra one or two laser fields can make.

2.7 Weak probe absorption and dispersion spectra

Another technique used by experimentalists to probe the dynamics of a strongly driven atom is to apply a second weak laser of frequency ω_p, and to scan this laser

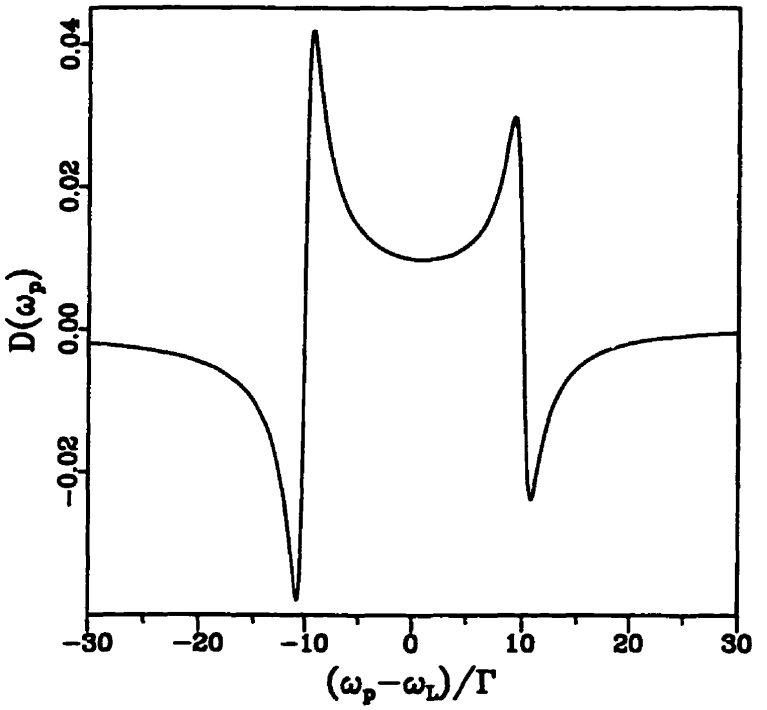

Figure 2.4 The weak probe dispersion spectrum for the same parameters as in Figure 2.2

through frequencies close to ω_0. This second laser is assumed weak enough not to appreciably affect the system dynamics. After passing through the system, the absorption and dispersion of this probe laser can be measured [5]. If the laser couples to a transition for which there is more population in the upper state than the lower then a net amplification will occur, while net absorption will occur if the population is greater in the lower state.

The absorption and dispersion (refractive index) profiles of the weak probe beam are given by the real and imaginary parts, respectively, of the Fourier transform of the two time commutator $\langle [S^-(t), S^+(t')] \rangle$. The term $\langle S^-(t)S^+(t') \rangle$ of the commutator is associated with absorption and the term $\langle S^+(t')S^-(t) \rangle$ with stimulated emission of the probe beam.

These spectra are derived in the dressed state picture in a manner similar to that of the fluorescence spectrum described above. The absorption spectrum is found to be given by

$$W(\omega_p) = \frac{\Gamma^{+-}(\Pi_{ss}^{-} - \Pi_{ss}^{+})\Gamma_s}{(\omega_p - (\omega_L + 2G))^2 + \Gamma_s^2} + \frac{\Gamma^{-+}(\Pi_{ss}^{+} - \Pi_{ss}^{-})\Gamma_s}{(\omega_p - (\omega_L - 2G))^2 + \Gamma_s^2}. \tag{2.18}$$

This spectrum is plotted in Figure 2.3, for the same parameters as used in Figure 2.2. Absorption is "upwards" in the diagram. The absorption and amplification occur because the dressed states are unequally populated. In this case $\Delta > 0$ and so from (2.9) and (2.4) we see that the upper (plus) states are more populated than the lower (minus) ones. This leads to absorption at $\omega_1 - 2G$ and amplification at $\omega_1 + 2G$.

Note that for the case of on resonance driving ($\Delta = 0$), a small amount of absorption and amplification at ω_0 *will* still occur, despite the fact that in the dressed state picture the steady state populations are equal and so the expression (2.18) vanishes. These effects are non-secular in nature (they arise from multiphoton processes [6]), and so are not easily derived within the dressed atom model.

The dispersion profile is given by

$$D(\omega_p) = \frac{\Gamma^{+-}(\Pi_{ss}^{-} - \Pi_{ss}^{+})(\omega_p - (\omega_L + 2G))}{(\omega_p - (\omega_L + 2G))^2 + \Gamma_s^2} + \frac{\Gamma^{-+}(\Pi_{ss}^{+} - \Pi_{ss}^{-})(\omega_p - (\omega_L - 2G))}{(\omega_p - (\omega_L - 2G))^2 + \Gamma_s^2}. \tag{2.19}$$

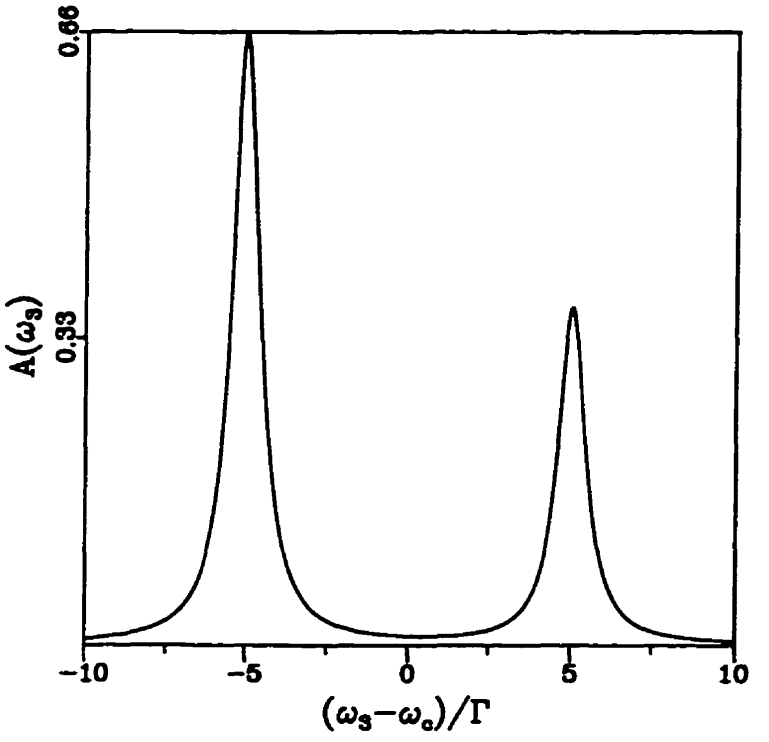

Figure 2.5 The Autler-Townes doublet for the same parameters as in Figure 2.2, and with $\Gamma_3/\Gamma = 3$.

This dispersion profile is plotted in Figure 2.4.

2.8 Autler-Townes absorption and dispersion spectra

Yet another way to investigate this system experimentally is to pick a third atomic level $|c\rangle$ which has a transition frequency ω_c from $|g\rangle$ (or $|e\rangle$) very different from ω_0. A weak laser of frequency ω_3 is now scanned across frequencies close to $\omega_c - \omega_g$, and the resulting absorption and dispersion of this laser measured [7]. If the laser is weak then it can be assumed to not appreciably affect the dressed state dynamics. The resulting "Autler-Townes" spectra can be easily derived,

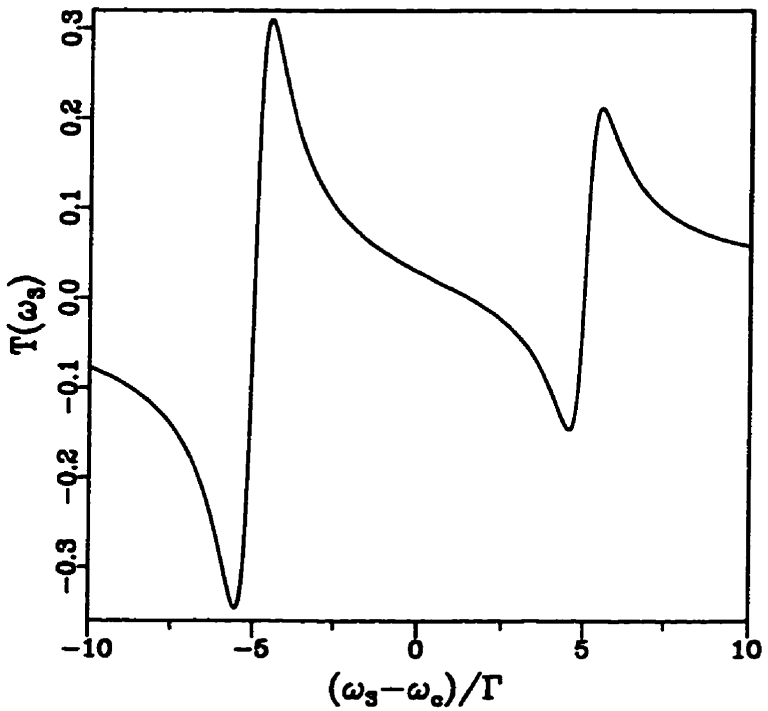

Figure 2.6 The Autler-Townes dispersion spectrum for the same parameters as in Figure 2.5.

and the Autler-Townes absorption spectrum is given by

$$A(\omega_3) = \frac{\Lambda^+ \Pi_{ss}^+ \Gamma_a}{(\omega_3 - (\omega_c - G))^2 + \Gamma_a^2} + \frac{\Lambda^- \Pi_{ss}^- \Gamma_a}{(\omega_3 - (\omega_c + G))^2 + \Gamma_a^2}, \tag{2.20}$$

while the corresponding Autler-Townes dispersion profile is

$$T(\omega_3) = \frac{\Lambda^+ \Pi_{ss}^+ (\omega_3 - (\omega_c - G))}{(\omega_3 - (\omega_c - G))^2 + \Gamma_a^2} + \frac{\Lambda^- \Pi_{ss}^- (\omega_3 - (\omega_c + G))}{(\omega_3 - (\omega_c + G))^2 + \Gamma_a^2}. \tag{2.21}$$

In the above, the weight factors $\Lambda^{\pm}$ determine the amount of the ground state (from which we are probing) "contaminating" the dressed states, and are given by

$$\Lambda^+ = |\langle N + |g, N\rangle|^2 = \sin^2\theta,$$

$$\Lambda^- = |\langle N - |g, N\rangle|^2 = \cos^2\theta.$$

The linewidth $\Gamma_a = \frac{1}{2}(\Gamma_s + \Gamma_3)$, where Γ_3 is the natural linewidth of level 3. These spectra are plotted in figures 5 and 6. Figure 5 shows the classic Autler-Townes doublet, which is split by $2G$. The doublet intensities are not equal because we have chosen parameters corresponding to off resonance driving ($\Delta > 0$).

2.9 Conclusions

We have examined in some detail the spectra associated with a two-level atom driven by a single intense laser field. These spectra will form the basis for our understanding, in the next three chapters, what differences are induced by the addition of an extra one or two laser fields with various detunings and intensities.

Hopefully it is clear that, at least in hindsight, all spectra presented in this chapter are very intuitive and easily understood from the dressed state picture. This understanding is not so easily obtained by solving density matrix equations of motion or the Bloch equations (either analytically or) numerically.

References

[1] C. Cohen-Tannoudji and S. Reynaud, J. Phys. B **10**, 345 (1977); C. Cohen-Tannoudji, J. Dupont-Roc, and G. Grynberg *Atom-Photon Interactions* (Wiley, New York, 1992).

[2] G.S. Agarwal in *Quantum Optics*, edited by G. Höhler, Springer Tracts in Modern Physics Vol. 70 (Springer, Berlin, 1974).

[3] B.R. Mollow, Phys. Rev. **188**, 1969 (1969).

[4] F. Schuda, C.R. Stroud, Jr., and M. Hercher, J. Phys. B **7**, L198 (1974); F.Y. Wu, R.E. Grove and S. Ezekiel, Phys. Rev. Lett. **35**, 1426 (1975).

[5] B.R. Mollow, Phys. Rev. A **5**, 2217 (1972); F.Y. Wu, S. Ezekiel, M. Ducloy and B.R. Mollow, Phys. Rev. Lett. **38**, 1077 (1977); C. Wei and N.B. Manson, Phys. Rev. A **49**, 4751 (1994); A.D. Wilson-Gordon and H. Friedmann, Optics Comm. **94**, 238 (1992); Tran Quang and Helen Freedhoff, Phys. Rev. A **48**, 3216 (1993).

[6] G. Grynberg and C. Cohen-Tannoudji, Optics. Commun. **96**, 150 (1993).

[7] S.H. Autler and C.H. Townes, Phys. Rev. **100**, 703 (1955); C. Wei, N.B. Manson and J.P.D. Martin, Phys. Rev. A **51**, 1438 (1995).

3. The multiphoton AC Stark effect

3.1 Introduction.

The interaction of a two-level atom with an intense, nearly resonant laser field is of fundamental interest in atomic spectroscopy and quantum optics and has been studied extensively for over 25 years. Early interest focussed on an atom driven by an intense monochromatic field and the resulting "dressed" system probed by a weak field, as briefly covered in chapter 2. Fluorescence by the system was first predicted [1] and then observed [2], as was the absorption and dispersion by the entangled atom+driving field system of a weak probe field nearly resonant with either the driven transition [3] or the transition from a driven level to a third atomic level (Autler-Townes effect) [4].

Another area of interest involves the atomic response to amplitude-modulated (AM) and bichromatic driving fields. A 100% amplitude-modulated field is equivalent to a bichromatic field whose (mutually coherent) components have equal intensities, and whose frequencies are separated by twice the modulation frequency. Various aspects of this problem have been studied. For example the fluorescence spectrum of an atom driven by a bichromatic field of equal amplitudes (Rabi frequencies) was observed [5] and interpreted using a dressed-atom analysis [6]. Since then a wide variety of studies have been performed on the fluorescence, near-resonant absorption, and Autler-Townes absorption of bichromatically driven atoms for both equal [7] and unequal [8] Rabi frequencies, and

for average driving field frequency both tuned to and detuned from the atomic resonance [9],[10].

Much attention has focussed, in these studies, on the appearance of the "subharmonic resonances" displayed by the absorption spectrum of a strong probe beam monitoring a strongly driven two-level system [10-13]. The experimental data collected to date relating to the subharmonic absorption maxima of the strong probe also corresponds to a study of the maxima of the integrated intensity of fluorescence by the atom when one component of the driving field (the "pump") is fixed in its frequency and intensity, while the frequency and/or intensity of the second component (the "probe") is varied. The connection of these subharmonic resonances with multi-photon gain has also been explored [14], and a two-photon optical lasing has been observed [15]. However, a "strong probe" is an intense field which itself alters the characteristics of the system it is supposed to be probing. Based on this observation, we will therefore consider this system from the point of view that both laser fields "dress" the atom and analyse the energy states of the resulting system. We will show that the system is both in principle and in practice more profitably regarded in the context of this bichromatic excitation.

In the studies of resonance fluorescence from two- or three-level atoms under bichromatic excitation, both driving fields couple to the same atomic transition. In the related studies of multi-level atoms driven by n coherent laser fields each of the fields couples to only one of the n possible one-photon transitions [16]; in this latter case a multiphoton absorption is possible, but the driving fields can lead to only a "one-photon AC Stark effect". In this chapter we will study a system

in which two fields drive the *same* atomic one-photon transition, yet nevertheless the second field can couple to multiphoton resonances between dressed states of the first field. We will find a new physical phenomenon: the splitting of the dressed states is due to an n-photon coupling between them, *i.e.* it represents an n-photon AC Stark effect. The fundamental dynamics of this system can be investigated by examining the fluorescence spectrum, as well as the weak probe absorption and Autler-Townes spectra. We will focus in this chapter on the driving of the singly dressed system by a laser field tuned to the subharmonic resonances, and use the dressed-atom model both to explain the physical origin of novel spectral effects and to demonstrate that far more detailed information is in fact obtainable by suitable probing. The calculated fluorescence, probe absorption and Autler-Townes spectra are extremely rich in detail, containing multiplets at the subharmonic as well as harmonic resonance frequencies with an intricate dependence on the order n of the resonance and on the relative Rabi frequencies of the driving field components.

In principle it is possible to write down and numerically solve the master equation or the Bloch equations of the system including all of these effects; this does not however lead to physical understanding of the problem. In order to gain insight into the dynamics of the system, we will use the "dressed atom" model, which was briefly discussed in Chapter 2, for our bichromatically driven atom [19].

The chapter is organised as follows. The energy levels of the entangled system of atom+driving fields (i.e. the doubly-dressed atom) are calculated first in

sections 3.2 and 3.3. Resonance fluorescence appears in this picture as a spontaneous emission cascade by the dressed atom down its ladder of energy manifolds. The absorption spectrum is interpreted as the net difference between absorption and stimulated emission of a weak, quasi-resonant probe between the manifold sublevels, while the Autler-Townes spectrum reflects the net absorption from the manifold sublevels of a weak probe tuned to a third atomic level. These spectra are calculated in section 3.4. In section 3.5 we discuss briefly the situation that occurs when the role of the two driving fields is reversed. In section 3.6 the results of this chapter are summarized. Appendix A contains details of the perturbation calculations involved in the determination of the dressed states.

3.2 The System

As in the last chapter, we will consider a two-level atom with ground state $|g\rangle$ and excited state $|e\rangle$ separated by a transition frequency ω_0 and connected by a transition dipole moment $\vec{\mu}$. The atom is driven by a bichromatic field with frequency components ω_1 and ω_2 and corresponding (on resonance) Rabi frequencies $2\Omega_1$ and $2\Omega_2$. The atom is also coupled to all other modes of the electromagnetic field, which are assumed to be initially in their vacuum states. This coupling leads to spontaneous emission with a rate Γ.

The time evolution of the atomic system can be described by the reduced atomic density operator ρ, which in the Schrödinger picture obeys the master equation ($\hbar = 1$) [20]

$$\frac{\partial \rho}{\partial t} = -i[H, \rho] - \frac{\Gamma}{2}(S^+S^-\rho + \rho S^+S^- - 2S^-\rho S^+), \tag{3.1}$$

where $S^+(S^-) = |e\rangle\langle g|$ ($|g\rangle\langle e|$) is the usual atomic raising (lowering) operator. The Hamiltonian H is composed of five terms,

$$H = H_a + H_1 + H_2 + V_1 + V_2, \tag{3.2}$$

where

$$H_a = \omega_0 S^z \tag{3.3}$$

is the Hamiltonian of the atom, and

$$H_i = \omega_i a_i^\dagger a_i, \quad i = 1, 2\ , \tag{3.4}$$

are the Hamiltonians of the driving field components. In equations (3.3) and (3.4), $S^z = \frac{1}{2}(|e\rangle\langle e| - |g\rangle\langle g|)$ is the atomic inversion, and $a_i(a_i^\dagger)$ are the annihilation (creation) operators for the driving field modes. The terms

$$V_i = g_i(a_i^\dagger S^- + S^+ a_i), \quad i = 1, 2. \tag{3.5}$$

where g_i are the atom-field coupling constants, describe the interaction of the laser fields with the atom (in the rotating-wave approximation).

We begin by diagonalising the Hamiltonian H to find the eigenstates (dressed states) of the combined atom+driving fields system. This approach is valid for

$$\omega_1, \omega_2 \gg \Omega_1, \Omega_2 > \Gamma. \tag{3.6}$$

For all but Section 3.5, we will consider the case of $\Omega_2 = \alpha\Omega_1$ with $\alpha < 1$, and thus we can examine the effect of the second field perturbatively. Moreover, we limit our calculations to the case in which the first field is on resonance with the

atomic transition, $\omega_1 = \omega_0$, and the second field is detuned from resonance by an integer fraction of the first field's Rabi frequency, so that

$$\omega_2 = \omega_0 + \frac{2\Omega_1}{n}. \tag{3.7}$$

This corresponds to driving the system by the second field at one of the "subharmonic resonances" of the Rabi frequency of the first field. The case of $n = 1$ has recently been examined both theoretically [21] and experimentally [22]. As we shall see the situation for $n = 2, 3, ...$ produces dramatically different results. An n-photon coupling between dressed states leads to the appearance of multiplet features at subharmonic as well as harmonic resonance frequencies in the spectra.

The diagonalisation of H leads to the dressed states of the system and their energies. However, instead of performing the diagonalisation of the total Hamiltonian by treating the driving fields as a single combined field, we first diagonalise the Hamiltonian $H_{da} = H_a + H_1 + V_1$ and calculate the dressed states of the atom+resonant field system. Next we couple the resulting singly-dressed atom to the detuned field and calculate the dressed states and their energies of this "doubly-dressed" atom. The eigenstates of the Hamiltonian H_{da} satisfy the eigenvalue equation

$$H_{da}|N\pm\rangle = [N\omega_0 \pm \Omega_1]|N\pm\rangle, \tag{3.8}$$

where

$$2\Omega_1 = 2g_1\sqrt{\langle N\rangle} \tag{3.9}$$

is the Rabi frequency of the resonant field[†]

$$|N\pm\rangle = \frac{1}{\sqrt{2}}(|g,N\rangle \pm |e,N-1\rangle) \tag{3.10}$$

are the singly-dressed states, and N is the number of photons in the resonant mode [19]. The singly-dressed states form a ladder of doublets, as shown in Figure 3.1(a), with adjacent doublets separated by ω_0, and intradoublet splitting $2\Omega_1$.

Next, we add the second field and find that the eigenstates of the combined system $H_{da} + H_2$ are degenerate doublets

$$\begin{aligned} |(N+n-m)+, M-n+m\rangle &\equiv |a_m^n\rangle, \\ |(N-m)-, M+m\rangle &\equiv |b_m^n\rangle, \end{aligned} \tag{3.11}$$

with energies

$$E_{a_m} \equiv E_{b_m} = (N+M)\omega_0 + \frac{\Omega_1}{n}[2(M+m)-n], \tag{3.12}$$

Here the second state of the tensor product denotes the number of photons in the detuned mode. In state $|b_m^n\rangle$, for example, the (singly-dressed) atom is in state $|(N-m)-\rangle$, and there are $M+m$ photons in the weaker field.

The degeneracy of the states (3.11) is due to an n-photon coupling between singly dressed states, as indicated for $n = 2$ by arrows in Figure 3.1(a). Thus, to this point, the energy structure of the system consists of an infinite number

[†] In the derivation of Eq. (3.6), we have ignored the variation of Ω_1 with N, on the basis that the resonant laser is in a (large amplitude coherent) state with an average number of photons $\langle N\rangle \gg 1$.

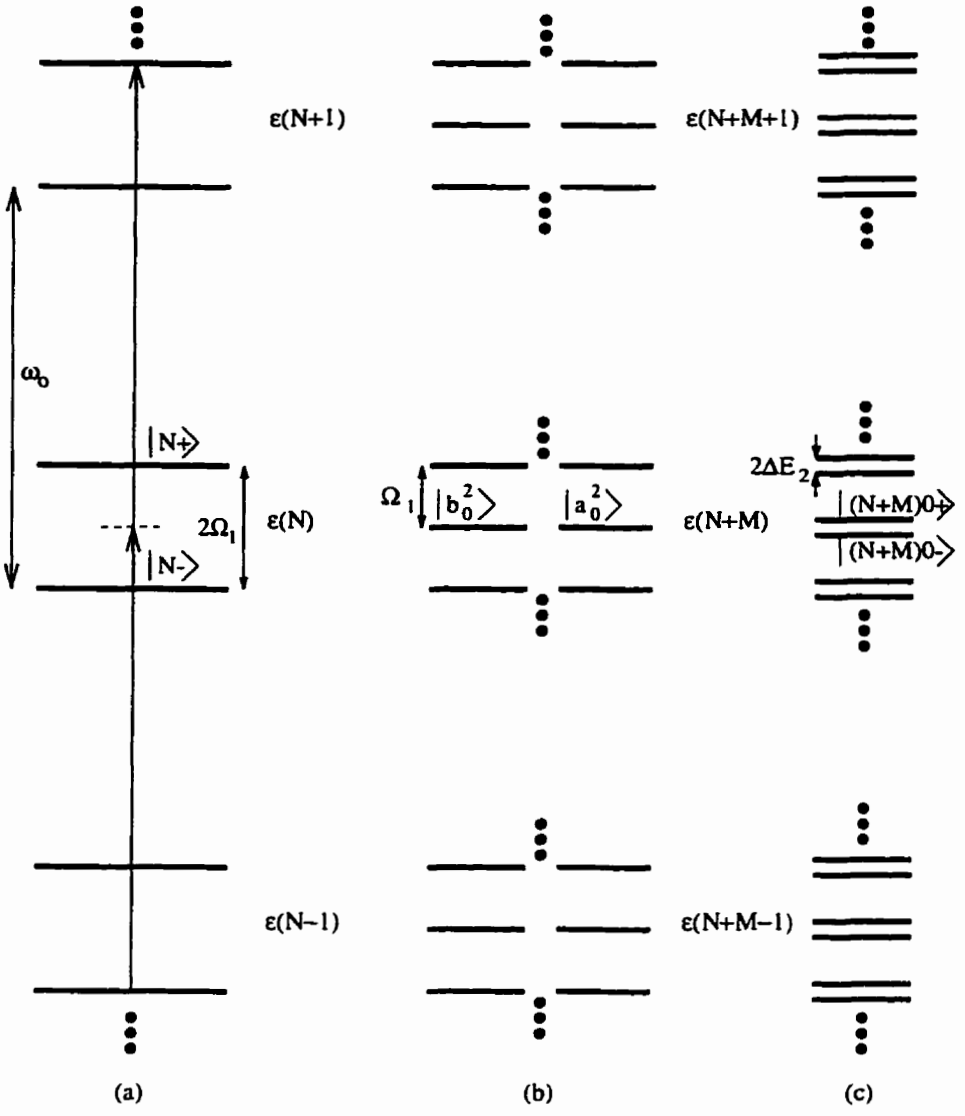

Figure 3.1 (a) Energy levels of the singly-dressed atom. Absorption of two laser 2 photons of frequency $\omega_2 = \omega_0 + \Omega_1$, corresponding to the case of $n = 2$, is indicated by the arrows. (b) Energy levels of the singly-dressed atom and laser 2 before the interaction between them is "turned on". The energy manifolds each contain an infinite number of degenerate doublets with interdoublet separation Ω_1. (c) Addition of the interaction with laser 2 removes the degeneracy and leads to the splitting of the degenerate levels into doublets with an intradoublet separation $2\Delta E_2$.

of manifolds (separated by ω_0), each containing an infinite number of degenerate doublets (separated by $2\Omega_1/n$), as shown in Figure 3.1(b).

3.3 The doubly-dressed states and energy splittings

The addition of the interaction V_2 between the atom and field mode 2 removes the degeneracy between the states $|a_m^n\rangle$ and $|b_m^n\rangle$ and results in "doubly-dressed" states. In order to show this, we diagonalise the Hamiltonian $H = H_{da} + H_2 + V_2$ in the basis of the degenerate states $|a_m^n\rangle$ and $|b_m^n\rangle$. We perform the diagonalisation using perturbation theory, and find that for $n = 2, 3, ...$ it is necessary to go to second-order degenerate perturbation theory to achieve this. This is due to the fact that the matrix elements $\langle\alpha|V_2|\beta\rangle$ $(\alpha, \beta = a, b)$ are zero, and the first non-vanishing perturbation calculations therefore involve diagonalisation of the operator

$$\mathcal{R}^1 \equiv \sum_{i \neq a,b} \frac{V_2|i\rangle\langle i|V_2}{E_a - E_i} \tag{3.13}$$

on the two dimensional degenerate subspace $\{|a\rangle, |b\rangle\}$.

The details of the perturbation calculations are shown in Appendix A. After lengthy calculations, we find that the eigenstates of H are composed of non-degenerate doublets with splitting $2\Delta E_n$ (as shown in Figure 1(c)), where ΔE_n, for $n = 2, 3$ and 4, are given by the series expansions

$$\begin{aligned}
\Delta E_2 &= \Omega_1\sqrt{13}\left(\frac{1}{6}\alpha^2 - \frac{493}{2808}\alpha^4 + \frac{9123107}{52565760}\alpha^6 + ...\right), \\
\Delta E_3 &= \Omega_1\left(\frac{9}{32}\alpha^2 + \frac{36117}{40960}\alpha^4 - \frac{132460191}{26214400}\alpha^6 + ...\right), \\
\Delta E_4 &= \Omega_1\left(\frac{4}{15}\alpha^2 + \frac{254}{3375}\alpha^4 + \frac{9384656}{5315625}\alpha^6 + ...\right).
\end{aligned} \tag{3.14}$$

The corresponding eigenstates (the doubly-dressed states), calculated as a perturbation expansion in α, are given by

$$\begin{aligned}
\mathbf{n=2:}\\
|(N+M)m+\rangle &= \mathcal{N}_2\Big(\eta|a\rangle+|b\rangle+\tfrac{1}{2}\alpha\Big[-(\eta+1)|a_1\rangle+|b_1\rangle+\eta|a_{-1}\rangle+(\eta-1)|b_{-1}\rangle\\
&\quad+\tfrac{1}{3}|a_3\rangle-\tfrac{1}{3}\eta|b_{-3}\rangle\Big]+\tfrac{1}{12}\alpha^2\Big[\tfrac{-27}{52}(|a\rangle-\eta|b\rangle)+(3\eta-2)|a_2\rangle+|b_2\rangle\\
&\quad+\eta|a_{-2}\rangle+(2\eta+3)|b_{-2}\rangle+\tfrac{1}{2}|a_4\rangle-\tfrac{1}{2}\eta|b_{-4}\rangle\Big]\Big),\\
|(N+M)m-\rangle &= \mathcal{N}_2\Big(|a\rangle-\eta|b\rangle+\tfrac{1}{2}\alpha\Big[(\eta-1)|a_1\rangle-\eta|b_1\rangle+|a_{-1}\rangle+(\eta+1)|b_{-1}\rangle\\
&\quad-\tfrac{1}{3}\eta|a_3\rangle-\tfrac{1}{3}|b_{-3}\rangle\Big]+\tfrac{1}{12}\alpha^2\Big[\tfrac{27}{52}(\eta|a\rangle+|b\rangle)+(3+2\eta)|a_2\rangle-\eta|b_2\rangle\\
&\quad+|a_{-2}\rangle+(2-3\eta)|b_{-2}\rangle-\tfrac{1}{2}\eta|a_4\rangle-\tfrac{1}{2}|b_{-4}\rangle\Big]\Big),
\end{aligned}\tag{3.15}$$

$$\begin{aligned}
\mathbf{n=3:}\\
|(N+M)m+\rangle &= \mathcal{N}_3\Big(|a\rangle+\tfrac{3}{4}\alpha\Big[\tfrac{3}{2}|b\rangle-|a_1\rangle+|a_{-1}\rangle+\tfrac{1}{2}|b_{-2}\rangle-\tfrac{1}{4}|b_{-4}\rangle\Big]\\
&\quad+\tfrac{27}{16}\alpha^2\Big[\tfrac{1}{2}|b_1\rangle-|b_{-1}\rangle+\tfrac{1}{8}|a_{-2}\rangle+\tfrac{7}{36}|b_{-3}\rangle+\tfrac{1}{8}|a_4\rangle-\tfrac{1}{20}|b_{-5}\rangle\Big]\Big),\\
|(N+M)m-\rangle &= \mathcal{N}_3\Big(|b\rangle+\tfrac{3}{4}\alpha\Big[\tfrac{-3}{2}|a\rangle+|b_1\rangle-|b_{-1}\rangle-\tfrac{1}{2}|a_2\rangle+\tfrac{1}{4}|a_4\rangle\Big]\\
&\quad+\tfrac{27}{16}\alpha^2\Big[|a_1\rangle-\tfrac{1}{2}|a_{-1}\rangle+\tfrac{1}{8}|b_2\rangle-\tfrac{7}{36}|a_3\rangle+\tfrac{1}{8}|b_{-4}\rangle+\tfrac{1}{20}|a_5\rangle\Big]\Big),
\end{aligned}\tag{3.16}$$

$$\begin{aligned}
\mathbf{n=4:}\\
|(N+M)m+\rangle &= \mathcal{N}_4\Big(|a\rangle+\alpha\Big[|a_{-1}\rangle-|a_1\rangle+\tfrac{1}{3}|b_{-3}\rangle-\tfrac{1}{5}|b_{-5}\rangle\Big]\\
&\quad+\alpha^2\Big[\tfrac{-5}{3}|b\rangle+\tfrac{2}{3}|a_2\rangle+\tfrac{2}{5}|a_{-2}\rangle-\tfrac{2}{3}|b_{-2}\rangle+\tfrac{7}{15}|b_{-4}\rangle-\tfrac{2}{15}|b_{-6}\rangle\Big]\Big),\\
|(N+M)m-\rangle &= \mathcal{N}_4\Big(|b\rangle+\alpha\Big[|b_1\rangle-|b_{-1}\rangle-\tfrac{1}{3}|a_3\rangle+\tfrac{1}{5}|a_5\rangle\Big]\\
&\quad+\alpha^2\Big[\tfrac{5}{3}|a\rangle+\tfrac{2}{3}|b_{-2}\rangle+\tfrac{2}{5}|b_2\rangle+\tfrac{2}{3}|a_2\rangle-\tfrac{7}{15}|a_4\rangle+\tfrac{2}{15}|a_6\rangle\Big]\Big),
\end{aligned}\tag{3.17}$$

where $\eta=-\frac{2}{3}-\frac{\sqrt{13}}{3}$, and $\mathcal{N}_2=[(1+\eta^2)(1+\frac{7}{9}\alpha^2)]^{-\frac{1}{2}}$, $\mathcal{N}_3=[1+\frac{484}{225}\alpha^2]^{-\frac{1}{2}}$, $\mathcal{N}_4=[1+\frac{657}{256}\alpha^2)]^{-\frac{1}{2}}$ are the normalization constants, and, for simplicity, we have introduced the notation $|a_i\rangle\equiv|a^n_{m+i}\rangle$, $|b_i\rangle\equiv|b^n_{m+i}\rangle$ for $i\neq 0$ and $|a_0\rangle=|a\rangle$, $|b_0\rangle=|b\rangle$.

We note the interesting effect that the operator R^1 in second-order lifts the degeneracy between the $|a\rangle$ and $|b\rangle$ states for all $n\geq 2$; however a mixture of these

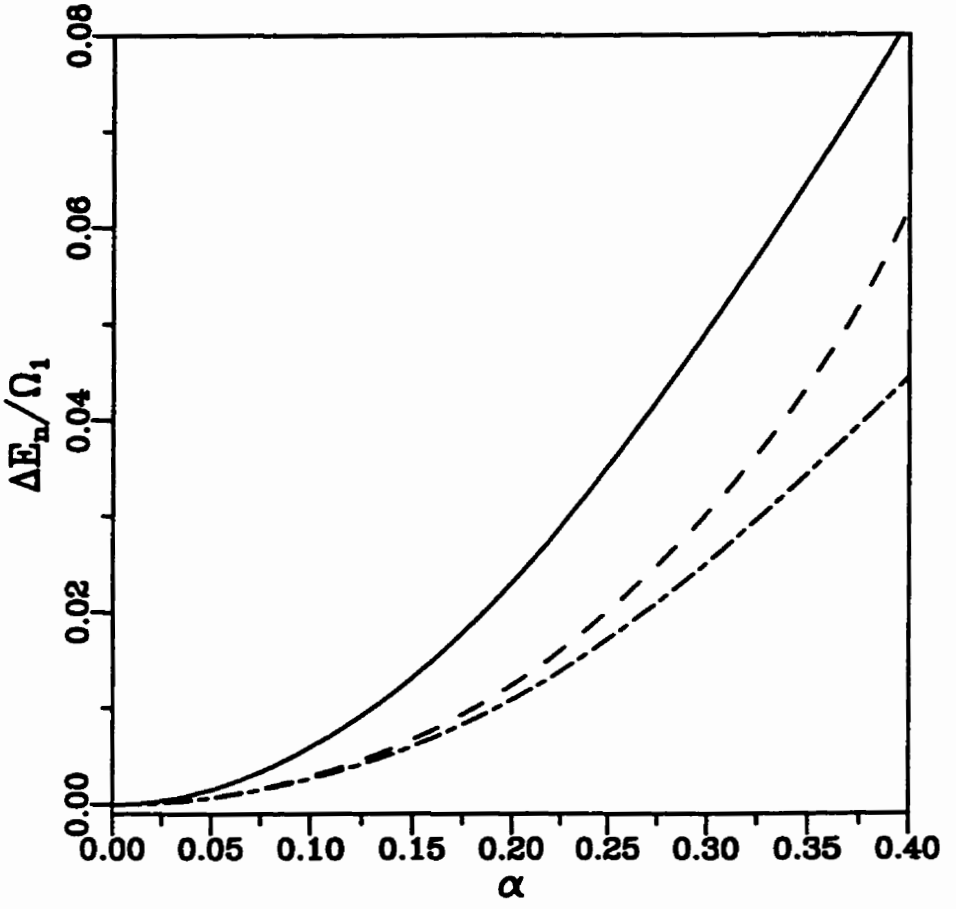

Figure 3.2 The n-photon energy splitting $\Delta E_n/\Omega_1$, plotted as a function of α for $n = 2$ (solid line), $n = 3$ (dashed line) and $n = 4$ (dashed-dotted line).

states *to zeroth-order in* α does not occur for $n > 2$. To understand this we refer to the operator $\mathcal{R}^1$, whose diagonal elements represent the shift of the degenerate states due to their coupling, through V_2, with other states of the manifold. Since $\langle a|\mathcal{R}^1|a\rangle = -\langle b|\mathcal{R}^1|b\rangle \neq 0$ for all n, the states are always shifted in opposite directions, which lifts the degeneracy at second order. The off-diagonal elements of $\mathcal{R}^1$ represent a coupling *between* the degenerate states through the other states of the manifold. It is not difficult to show that for $n > 2$ these off-diagonal elements are zero; hence the matrix representation of $\mathcal{R}^1$ is diagonal and no superposition of the states occurs until order α^{n-2}.

The splittings ΔE_n are plotted in Figure 3.2 as a function of α. Clearly for small α the splittings exhibit a quadratic dependence on α, and decrease with increasing n. Moreover for $\alpha < 0.1$ the splittings for $n = 3$ and 4 are almost exactly equal. This is a consequence again of the fact that for $n \geq 3$ the states $|a\rangle$ and $|b\rangle$ do not couple to each other through $\mathcal{R}^1$, which results in the leading term of the expansion for ΔE_n rapidly approaching $\frac{1}{4}\Omega_1\alpha^2$ for large n. Thus as n increases, the small α behaviour of the splittings becomes almost identical.

3.4 The fluorescence, weak probe and Autler-Townes absorption and dispersion spectra

3.4.1 Spectral frequencies and transition rates

The interaction between the atom and the vacuum modes of the electromagnetic field leads to a spontaneous emission cascade down the energy manifold ladder of the dressed atom. Transitions occur between any pair of dressed states with a probability proportional to the absolute square of the dipole transition moment connecting them. Using the dressed states (3.15)-(3.17) we find that the transitions from $|(N+M)m\sigma\rangle$ to $|(N+M-1)(m+j)\epsilon\rangle$ $(\epsilon, \sigma \in \{+,-\})$ occur at frequencies

$$\omega_j^{\pm\pm} = \omega_0 - j\frac{2\Omega_1}{n} \qquad (3.18),$$

and

$$\omega_j^{\pm\mp} = \omega_0 - j\frac{2\Omega_1}{n} \pm 2\Delta E_n, \qquad (3.19)$$

indicating that the fluorescence spectrum will consist of a series of triplets with intratriplet spacing $2\Delta E_n$ centred at integer multiples of $2\Omega_1/n$, *i.e.* at both

sub- and super- harmonics of the strong field Rabi frequency. Non-zero transition probabilities occur only between states within neighbouring manifolds. The relevant transition rates are therefore of the form

$$\Gamma_j^{\sigma\epsilon} = \Gamma \left| \langle (N+M)m\sigma | \, S^+ \, | (N+M-1)(m+j)\epsilon \rangle \right|^2 \qquad (3.20).$$

These transition rates (normalised to Γ, as are all relevant results presented henceforth) are presented explicitly below. In order to show the first non-vanishing terms in the transition rates, the calculations for $n = 2$ are presented correct to order α^2, whereas for $n = 3, 4$ they are presented correct to order α^4.

For $n = 2$ the transition rates (3.20) are given by

$$\begin{array}{llll}
\Gamma_{-3}^{\pm\pm} & = \frac{1}{13}\alpha^2 & \Gamma_{-3}^{\pm\mp} & = \left(\frac{17}{117} \pm \frac{4\sqrt{13}}{117}\right)\alpha^2 \\
\Gamma_{-2}^{\pm\pm} & = \frac{9}{208} - \frac{1405}{5408}\alpha^2 & \Gamma_{-2}^{\pm\mp} & = \frac{17}{208} \pm \frac{\sqrt{13}}{52} - \left(\frac{17099}{48672} \mp \frac{6803\sqrt{13}}{97344}\right)\alpha^2 \\
\Gamma_{-1}^{\pm\pm} & = \frac{13}{36}\alpha^2 & \Gamma_{-1}^{\pm\mp} & = \frac{1}{4}\alpha^2 \\
\Gamma_{0}^{\pm\pm} & = \frac{1}{13} - \frac{2201}{12168}\alpha^2 & \Gamma_{0}^{\pm\mp} & = \frac{9}{52} - \left(\frac{131}{1352} \mp \frac{3\sqrt{13}}{26}\right)\alpha^2 \\
\Gamma_{1}^{\pm\pm} & = \frac{4}{117}\alpha^2 & \Gamma_{1}^{\pm\mp} & = \frac{1}{13}\alpha^2 \\
\Gamma_{2}^{\pm\pm} & = \frac{9}{208} - \frac{261}{5408}\alpha^2 & \Gamma_{2}^{\pm\mp} & = \frac{17}{208} \mp \frac{\sqrt{13}}{52} - \left(\frac{3059}{48672} \mp \frac{1187\sqrt{13}}{97344}\right)\alpha^2 \\
\Gamma_{3}^{\pm\pm} & = \frac{1}{52}\alpha^2 & \Gamma_{3}^{\pm\mp} & = \left(\frac{17}{468} \mp \frac{\sqrt{13}}{117}\right)\alpha^2.
\end{array} \qquad (3.21)$$

The left hand column of (3.21) consists of those transition rates which contribute to the central components of the fluorescence triplets, the right hand column are transition rates which govern the intensities of the triplet sidebands.

For $n = 3$ we find the transition rates which govern the intensities of the central component in each fluorescence triplet are given by

$$\begin{aligned}
\Gamma_0^{\pm\pm} &= \tfrac{1}{4} - \tfrac{369}{256}\alpha^2 + \tfrac{4844169}{409600}\alpha^4 & \Gamma_1^{\pm\pm} &= \tfrac{81}{1024}\alpha^2 - \tfrac{45927}{65536}\alpha^4 \\
\Gamma_{-1}^{\pm\pm} &= \tfrac{81}{1024}\alpha^2 + \tfrac{325053}{327680}\alpha^4 & \Gamma_2^{\pm\pm} &= \tfrac{263169}{409600}\alpha^4 \\
\Gamma_{-2}^{\pm\pm} &= \tfrac{927369}{409600}\alpha^4 & \Gamma_3^{\pm\pm} &= \tfrac{81}{256}\alpha^2 - \tfrac{677889}{163840}\alpha^4 \\
\Gamma_{-3}^{\pm\pm} &= \tfrac{81}{256}\alpha^2 - \tfrac{207117}{32768}\alpha^4 & \Gamma_4^{\pm\pm} &= \tfrac{6561}{16384}\alpha^4 \\
\Gamma_{-4}^{\pm\pm} &= \tfrac{18225}{16384}\alpha^4,
\end{aligned} \tag{3.22a}$$

while those governing the intensities of the sideband components of each triplet are given by

$$\begin{aligned}
\Gamma_0^{+-} &= \tfrac{81}{64}\alpha^2 - \tfrac{26163}{2560}\alpha^4 & \Gamma_0^{-+} &= \tfrac{81}{64}\alpha^2 - \tfrac{18549}{1280}\alpha^4 \\
\Gamma_1^{+-} &= \tfrac{6561}{16384}\alpha^4 & \Gamma_1^{-+} &= \tfrac{3969}{4096}\alpha^4 \\
\Gamma_{-1}^{+-} &= \tfrac{6561}{4096}\alpha^4 & \Gamma_{-1}^{-+} &= \tfrac{6561}{16384}\alpha^4 \\
\Gamma_{-2}^{+-} &= \tfrac{81}{64}\alpha^2 - \tfrac{485757}{40960}\alpha^4 & \Gamma_2^{-+} &= \tfrac{9}{64}\alpha^2 - \tfrac{50949}{40960}\alpha^4 \\
\Gamma_3^{+-} &= \tfrac{6561}{16384}\alpha^4 & \Gamma_3^{-+} &= \tfrac{1}{4} - \tfrac{597}{512}\alpha^2 + \tfrac{55103607}{6553600}\alpha^4 \\
\Gamma_{-3}^{+-} &= \tfrac{1}{4} - \tfrac{1365}{512}\alpha^2 + \tfrac{125778807}{6553600}\alpha^4 & \Gamma_{-3}^{-+} &= \tfrac{6561}{16384}\alpha^4 \\
\Gamma_{-4}^{+-} &= \tfrac{225}{256}\alpha^2 - \tfrac{89343}{16384}\alpha^4 & \Gamma_4^{-+} &= \tfrac{81}{256}\alpha^2 - \tfrac{105219}{81920}\alpha^4 \\
\Gamma_{-5}^{+-} &= \tfrac{3538161}{6553600}\alpha^4 & \Gamma_5^{-+} &= \tfrac{6561}{16384}\alpha^4.
\end{aligned} \tag{3.22b}$$

For $n = 4$ we find the central component transition rates are given by

$$\begin{aligned}
\Gamma_0^{\pm\pm} &= \tfrac{1}{4} - \tfrac{34}{225}\alpha^2 - \tfrac{149486}{50625}\alpha^4 & \Gamma_1^{\pm\pm} &= \tfrac{16}{225}\alpha^2 - \tfrac{3136}{50625}\alpha^4 \\
\Gamma_{-1}^{\pm\pm} &= \tfrac{16}{225}\alpha^2 + \tfrac{4064}{50625}\alpha^4 & \Gamma_2^{\pm\pm} &= \tfrac{16}{225}\alpha^4 \\
\Gamma_{-2}^{\pm\pm} &= \tfrac{4}{225}\alpha^4 & \Gamma_4^{\pm\pm} &= \tfrac{25}{36}\alpha^4 \\
\Gamma_{-4}^{\pm\pm} &= \tfrac{25}{36}\alpha^4,
\end{aligned} \tag{3.23a}$$

while the sideband transition rates are given by

$$\begin{aligned}
\Gamma_0^{+-} &= \tfrac{25}{9}\alpha^4 & \Gamma_0^{-+} &= \tfrac{25}{9}\alpha^4 \\
\Gamma_{-2}^{+-} &= \tfrac{400}{81}\alpha^4 & \Gamma_2^{-+} &= \tfrac{4}{81}\alpha^4 \\
\Gamma_{-3}^{+-} &= \tfrac{16}{9}\alpha^2 - \tfrac{28288}{2025}\alpha^4 & \Gamma_3^{-+} &= \tfrac{4}{9}\alpha^2 - \tfrac{2272}{2025}\alpha^4 \\
\Gamma_{-4}^{+-} &= \tfrac{1}{4} - \tfrac{707}{225}\alpha^2 + \tfrac{1463321}{101250}\alpha^4 & \Gamma_4^{-+} &= \tfrac{1}{4} - \tfrac{257}{225}\alpha^2 + \tfrac{95321}{101250}\alpha^4 \\
\Gamma_{-5}^{+-} &= \tfrac{36}{25}\alpha^2 - \tfrac{15392}{1875}\alpha^4 & \Gamma_5^{-+} &= \tfrac{16}{25}\alpha^2 - \tfrac{1024}{625}\alpha^4 \\
\Gamma_{-6}^{+-} &= \tfrac{8836}{5625}\alpha^4 & \Gamma_6^{-+} &= \tfrac{1936}{5625}\alpha^4
\end{aligned} \tag{3.23b}$$

An examination of (3.22) and (3.23) reveals that the only transition rates which have nonvanishing terms independent of α are $\Gamma_0^{\pm\pm}$, which correspond to transitions at ω_0, and $\Gamma_{\mp n}^{\pm\mp}$, which correspond to sidebands of the triplets at $\pm 2\Omega_1$. These are the locations of the Rabi sidebands for monochromatic driving.

3.4.2 Populations of the dressed states

We use the master equation (3.1) to find the time evolution of the populations of the doubly-dressed states and of the coherences between them. To study the populations, we project the master equation onto $|(N+M)m\pm\rangle$ on the right and $\langle(N+M)m\pm|$ on the left. We make the secular approximation in which we ignore couplings between populations and coherences and introduce the "reduced populations" [19]

$$\Pi_m^{\pm} = \sum_{N,M} \langle (N+M)m \pm |\rho| (N+M)m\pm\rangle. \tag{3.24}$$

Because $N, M \gg 1$ we can also assume that the populations vary very slowly with m, and so

$$\Pi_m^{\pm} \simeq \Pi_{m\pm 1}^{\pm} \simeq \ldots \equiv \Pi^{\pm}. \tag{3.25}$$

The population equations then reduce to a pair of coupled equations

$$\dot{\Pi}^{\pm} = \mp A^{+}\Pi^{+} \pm A^{-}\Pi^{-}, \tag{3.26}$$

where the dot denotes differentiation with respect to Γt, and the coefficients $A^{\pm}$ are given by

$$\begin{aligned}
&\mathbf{n=2}: \\
&\quad A^{\pm} = \frac{35}{104} - \left(\frac{61}{24336} \pm \frac{\sqrt{13}}{12}\right)\alpha^2 + \left(\frac{99556813}{455569920} \mp \frac{259\sqrt{13}}{2808}\right)\alpha^4; \\
&\mathbf{n=3}: \\
&\quad A^{+} = \frac{1}{4} + \frac{381}{512}\alpha^2 - \frac{4421529}{819200}\alpha^4, \\
&\quad A^{-} = \frac{1}{4} - \frac{285}{512}\alpha^2 - \frac{5538249}{819200}\alpha^4; \\
&\mathbf{n=4}: \\
&\quad A^{+} = \frac{1}{4} + \frac{17}{225}\alpha^2 + \frac{158051}{101250}\alpha^4, \\
&\quad A^{-} = \frac{1}{4} - \frac{13}{225}\alpha^2 + \frac{136931}{101250}\alpha^4.
\end{aligned} \tag{3.27}$$

The equations (3.26) have steady state solutions

$$\Pi_{ss}^{\pm} = \frac{A^{\mp}}{A^{+} + A^{-}}, \tag{3.28}$$

which yield explicitly

$$\begin{aligned}
&\mathbf{n=2}: \\
&\quad \Pi_{ss}^{\pm} = \frac{1}{2} \mp \frac{13\sqrt{13}}{105}\alpha^2 \pm \frac{4502\sqrt{13}}{33075}\alpha^4, \\
&\mathbf{n=3}: \\
&\quad \Pi_{ss}^{\pm} = \frac{1}{2} \mp \frac{3}{16}\alpha^2 \mp \frac{2241}{2560}\alpha^4, \\
&\mathbf{n=4}: \\
&\quad \Pi_{ss}^{\pm} = \frac{1}{2} \mp \frac{2}{15}\alpha^2 \mp \frac{688}{3375}\alpha^4.
\end{aligned} \tag{3.29}$$

In the case of resonant monochromatic excitation, the dressed states are equally populated (in the secular approximation). However the atom still exhibits

weak emissive and absorptive properties which arise from multiphoton processes [17],[18]. In the case of bichromatic driving however, the populations $\Pi_{ss}^{\pm}$ depend on α and are unequal even within the secular approximation. This results in first-order absorption and emission at all sideband frequencies, with central components which still vanish, because they correspond to $+ \Leftrightarrow +$ and $- \Leftrightarrow -$ transitions (which involve equal upper and lower state populations). The difference between the populations depends intricately upon the strength of the second laser and decreases with increasing n, indicating a decreasing efficiency of the second laser. The effective Rabi frequency of the second laser decreases with increasing n, as the laser drives the higher order resonances.

3.4.3 Coherences and spectral linewidths

All spectra of the system are related to the time evolution of the atomic dipole moment operator S^+ given by

$$S^+ = \sum_{\substack{l\epsilon,m\sigma \\ N,M}} S^+_{l\epsilon,m\sigma}\rho^{(+)}_{l\epsilon,m\sigma,N,M}, \tag{3.30}$$

where $S^+_{l\epsilon,m\sigma} = \langle (N+M)l\epsilon|S^+|(N+M-1)m\sigma\rangle$, and

$$\rho^{(+)}_{l\epsilon,m\sigma,N,M} = |(N+M)l\epsilon >< (N+M-1)m\sigma|. \tag{3.31}$$

The matrix elements of the off diagonal operators (3.31) represent coherences between the dressed states, and these oscillate at frequencies (3.18) and (3.19).

First, we consider transitions at the frequencies of the sidebands (3.19). For values of Ω_1 and Ω_2 corresponding to the range (3.6), it is easily verified that

the spectral lines are all nonoverlapping. The equations of motion of the corresponding density matrix elements are therefore uncoupled and from the master equation (3.1) we find that they are given by

$$\dot{\rho}_{l\pm,m\mp,N,M} = -(i\omega_{l-m}^{\pm\mp} + \Gamma_s)\rho_{l\pm,m\mp,N,M}, \tag{3.32}$$

where the linewidths Γ_s are

$$\begin{aligned}
&\mathbf{n = 2}: \\
&\qquad \Gamma_s = \frac{69}{104} + \frac{61}{24336}\alpha^2 + \frac{99556813}{227784960}\alpha^4, \\
&\mathbf{n = 3}: \\
&\qquad \Gamma_s = \frac{3}{4} - \frac{333}{512}\alpha^2 + \frac{4979889}{819200}\alpha^4, \\
&\mathbf{n = 4}: \\
&\qquad \Gamma_s = \frac{3}{4} - \frac{2}{225}\alpha^2 - \frac{147491}{101250}\alpha^4.
\end{aligned} \tag{3.33}$$

Next we consider the transitions at the central component of each triplet. In this case the two matrix elements $\rho^{(+)}_{l+,m+,N,M}$ and $\rho^{(+)}_{l-,m-,N,M}$ oscillate at the same frequency (3.18), and therefore have coupled equations of motion. When we average over the driving field, the reduced coherences $\rho^{(+)}_{l\pm,m\pm} = \sum_{NM} \rho^{(+)}_{l\pm,m\pm,N,M}$ are found to obey the same coupled equations of motion as do the populations $\Pi^{\pm}$, with the addition in each of the freely oscillating term $-i\omega^{\pm\pm}_{l-m}\rho^{(+)}_{l\pm,m\pm}$, given by

$$\dot{\rho}_{l\pm,m\pm} = -(i\omega^{\pm\pm}_{l-m} + A^{\pm})\rho_{l\pm,m\pm} + A^{\mp}\rho_{l\mp,m\mp}. \tag{3.34}$$

The associated dipole moments $p^{(+)}_{l\pm,m\pm} = S^{+}_{l\pm,m\pm}\rho^{(+)}_{l\pm,m\pm}$ then obey the equations

$$\dot{p}^{(+)}_{l\pm,m\pm}(t) = -(i\omega^{\pm\pm}_{l-m} + A^{\pm})p^{(+)}_{l\pm,m\pm}(t) - A^{\mp}p^{(+)}_{l\mp,m\mp}(t), \tag{3.35}$$

whose solutions are readily found to be

$$p^{(+)}_{l\pm,m\pm}(t) = \frac{\pm u_1}{\sqrt{(A^{+})^2 + (A^{-})^2}}A^{\mp}e^{-i\omega^{\pm\pm}_{l-m}t} + u_2 e^{-(i\omega^{\pm\pm}_{l-m}+\Gamma_c)t}, \tag{3.36}$$

where the constants u_1 and u_2 can be found from initial conditions. We do not however require the values of u_1 and u_2 in order to calculate the spectra and therefore do not solve for them. The first term in (3.36) corresponds to the elastic components, while the second term corresponds to the inelastic central components at frequencies $\omega^{\pm\pm}_{l-m}$ with linewidth given by

$$\Gamma_c = A^{+} + A^{-}. \tag{3.37}$$

For all n we find $\Gamma_c = 2(1 - \Gamma_s)$. We see from (3.33) and (3.37) that the spectral linewidths depend on α such that the linewidths of the sideband components of the triplets decrease with increasing n, whereas the linewidths of the central components increase with increasing n.

3.4.4 Fluorescence spectrum

The fluorescence spectrum is given by the real part of the Fourier transform of the correlation function of the dipole-moment operator $\langle p^{(+)}(t)p^{(-)}(t')\rangle$, $t > t'$. From the quantum regression theorem [24], it is well known that for $t > t'$ the

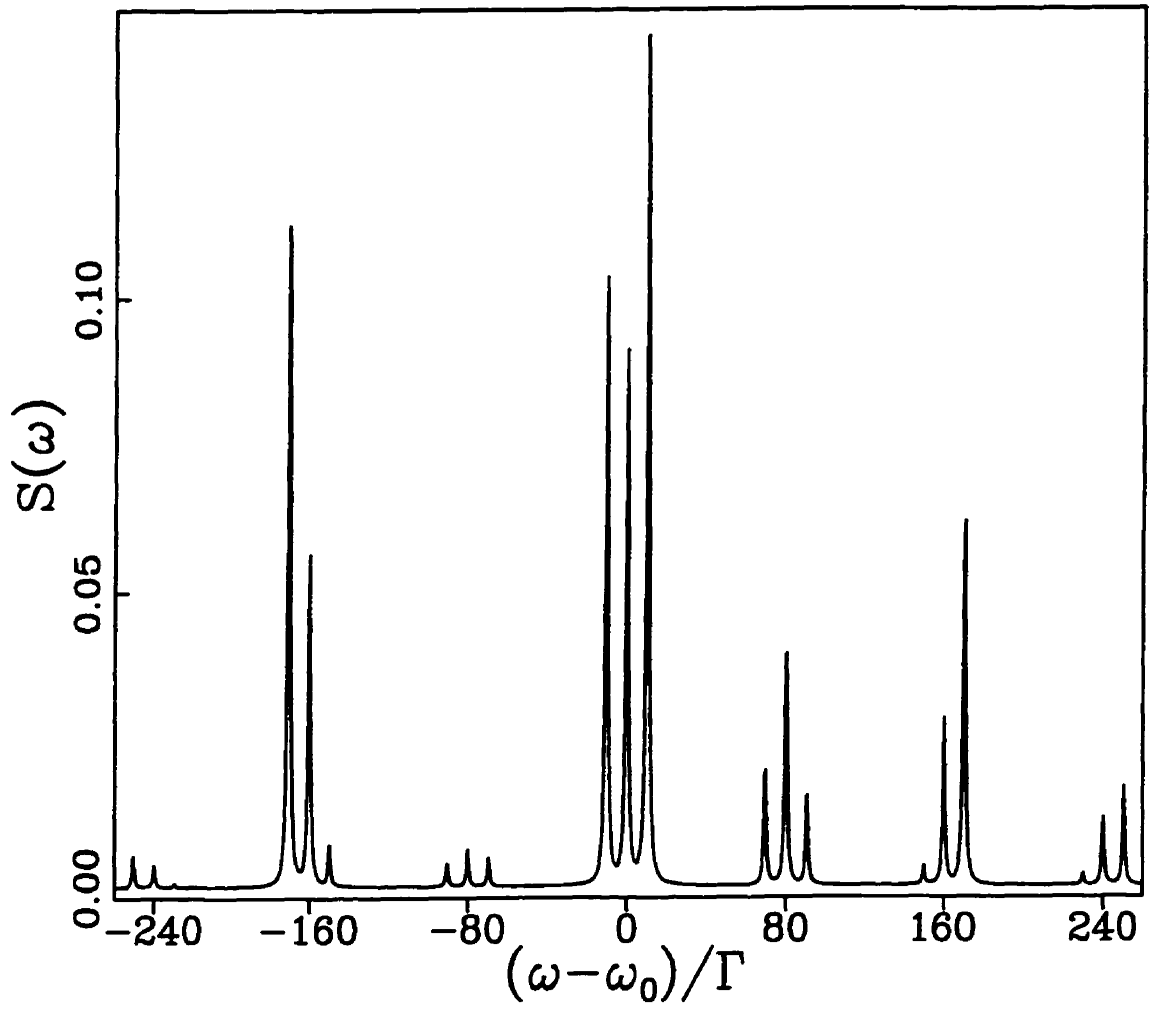

Figure 3.3(a) The fluorescence spectrum for $\omega_1 = \omega_0$, $\omega_2 = \omega_0 + 2\Omega_1/n$, with $2\Omega_1 = 160\Gamma$, $\alpha = 0.35$, and n=2.

two-time average $\langle p^{(+)}_{l\epsilon,m\sigma}(t)p^{(-)}(t')\rangle$ satisfies the same equation of motion as the one-time average $\langle p^{(+)}_{l\epsilon,m\sigma}(t)\rangle$, with the initial conditions

$$\langle p^{(+)}_{l\epsilon,m\sigma}(t')p^{(-)}(t')\rangle = \Gamma^{\epsilon\sigma}_{l-m}\Pi^{\epsilon}_{ss}, \tag{3.38}$$

where $\Gamma^{\epsilon\sigma}_{l-m}$ are the transition rates given by (3.21)-(3.24), and Π^{ϵ}_{ss} are the steady-state populations of the dressed states given by (3.29). The equations of motion for the one-time averages $\langle p^{(+)}_{l\epsilon,m\sigma}(t)\rangle$ were obtained in section 3.4.3. Thus, in the

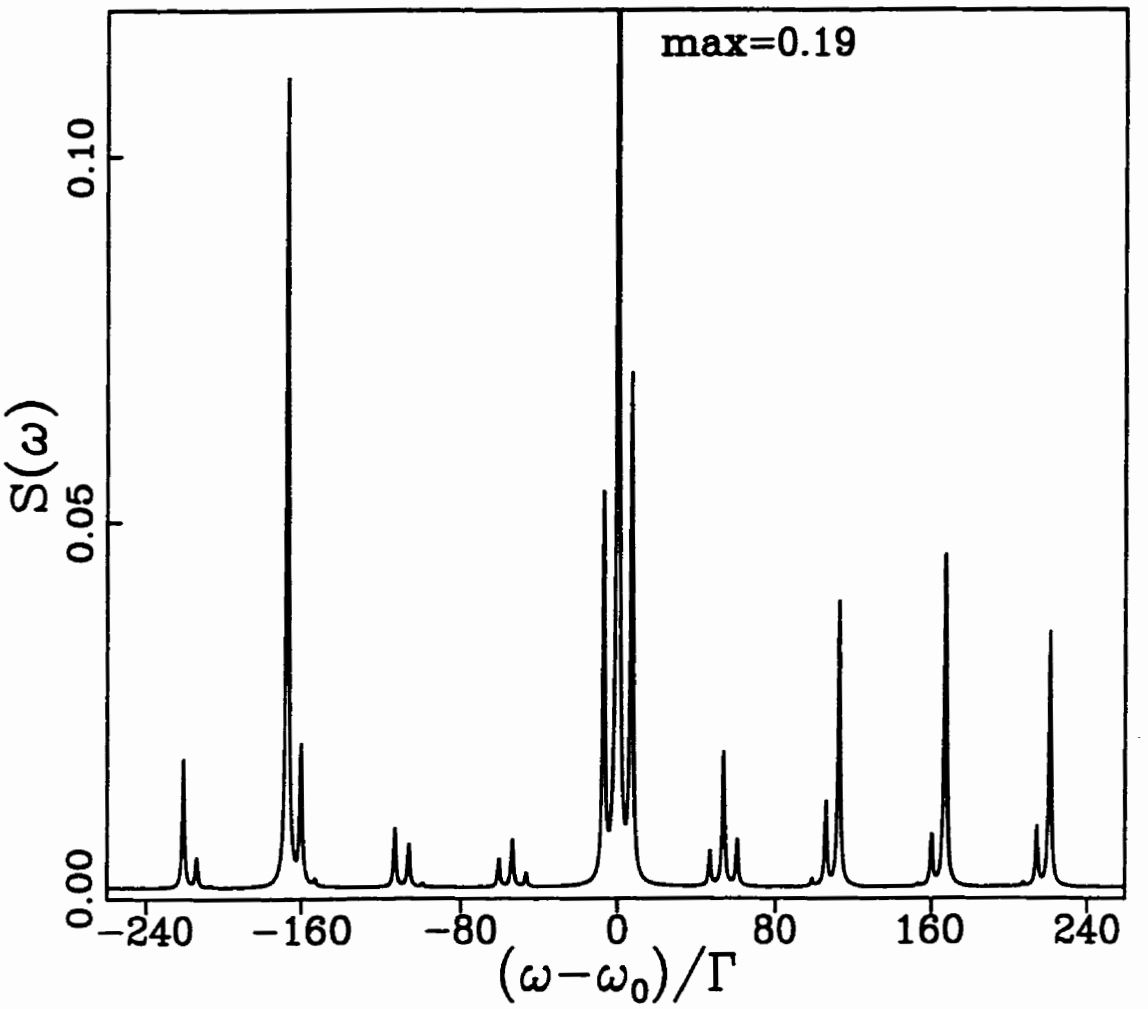

Figure 3.3(b) The fluorescence spectrum for $\omega_1 = \omega_0$, $\omega_2 = \omega_0 + 2\Omega_1/n$, with $2\Omega_1 = 160\Gamma$, $\alpha = 0.35$, and n=3.

limit of large Ω_2 ($\Omega_2 > \Gamma$), where the spectral lines do not overlap, the fluorescence spectrum (apart from geometrical and atomic factors) is given by

$$S(\omega) = \sum_{j=-\infty}^{\infty} \left(\frac{\Gamma_j^{+-}\Pi_{ss}^{+}\Gamma_s}{(\omega-\omega_j^{+-})^2+\Gamma_s^2} + \frac{\Gamma_j^{-+}\Pi_{ss}^{-}\Gamma_s}{(\omega-\omega_j^{-+})^2+\Gamma_s^2} + \frac{(\Gamma_j^{++}\Pi_{ss}^{+}+\Gamma_j^{--}\Pi_{ss}^{-})\Gamma_c}{(\omega-\omega_j^{++})^2+\Gamma_c^2} \right), \tag{3.39}$$

where the sum over j indicates a sum over the nonvanishing transitions as given by (3.21)-(3.23). In Figure 3.3 we plot this analytical expression for the fluorescence

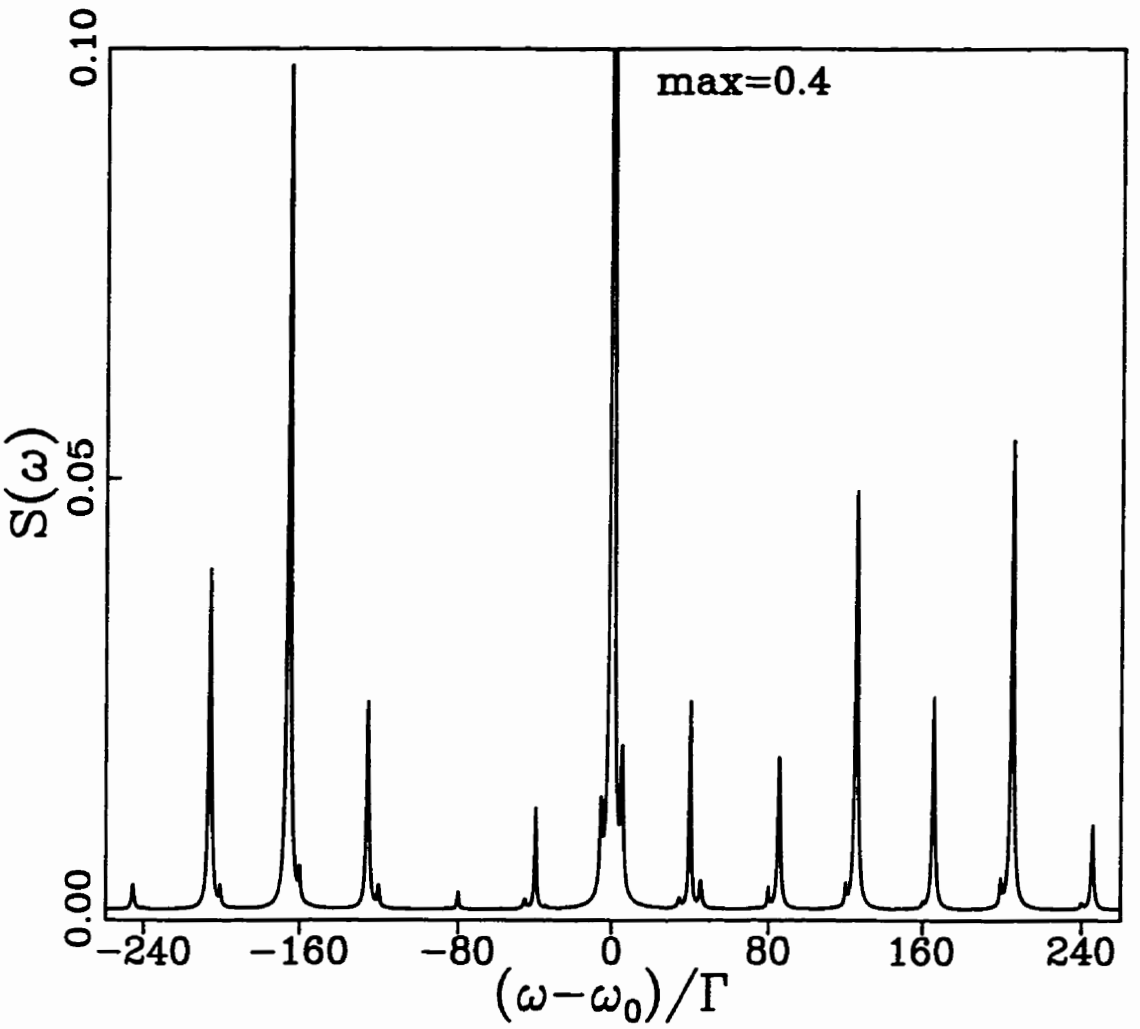

Figure 3.3(c) The fluorescence spectrum for $\omega_1 = \omega_0$, $\omega_2 = \omega_0 + 2\Omega_1/n$, with $2\Omega_1 = 160\Gamma$, $\alpha = 0.35$, and n=4.

spectrum for $n = 2, 3$ and 4.† It is seen that for all n the spectrum consists of a series of triplets with intertriplet spacing $2\Omega_1/n$ and intratriplet spacing $2\Delta E_n$. With increasing n, the number of triplets increases while the splitting of each triplet decreases. The structure of the spectrum reveals the presence of both

† We note here that the master equation (3.1) has also been solved numerically, and we have found that in order to get excellent agreement between the numerical and the present analytical results, we have to extend the dressed atom calculations to order α^6. Therefore, all the spectra plotted here include the populations and transition rates correct to α^6.

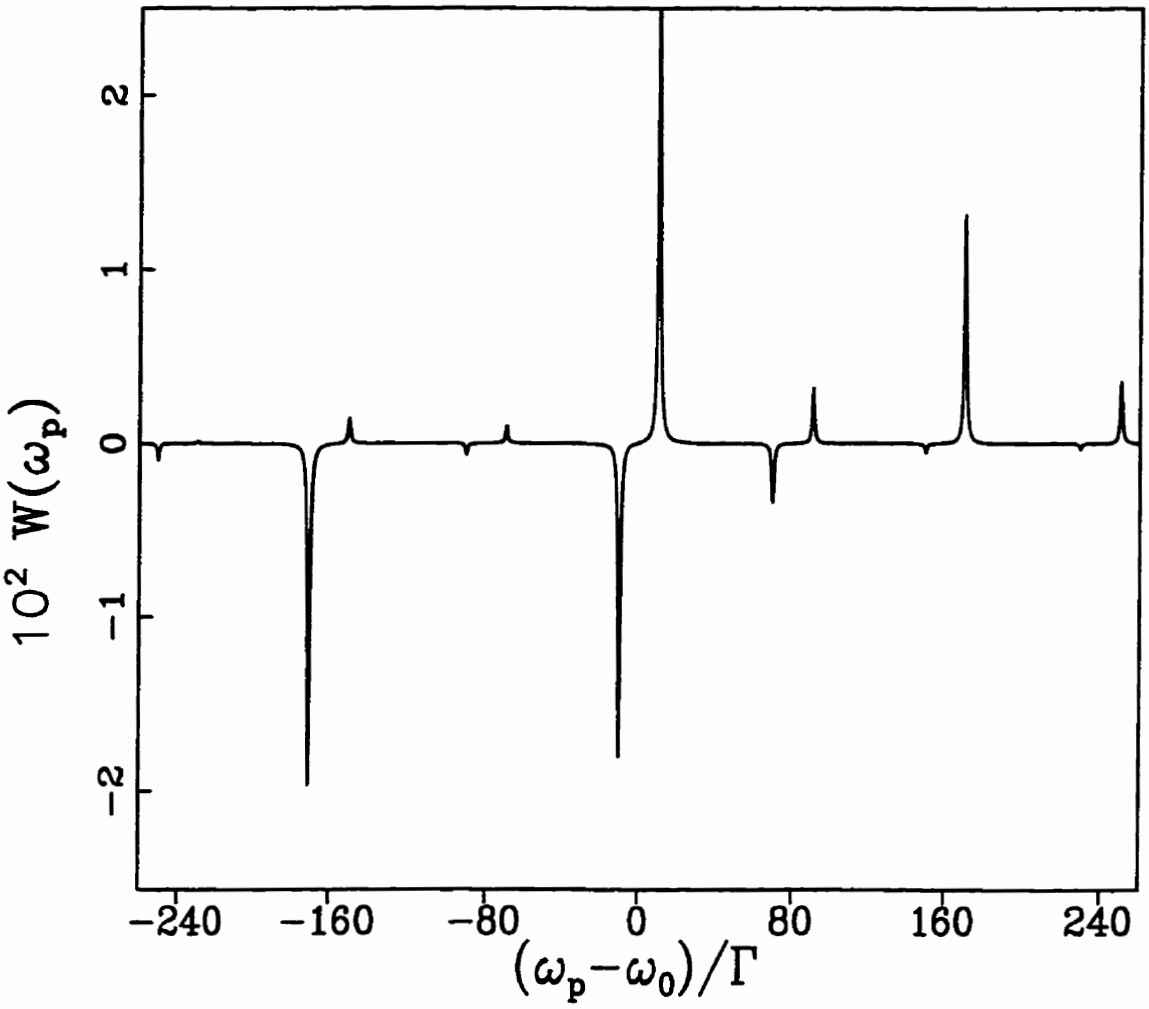

Figure 3.4(a) The near resonance weak probe absorption spectrum for $\omega_1 = \omega_0$, $\omega_2 = \omega_0 + 2\Omega_1/n$, with $2\Omega_1 = 160\Gamma$, $\alpha = 0.35$, and n=2.

the multiphoton transitions (in the appearance of the subharmonic and harmonic features) and the multiphoton AC Stark effect (in the intratriplet splitting).

3.4.5 Weak probe nearly resonant with ω_0: absorption and dispersion

It is interesting to consider as well the absorption and dispersion of a weak beam probing the doubly-dressed atom. Since the dressed states are unequally

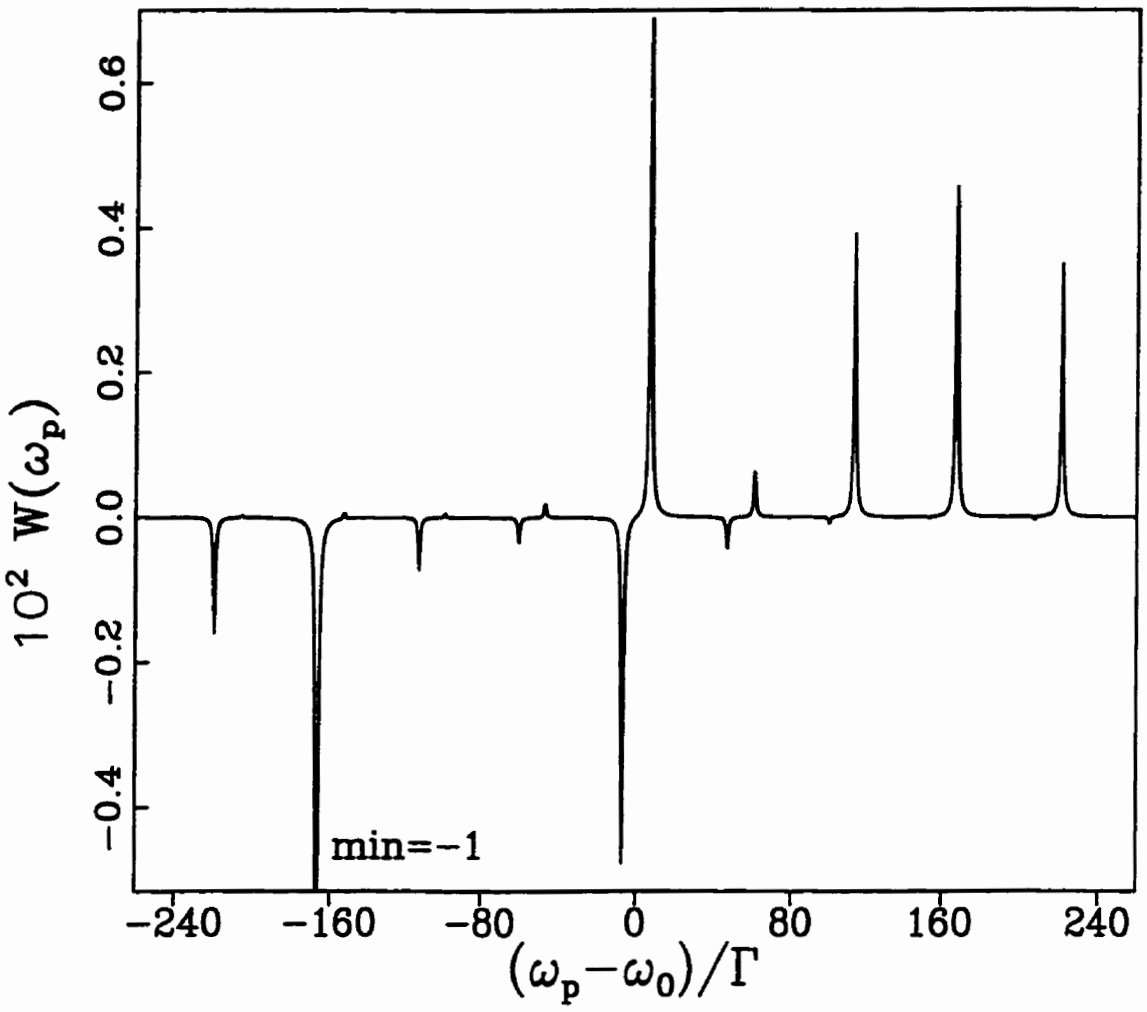

Figure 3.4(b) The near resonance weak probe absorption spectrum for $\omega_1 = \omega_0$, $\omega_2 = \omega_0 + 2\Omega_1/n$, with $2\Omega_1 = 160\Gamma$, $\alpha = 0.35$, and n=3.

populated, the absorption spectrum can give information about population inversions between the dressed states. The absorption and dispersion profiles of a weak probe beam of frequency ω_p are given by the real and imaginary parts, respectively, of the Fourier transform of the commutator $\langle [S^-(t), S^+(t')] \rangle$. The term $\langle S^-(t)S^+(t') \rangle$ of the commutator is associated with absorption and the term $\langle S^+(t')S^-(t) \rangle$ with stimulated emission of the probe beam. From the quantum

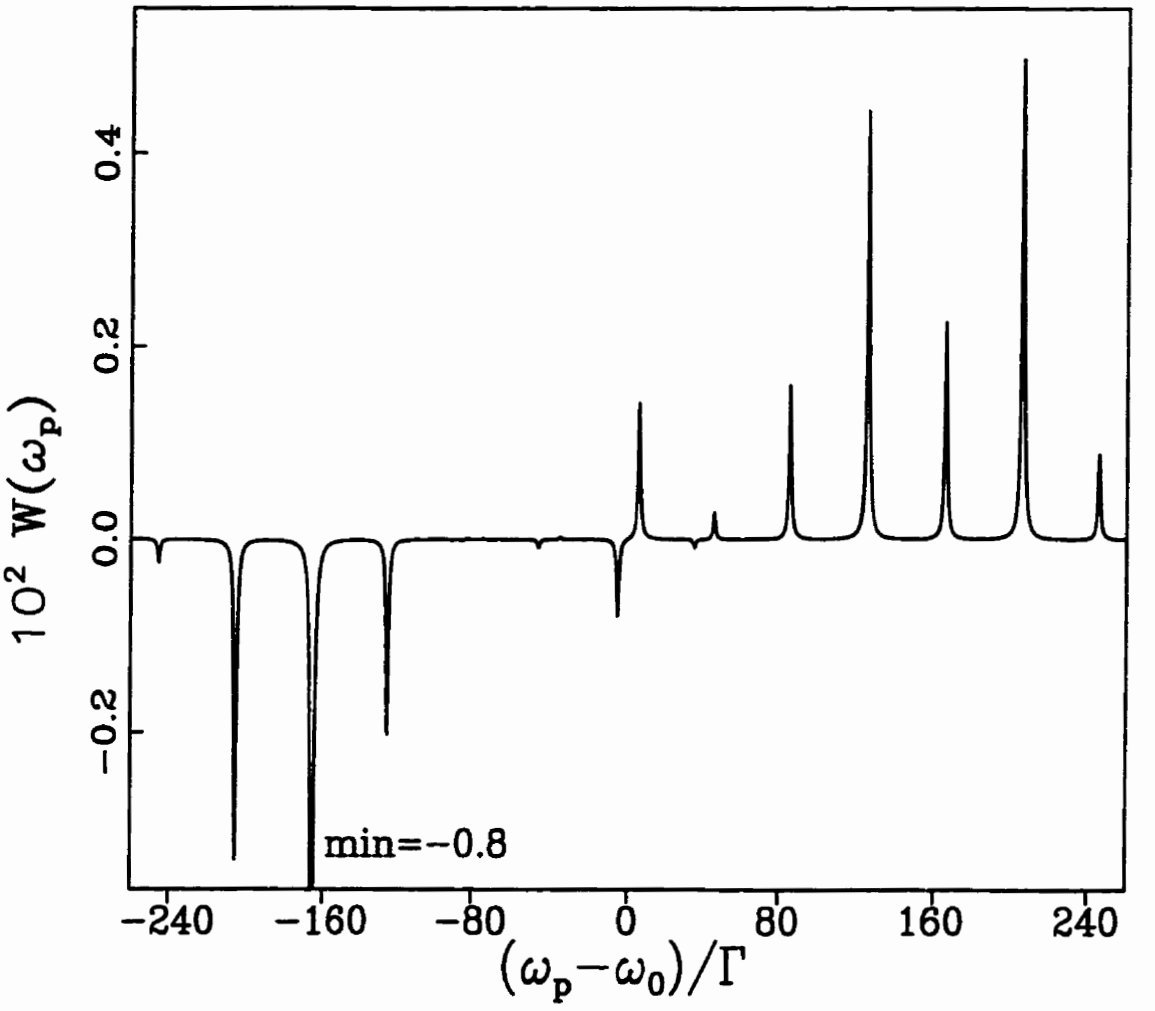

Figure 3.4(c) The near resonance weak probe absorption spectrum for $\omega_1 = \omega_0$, $\omega_2 = \omega_0 + 2\Omega_1/n$, with $2\Omega_1 = 160\Gamma$, $\alpha = 0.35$, and n=4.

regression theorem [24], it is well known that for $t > t'$ the two-time commutator $\langle[S^-_{l\epsilon,m\sigma}(t), S^+(t')]\rangle$ satisfies the same equation of motion as does the density matrix element $\left[\rho^{(+)}_{l\epsilon,m\sigma}(t)\right]^*$, with the initial condition

$$\langle[S^-_{l\epsilon,m\sigma}(t'), S^+(t')]\rangle = \Gamma^{\epsilon\sigma}_{l-m}\left(\Pi^{\epsilon}_{ss} - \Pi^{\sigma}_{ss}\right). \tag{3.40}$$

Thus, it is straightforward to show that in the case of nonoverlapping spectral components the absorption spectrum of a probe beam nearly resonant with the

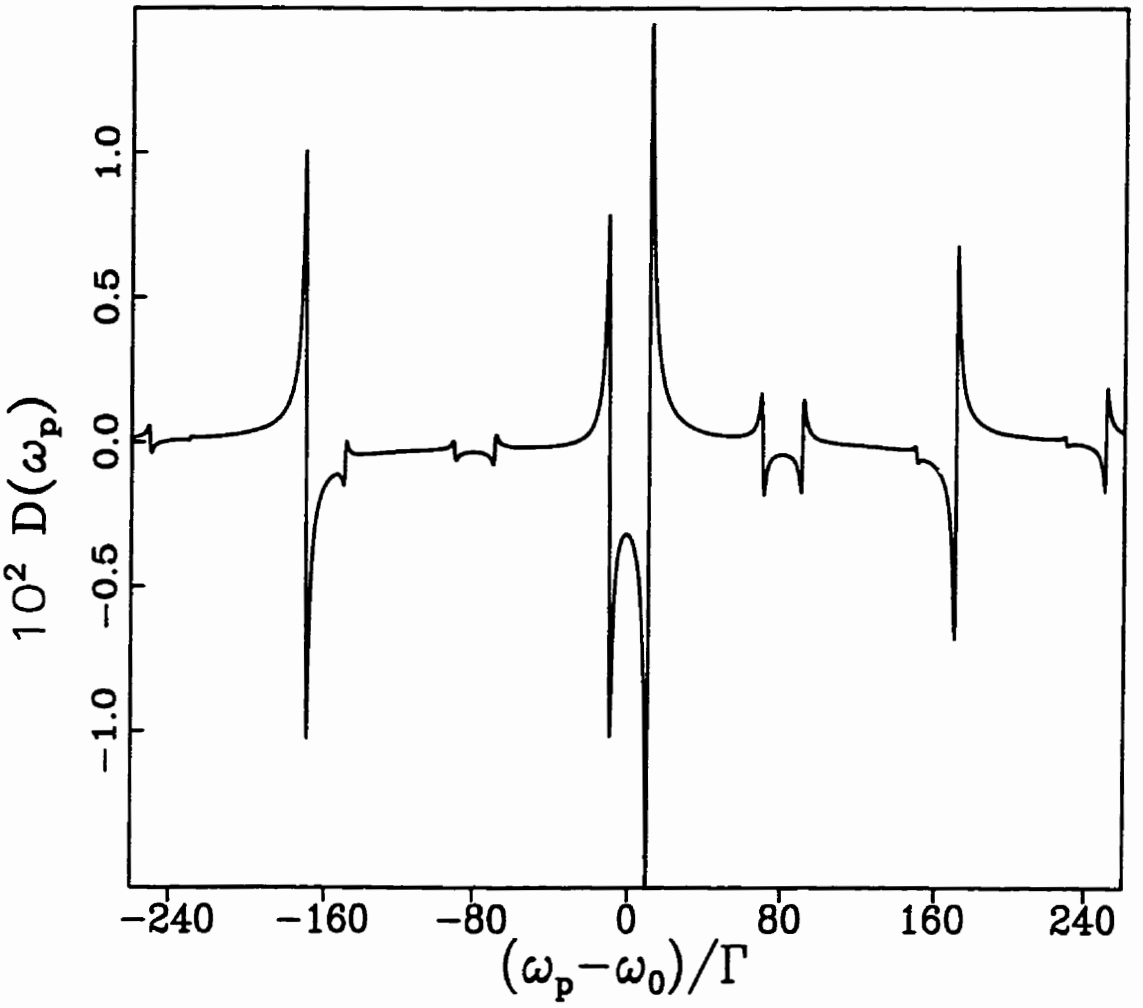

Figure 3.5(a) The near resonance weak probe dispersion profile for $\omega_1 = \omega_0$, $\omega_2 = \omega_0 + 2\Omega_1/n$, with $2\Omega_1 = 160\Gamma$, $\alpha = 0.35$, and n=2.

atomic transition frequency is given by

$$W(\omega_p) = \sum_{j=-\infty}^{\infty} \left(\frac{\Gamma_j^{+-}(\Pi_{ss}^{-} - \Pi_{ss}^{+})\Gamma_s}{(\omega_p - \omega_j^{+-})^2 + \Gamma_s^2} + \frac{\Gamma_j^{-+}(\Pi_{ss}^{+} - \Pi_{ss}^{-})\Gamma_s}{(\omega_p - \omega_j^{-+})^2 + \Gamma_s^2} \right), \tag{3.41}$$

and the dispersion profile by

$$D(\omega_p) = \sum_{j=-\infty}^{\infty} \left(\frac{\Gamma_j^{+-}(\Pi_{ss}^{-} - \Pi_{ss}^{+})(\omega_p - \omega_j^{+-})}{(\omega_p - \omega_j^{+-})^2 + \Gamma_s^2} + \frac{\Gamma_j^{-+}(\Pi_{ss}^{+} - \Pi_{ss}^{-})(\omega_p - \omega_j^{-+})}{(\omega_p - \omega_j^{-+})^2 + \Gamma_s^2} \right). \tag{3.42}$$

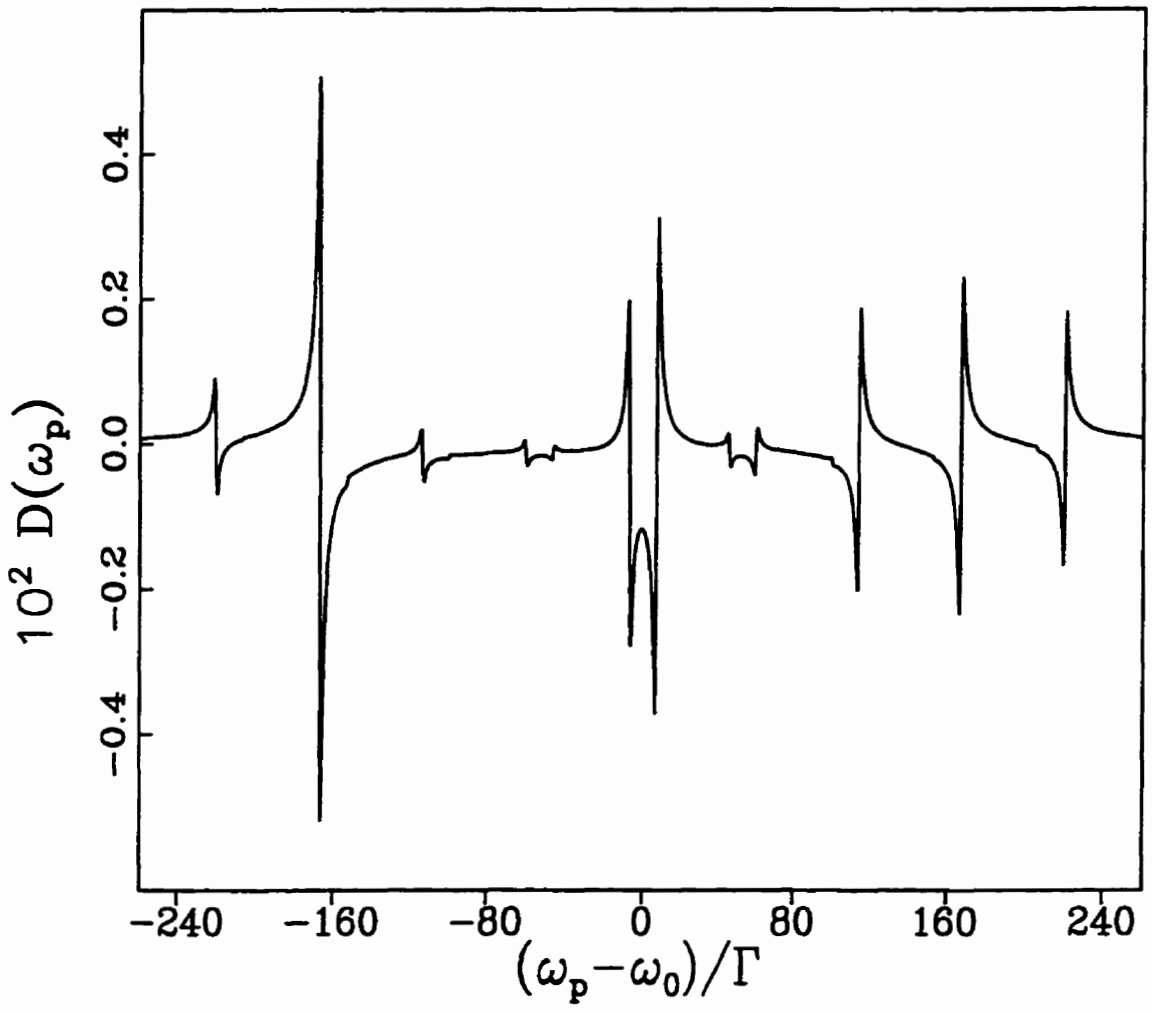

Figure 3.5(b) The near resonance weak probe dispersion profile for $\omega_1 = \omega_0$, $\omega_2 = \omega_0 + 2\Omega_1/n$, with $2\Omega_1 = 160\Gamma$, $\alpha = 0.35$, and n=3.

The expressions (3.41) and (3.42) are plotted respectively in Figures 3.4 and 3.5 (absorption is upwards in the diagram). They contain features at the same frequencies and with the same linewidths as their counterparts in $S(\omega)$, but with widely differing intensities depending on α. As the calculations have been made within the secular approximation, there are no (small) central features in the components of the absorption spectra. Therefore the absorption spectrum and the dispersion profile are composed of doublets centred at the frequencies $\omega_j^{\pm\mp}$.

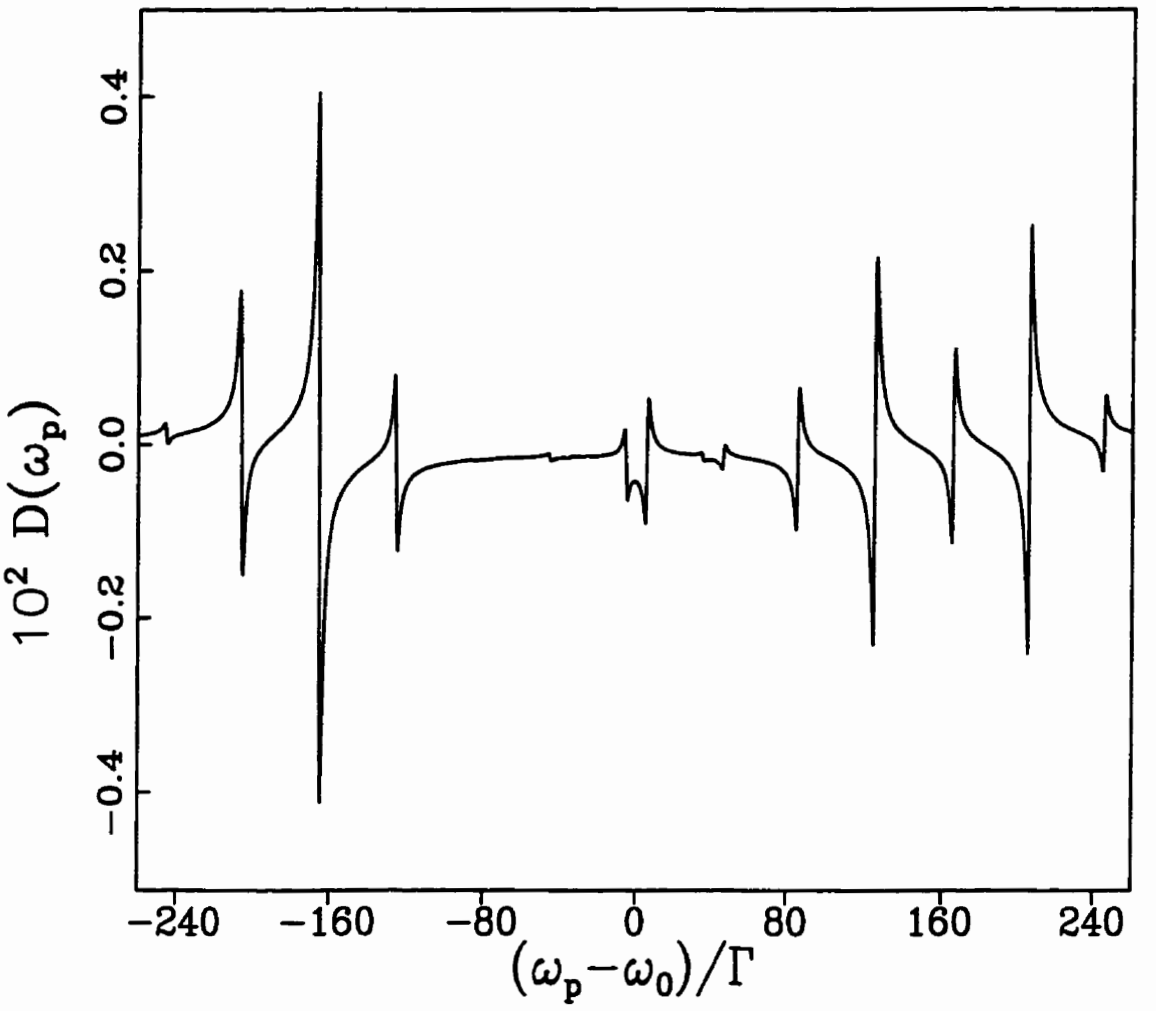

Figure 3.5(c) The near resonance weak probe dispersion profile for $\omega_1 = \omega_0$, $\omega_2 = \omega_0 + 2\Omega_1/n$, with $2\Omega_1 = 160\Gamma$, $\alpha = 0.35$, and n=4.

In each doublet of the absorption spectrum one sideband is absorbing and the other amplifying depending on the difference in steady-state populations of the lower and upper levels of the transition.

It is interesting to note from Figure 3.4, that with increasing n the maximum of amplification and absorption shifts from the central doublet to the Rabi sidebands. The same occurs with the dispersion, as seen in Figure 5. Moreover, as n increases the red features become exclusively emissive whereas the blue features become

only absorptive. The amplification at frequencies smaller than ω_0 is relatively large compared to the absorption at frequencies greater than ω_0, in contrast with the monochromatic case, where the amplification at one of the sidebands is always small compared to the absorption at the other sideband [3].

The dispersion, shown in Figure 5, also exhibits interesting modifications. For example, in the region between the central doublet there is a strong negative dispersion with minimal absorption. For $n = 2$, this effect is also seen in all harmonic and subharmonic doublets. With increasing n the negative dispersion decreases in the harmonic and subharmonic doublets whereas the central structure is remarkably stable against variation in n.

It should be emphasised here that this system may prove useful in the production of optical materials having a large index of refraction accompanied by vanishing absorption [25]. An advantage of this system is that near the central frequency, where the absorption vanishes, both the absorption and dispersion change slowly with frequency. Therefore, our system is a convenient candidate for this experimental application, since it does not require a precise matching of the probe beam frequency to the point of vanishing absorption.

3.4.6 Autler-Townes absorption and dispersion profiles

The structure and properties of the doubly-dressed atom can also be studied by monitoring the system with a weak probe beam coupled to a third (bare) atomic state. We assume that a third atomic level $|c\rangle$ is connected to $|g\rangle$ with a non-zero dipole moment, and with a transition frequency ω_c (from $|g\rangle$) much different from

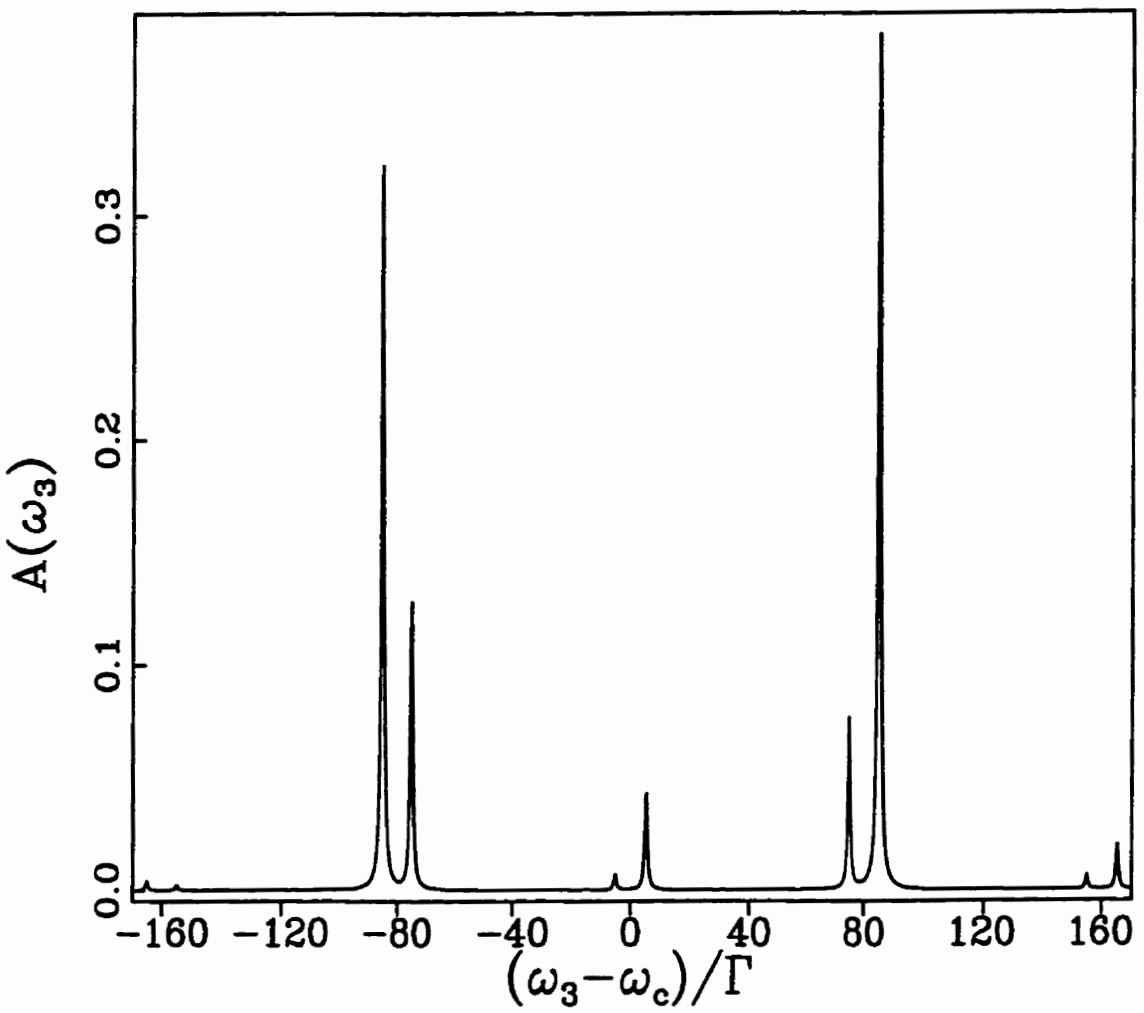

Figure 3.6(a) The Autler-Townes absorption spectrum for $\omega_1 = \omega_0$, $\omega_2 = \omega_0 + 2\Omega_1/n$, with $2\Omega_1 = 160\Gamma$, $\alpha = 0.35$, $\Gamma_3 = \Gamma/3$ and n=2.

ω_0. The transition is monitored by a weak probe beam of frequency ω_3 tuned close to ω_c. The intensity of the features corresponding to absorption from the dressed state $|(N+M)m\pm\rangle$ is proportional to the product of the steady state population $\Pi_{ss}^{\pm}$ and the transition rate from $|(N+M)m\pm\rangle$ to $|c,N,M\rangle$, which itself is proportional to [19]

$$\Lambda_m^{\pm} = \Gamma_3 |\langle (N+M)m \pm |g,N,M\rangle|^2, \tag{3.43}$$

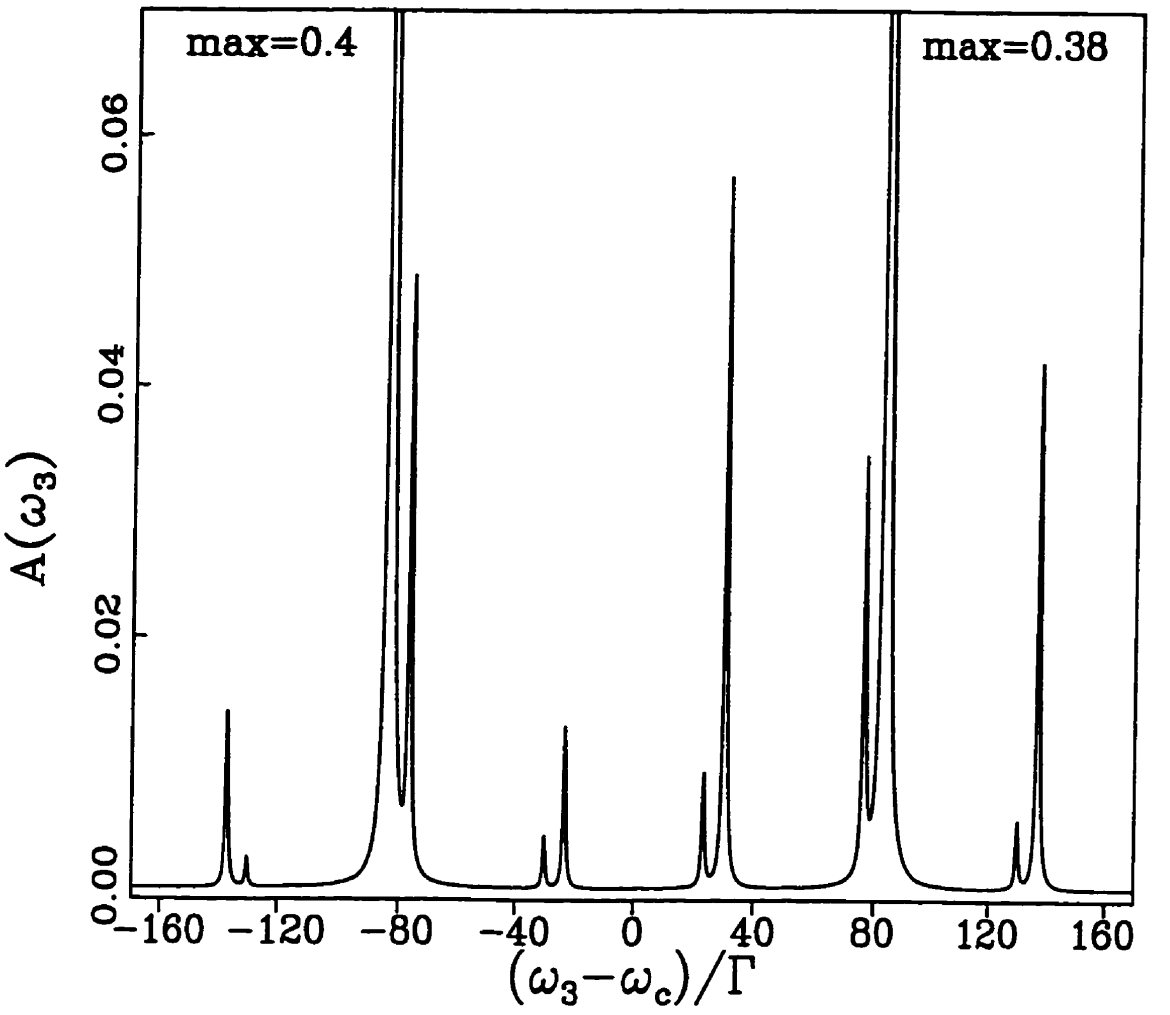

Figure 3.6(b) The Autler-Townes absorption spectrum for $\omega_1 = \omega_0$, $\omega_2 = \omega_0 + 2\Omega_1/n$, with $2\Omega_1 = 160\Gamma$, $\alpha = 0.35$, $\Gamma_3 = \Gamma/3$ and n=3.

where Γ_3 is the natural width of level $|c\rangle$. These quantities are readily evaluated using the dressed states (3.15)-(3.17). Intuitively the quantities (3.43) are a measurement of how much of the ground state $|g\rangle$ is "mixed" in each dressed state, and is therefore available to be probed up to the third level. The $\Lambda_m^{\pm}$, normalised

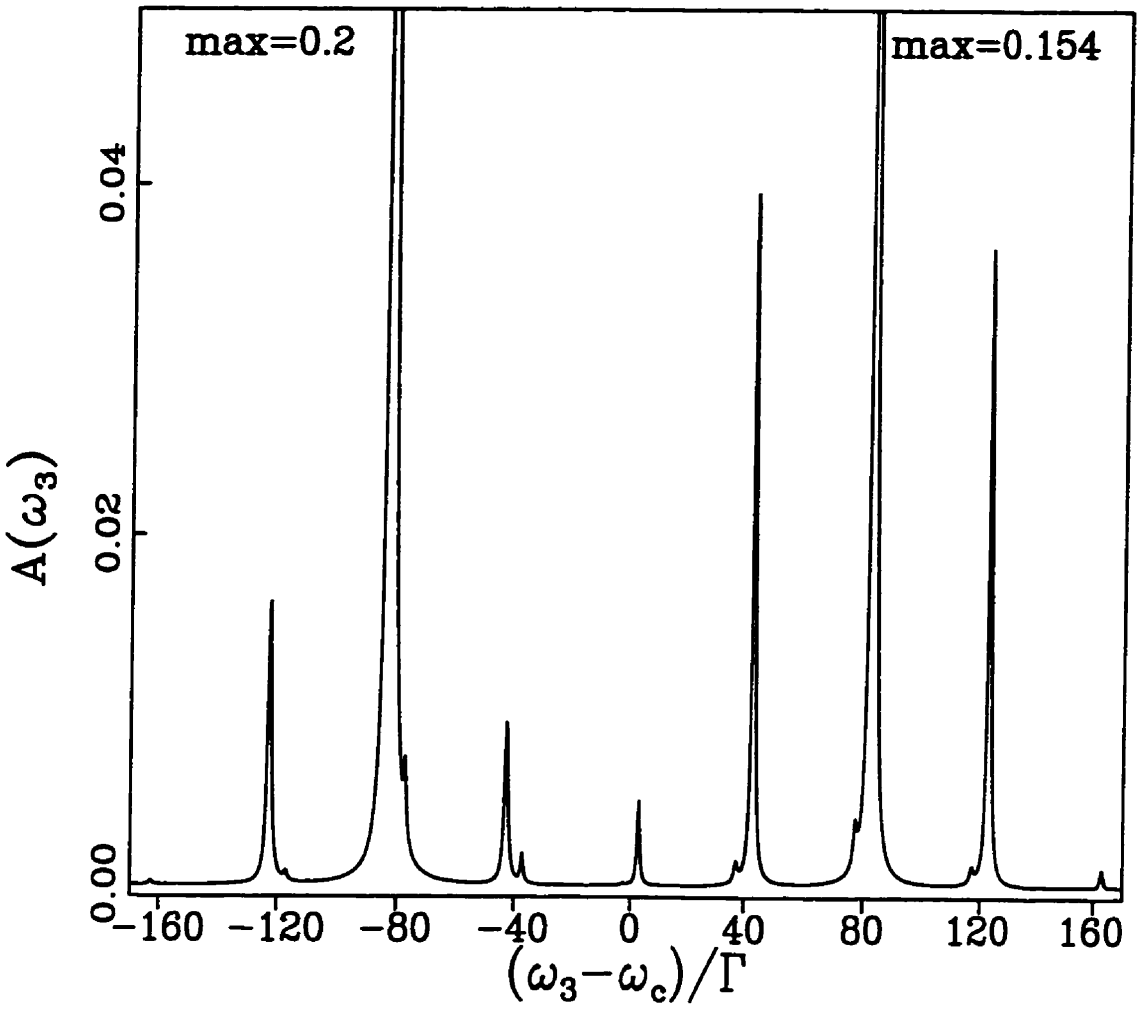

Figure 3.6(c) The Autler-Townes absorption spectrum for $\omega_1 = \omega_0$, $\omega_2 = \omega_0 + 2\Omega_1/n$, with $2\Omega_1 = 160\Gamma$, $\alpha = 0.35$, $\Gamma_3 = \Gamma/3$ and n=4.

to Γ_3, are found to be given by

$$\mathbf{n = 2}:$$

$$\Lambda_{-1}^{\pm} = (\tfrac{1}{9} \mp \tfrac{2\sqrt{13}}{117})\alpha^2 \qquad \Lambda_0^{\pm} = (\tfrac{1}{4} \mp \tfrac{\sqrt{13}}{26}) - (\tfrac{5}{18} \mp \tfrac{433\sqrt{13}}{48672})\alpha^2$$

$$\Lambda_2^{\pm} = (\tfrac{1}{4} \pm \tfrac{\sqrt{13}}{26}) - (\tfrac{1}{9} \pm \tfrac{1993\sqrt{13}}{48672})\alpha^2 \qquad \Lambda_1^{\pm} = (\tfrac{1}{4} \mp \tfrac{\sqrt{13}}{26})\alpha^2 \tag{3.44}$$

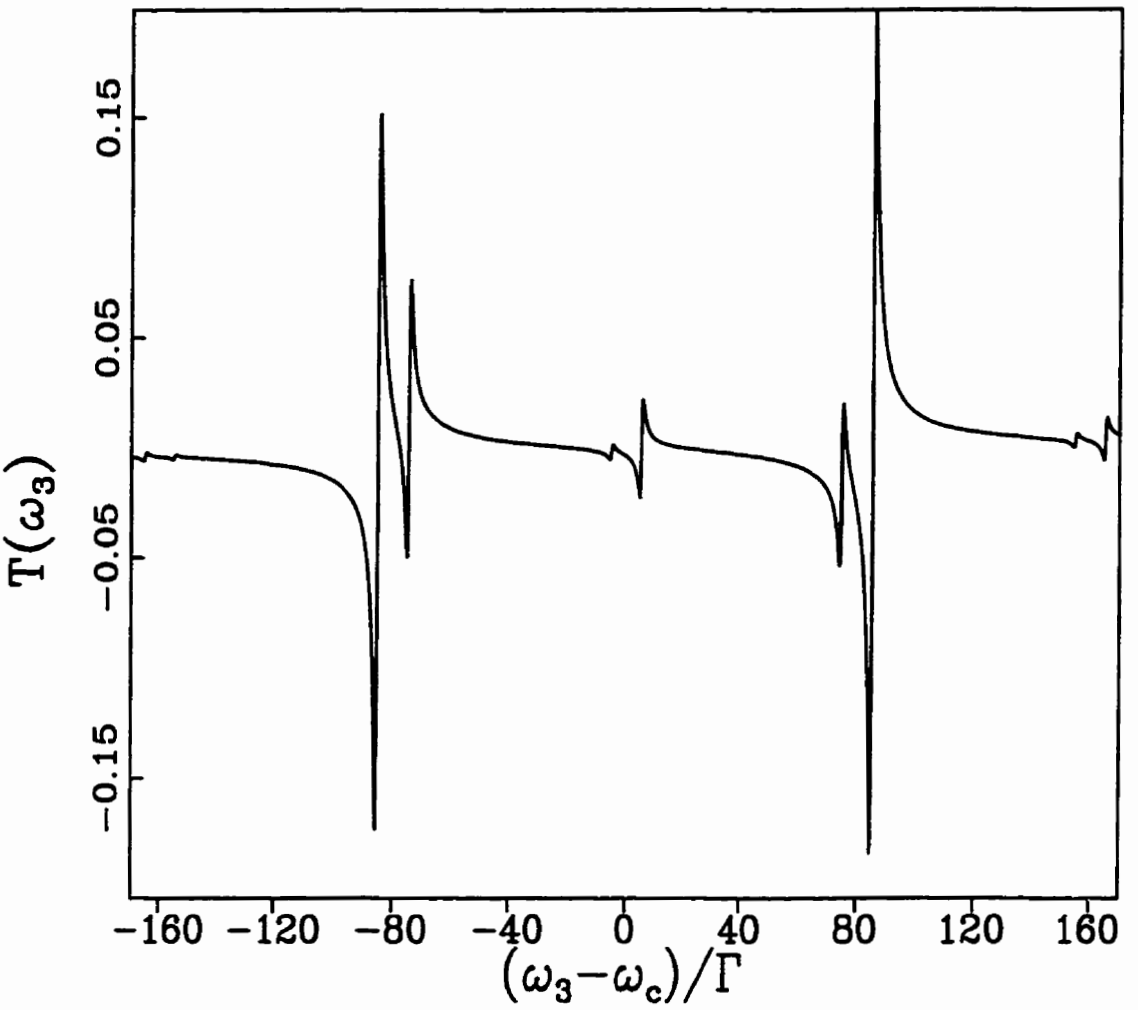

Figure 3.7(a) The Autler-Townes dispersion profile for $\omega_1 = \omega_0$, $\omega_2 = \omega_0 + 2\Omega_1/n$, with $2\Omega_1 = 160\Gamma$, $\alpha = 0.35$, $\Gamma_3 = \Gamma/3$ and n=2.

$\mathbf{n = 3}$:

$$
\begin{aligned}
\Lambda_0^+ &= \tfrac{81}{128}\alpha^2 - \tfrac{1215081}{163840}\alpha^4 & \Lambda_0^- &= \tfrac{1}{2} - \tfrac{825}{512}\alpha^2 + \tfrac{27429651}{3276800}\alpha^4 \\
\Lambda_1^+ &= \tfrac{729}{512}\alpha^4 & \Lambda_1^- &= \tfrac{81}{128}\alpha^2 - \tfrac{81405}{32768}\alpha^4 \\
\Lambda_{-1}^+ &= \tfrac{18225}{32768}\alpha^4 & \Lambda_{-1}^- &= \tfrac{225}{512}\alpha^2 - \tfrac{130923}{131072}\alpha^4 \\
\Lambda_2^+ &= \tfrac{9}{128}\alpha^2 - \tfrac{25893}{32768}\alpha^4 & \Lambda_2^- &= \tfrac{729}{512}\alpha^4 \\
\Lambda_3^+ &= \tfrac{1}{2} - \tfrac{489}{512}\alpha^2 + \tfrac{19169811}{3276800}\alpha^4 & \Lambda_{-2}^- &= \tfrac{35721}{819200}\alpha^4 \\
\Lambda_4^+ &= \tfrac{81}{512}\alpha^2 - \tfrac{41067}{131072}\alpha^4 & \Lambda_3^- &= \tfrac{81}{128}\alpha^2 - \tfrac{962361}{163840}\alpha^4 \\
\Lambda_5^+ &= \tfrac{6561}{819200}\alpha^4 & \Lambda_4^- &= \tfrac{6561}{32768}\alpha^4
\end{aligned}
\tag{3.45}
$$

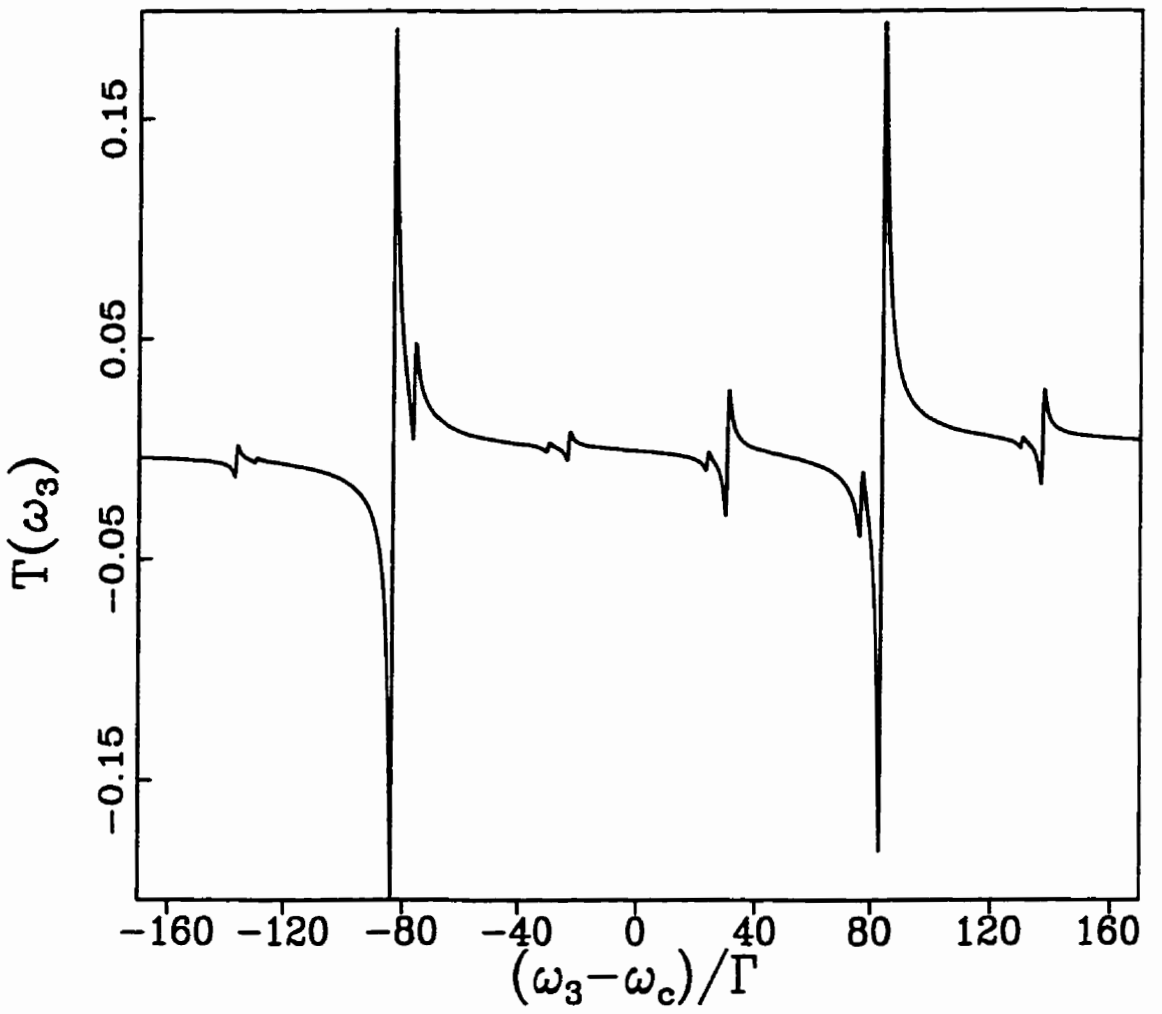

Figure 3.7(b) The Autler-Townes dispersion profile for $\omega_1 = \omega_0$, $\omega_2 = \omega_0 + 2\Omega_1/n$, with $2\Omega_1 = 160\Gamma$, $\alpha = 0.35$, $\Gamma_3 = \Gamma/3$ and n=3.

$\mathbf{n = 4}$:

$$\begin{aligned}
\Lambda_0^+ &= \tfrac{25}{18}\alpha^4 & \Lambda_0^- &= \tfrac{1}{2} - \tfrac{347}{225}\alpha^2 + \tfrac{27821}{33750}\alpha^4 \\
\Lambda_3^+ &= \tfrac{2}{9}\alpha^2 - \tfrac{196}{675}\alpha^4 & \Lambda_1^- &= \tfrac{8}{9}\alpha^2 - \tfrac{1424}{675}\alpha^4 \\
\Lambda_4^+ &= \tfrac{1}{2} - \tfrac{137}{225}\alpha^2 - \tfrac{32099}{33750}\alpha^4 & \Lambda_{-1}^- &= \tfrac{18}{25}\alpha^2 - \tfrac{644}{625}\alpha^4 \\
\Lambda_5^+ &= \tfrac{8}{25}\alpha^2 - \tfrac{1616}{5625}\alpha^4 & \Lambda_2^- &= \tfrac{8}{9}\alpha^4 \\
\Lambda_6^+ &= \tfrac{8}{225}\alpha^4 & \Lambda_{-2}^- &= \tfrac{32}{225}\alpha^4 \\
& & \Lambda_4^- &= \tfrac{25}{18}\alpha^4.
\end{aligned} \tag{3.46}$$

These are correct to order α^2 for $n = 2$, and order α^4 for $n = 3, 4$.

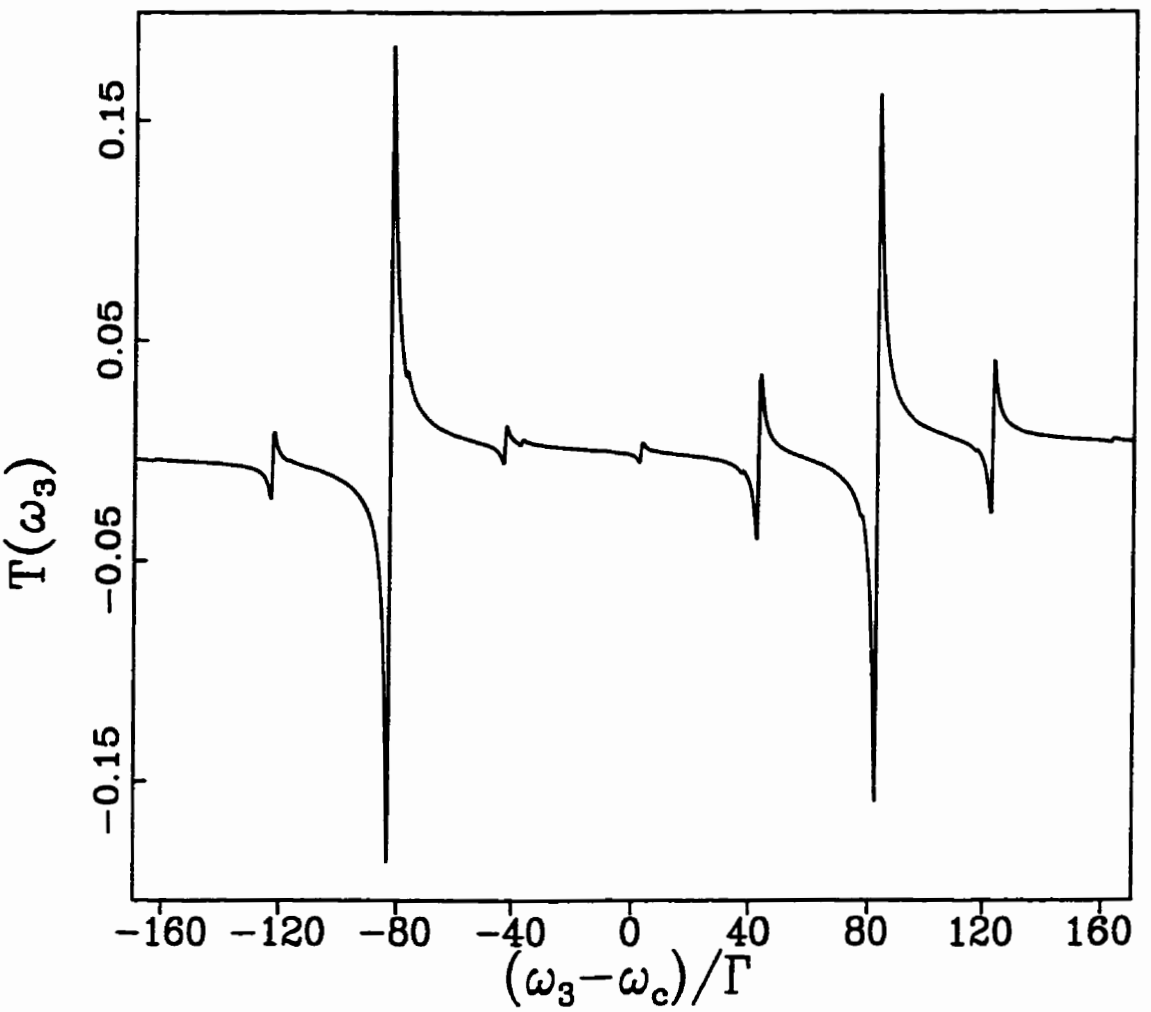

Figure 3.7(c) The Autler-Townes dispersion profile for $\omega_1 = \omega_0$, $\omega_2 = \omega_0 + 2\Omega_1/n$, with $2\Omega_1 = 160\Gamma$, $\alpha = 0.35$, $\Gamma_3 = \Gamma/3$ and n=4.

The frequencies at which the absorption occurs from $|(N+M)m\pm\rangle$ to $|c, N, M\rangle$ are given by

$$\omega_j^{\pm} = \omega_c - \Big(\frac{2j}{n} - 1\Big)\Omega_1 \mp \Delta E_n, \tag{3.47}$$

while the linewidths are given by

$$\Gamma_a = \frac{\Gamma_s + \Gamma_3/\Gamma}{2}, \tag{3.48}$$

Accordingly, the Autler-Townes absorption spectrum can be written as

$$A(\omega_3) = \sum_j \left(\frac{\Lambda_j^+ \Pi_{ss}^+ \Gamma_a}{(\omega_3 - \omega_j^+)^2 + \Gamma_a^2} + \frac{\Lambda_j^- \Pi_{ss}^- \Gamma_a}{(\omega_3 - \omega_j^-)^2 + \Gamma_a^2} \right), \tag{3.49}$$

and the corresponding dispersion profile is

$$T(\omega_3) = \sum_j \left(\frac{\Lambda_j^+ \Pi_{ss}^+ (\omega_3 - \omega_j^+)}{(\omega_3 - \omega_j^+)^2 + \Gamma_a^2} + \frac{\Lambda_j^- \Pi_{ss}^- (\omega_3 - \omega_j^-)}{(\omega_3 - \omega_j^-)^2 + \Gamma_a^2} \right). \tag{3.50}$$

In Figures 3.6 and 3.7 we plot the Autler-Townes absorption and dispersion spectra, respectively, for the same parameters as in Figure 3. Each consists of a series of doublets, located at frequencies $2m\Omega_1/n$, where $m = 0, \pm 1, \pm 2, ...$ for n even and $m = \pm\frac{1}{2}, \pm\frac{3}{2}, \pm\frac{5}{2}, ...$ for n odd. The intradoublet separation is $2\Delta E_n$. The most intense doublets are those centred at the frequencies $\omega_c \pm \Omega_1$, which correspond to the Autler-Townes frequencies of a monochromatically driven atom. The width of all lines is Γ_a, and once again an intricate dependence of the peak intensities on α is evident. Care must be taken when comparing the transition rates (3.44)-(3.46) with the doublets in Figure 3.6. The transition rates $\Lambda_0^\pm$ correspond to the sideband doublet at $\omega_3 = \omega_c + \Omega_1$, not to the central one, whereas $\Lambda_i^\pm$ corresponds to the ith doublet to the left (right) of this intense doublet if i is positive (negative).

3.5 Reversing the roles of the driving fields - the $\alpha > 1$ case

In sections 3.1 to 3.4 we considered the multiphoton processes that arise when an atom driven by a strong, on resonance field is simultaneously driven by a

second field detuned to a subharmonic resonance of the first. In this situation, it is particularly easy to see, from the dressed atom picture, why scanning the second field through detunings from $2\Omega_1$ to zero picks up multiphoton effects at the subharmonic resonances, *i.e.* at integer fractions of $2\Omega_1$. However we considered only the regime where $\alpha \equiv \Omega_2/\Omega_1$ was small. Experimentally, another interesting phenomenon was noticed [26]. When the detuning of the second field was held fixed but the strength was increased, for certain values of α which were greater than one, more multiphoton resonances were observed. For instance, if the second field started at a detuning corresponding to a two-photon resonance, then for special values of α a three-photon resonance was observed. This section will explain this phenomenon as an effect similar to that described above, although we will look at it in considerably less detail than the "normal" multiphoton effect considered previously.

Since the effect occurs when the second (off resonance) laser field is stronger than the first (on resonance) field we will dress first around the second detuned field. Remembering that there are M photons in this mode, and assuming an arbitrary detuning Δ_2 for the present (rather than the $2\Omega_1/n$ considered previously), we obtain the well known singly dressed states

$$\begin{aligned} |M+\rangle &= \sin\theta|g,M\rangle + \cos\theta|e,M-1\rangle \\ |M-\rangle &= \cos\theta|g,M\rangle - \sin\theta|e,M-1\rangle, \end{aligned} \tag{3.51}$$

which are separated by a generalised Rabi frequency $2G = \sqrt{4\Omega_2^2 + \Delta_2^2}$ (see Chapter 2). Here

$$\sin^2\theta = \frac{1}{2} + \frac{\Delta_2}{4\Omega}. \tag{3.52}$$

These dressed state manifolds are a distance $\omega_2 = \omega_0 + \Delta_2$ apart. In analogy with Figure 3.1(a) therefore, we expect that when we add in the first, on resonance, field we will see a k photon coupling ($k = 2, 3, ...$) between the dressed states (3.51) whenever

$$2G = k\Delta_2, \tag{3.53}$$

or, in terms of the strong field's on resonance Rabi frequency, when

$$2\Omega_2 = \sqrt{k^2 - 1}\Delta_2. \tag{3.54}$$

Notice that (3.54) is a criterion which involves only parameters of the second (assumed strong) field. Now if Δ_2 was $2\Omega_1/n$, we can easily see from (3.54) that the values of α for which the k photon resonance will occur are given by

$$\alpha = \sqrt{k^2 - 1}/n. \tag{3.55}$$

Obviously we must have $k > n$, since we have implicitly assumed that α is greater than 1.

Another way of interpreting (3.54) is as a condition on the value of Δ_2. This is in fact what we will do in this section, since the calculations will then be similar to those of the previous sections. In particular we shall treat the first, on resonance, field as a perturber and redo the previous analysis in terms of the parameter $\beta \equiv 1/\alpha = \Omega_1/\Omega_2$. Thus we have $\Delta_2 = 2\Omega_2/\sqrt{k^2 - 1}$, $\sin^2\theta = \frac{1}{2} + \frac{1}{2k}$ and $G = k\Omega_2/\sqrt{k^2 - 1}$.

For the sake of brevity, we will examine only the two photon resonance that occurs when $\Delta_2 = 2\Omega_2/\sqrt{3}$. The analysis is very similar to that outlined in the previous sections, and only a summary of the results will be presented here. Once again we find pairs of degenerate doublets (k=2)

$$\begin{aligned} |(M-k+m)+, N+k-m\rangle &\equiv |a_m^k\rangle, \\ |(M+m)-, N-m\rangle &\equiv |b_m^k\rangle, \end{aligned} \tag{3.56}$$

Notice that we dress the atom first by the field ω_2, and thus the first state in the tensor product corresponds to this (detuned) field, while the second state corresponds to the number of photons in the $\omega_1 = \omega_0$ mode.

We proceed as before to find the dressed states. As before, these form an infinite set of doublets on manifold $(N+M)$ (see Figure 3.1), with the manifolds now a distance ω_2 apart, the interdoublet splitting now $2G$, and the intradoublet splitting given by

$$\Delta E = \Omega_2\sqrt{3}\sqrt{439}\left(\frac{1}{48}\beta^2 - \frac{65077}{4045824}\beta^4 + \ldots\right). \tag{3.56}$$

We notice that this two photon splitting is bigger than the corresponding expression (3.14a), and thus may be more experimentally accessible.

The transition frequencies analogous to (3.18) and (3.19), which determine the positions of the fluorescence and near-resonance absorption spectral lines, are given by

$$\omega_j^{\pm\pm} = \omega_0 - j\Delta_2 \tag{3.57},$$

and

$$\omega_j^{\pm\mp} = \omega_0 - j\Delta_2 \pm 2\Delta E, \tag{3.58},$$

while the Autler-Townes transition frequencies are given by

$$\omega_j^{\pm\mp} = \omega_3 - (j - \frac{k}{2})\Delta_2 \pm 2\Delta E. \tag{3.59}$$

Proceeding as before, we find the steady state populations to be given by

$$\Pi_{ss}^{\pm} = \frac{1}{2} \pm \frac{56\sqrt{439}}{4633} \mp \frac{3633899527\sqrt{439}}{603071902144}\beta^2, \tag{3.60}$$

and the linewidths by

$$\Gamma_c = \frac{4633}{7024} + \left(-\frac{58120913}{592038912} - \frac{5629095\sqrt{439}}{173270054912}\right)\beta^2, \tag{3.61}$$

$$\Gamma_s = \frac{9415}{14048} + \left(\frac{58120913}{1184077824} - \frac{7172145\sqrt{439}}{346540109824}\right)\beta^2. \tag{3.62}$$

To compute the fluorescence we need the transition rates. These are given by

$$\begin{aligned}
\Gamma_{-3}^{++} &= \tfrac{243}{112384}\beta^2 \\
\Gamma_{-2}^{++} &= \left(\tfrac{59535\sqrt{439}}{173270054912} - \tfrac{2978451}{789385216}\right)\beta^2 + \tfrac{243}{28096} \\
\Gamma_{-1}^{++} &= \tfrac{3}{112384}\beta^2 \\
\Gamma_{0}^{++} &= \tfrac{147}{1756} + \left(-\tfrac{178605\sqrt{439}}{43317513728} - \tfrac{54429907}{197346304}\right)\beta^2 \\
\Gamma_{1}^{++} &= \tfrac{439}{768}\beta^2 \\
\Gamma_{2}^{++} &= \left(\tfrac{535815\sqrt{439}}{173270054912} - \tfrac{236177451}{789385216}\right)\beta^2 + \tfrac{2187}{28096} \\
\Gamma_{3}^{++} &= \tfrac{6075}{112384}\beta^2,
\end{aligned} \tag{3.63}$$

$$\begin{aligned}
\Gamma_{-3}^{--} &= \tfrac{243}{112384}\beta^2 \\
\Gamma_{-2}^{--} &= \left(-\tfrac{414315\sqrt{439}}{346540109824} - \tfrac{2978451}{789385216}\right)\beta^2 + \tfrac{243}{28096} \\
\Gamma_{-1}^{--} &= \tfrac{3}{112384}\beta^2 \\
\Gamma_{0}^{--} &= \tfrac{147}{1756} + \left(-\tfrac{178605\sqrt{439}}{43317513728} - \tfrac{54429907}{197346304}\right)\beta^2 \\
\Gamma_{1}^{--} &= \tfrac{439}{768}\beta^2 \\
\Gamma_{2}^{--} &= \left(-\tfrac{3728835\sqrt{439}}{346540109824} - \tfrac{236177451}{789385216}\right)\beta^2 + \tfrac{2187}{28096} \\
\Gamma_{3}^{--} &= \tfrac{6075}{112384}\beta^2,
\end{aligned} \tag{3.64}$$

$$
\begin{aligned}
\Gamma_{-3}^{-+} &= \left(\frac{635}{112384} - \frac{7\sqrt{439}}{28096}\right)\beta^2 \\
\Gamma_{-2}^{-+} &= \left(\frac{50822\sqrt{439}}{253813557} - \frac{12598369}{2368155648}\right)\beta^2 + \frac{635}{28096} - \frac{7\sqrt{439}}{7024} \\
\Gamma_{-1}^{-+} &= \left(\frac{13167}{112384} - \frac{9\sqrt{439}}{1756}\right)\beta^2 \\
\Gamma_{0}^{-+} &= \left(\frac{2247012009\sqrt{439}}{173270054912} - \frac{27283797}{197346304}\right)\beta^2 + \frac{729}{7024} \\
\Gamma_{1}^{-+} &= \frac{81}{256}\beta^2 \\
\Gamma_{2}^{-+} &= \left(-\frac{6653590269\sqrt{439}}{346540109824} - \frac{383766375}{789385216}\right)\beta^2 + \frac{5715}{28096} + \frac{63\sqrt{439}}{7024} \\
\Gamma_{3}^{-+} &= \left(\frac{15875}{112384} + \frac{175\sqrt{439}}{28096}\right)\beta^2,
\end{aligned}
\tag{3.65}
$$

and

$$
\begin{aligned}
\Gamma_{-3}^{+-} &= \left(\frac{635}{112384} + \frac{7\sqrt{439}}{28096}\right)\beta^2 \\
\Gamma_{-2}^{+-} &= \left(-\frac{210481487\sqrt{439}}{1039620329472} - \frac{12700429}{2368155648}\right)\beta^2 + \frac{635}{28096} + \frac{7\sqrt{439}}{7024} \\
\Gamma_{-1}^{+-} &= \left(\frac{13167}{112384} + \frac{9\sqrt{439}}{1756}\right)\beta^2 \\
\Gamma_{0}^{+-} &= \left(-\frac{2248783479\sqrt{439}}{173270054912} - \frac{27283797}{197346304}\right)\beta^2 + \frac{729}{7024} \\
\Gamma_{1}^{+-} &= \frac{81}{256}\beta^2 \\
\Gamma_{2}^{+-} &= \left(\frac{415415409\sqrt{439}}{21658756864} - \frac{383460195}{789385216}\right)\beta^2 + \frac{5715}{28096} - \frac{63\sqrt{439}}{7024} \\
\Gamma_{3}^{+-} &= \left(\frac{15875}{112384} - \frac{175\sqrt{439}}{28096}\right)\beta^2.
\end{aligned}
\tag{3.66}
$$

The expression for the fluorescence spectrum is the same as in equation (3.39), and is plotted in Figure 3.8. Note that we plot $S(\omega)$ versus $(\omega - \omega_0)/\Gamma$, not the more natural $(\omega - \omega_2)/\Gamma$. This is done purely to make the spectrum more symmetrical and easier to compare with Figure 3.3(a).

The Autler-Townes spectrum is also easy to compute. The line weights are

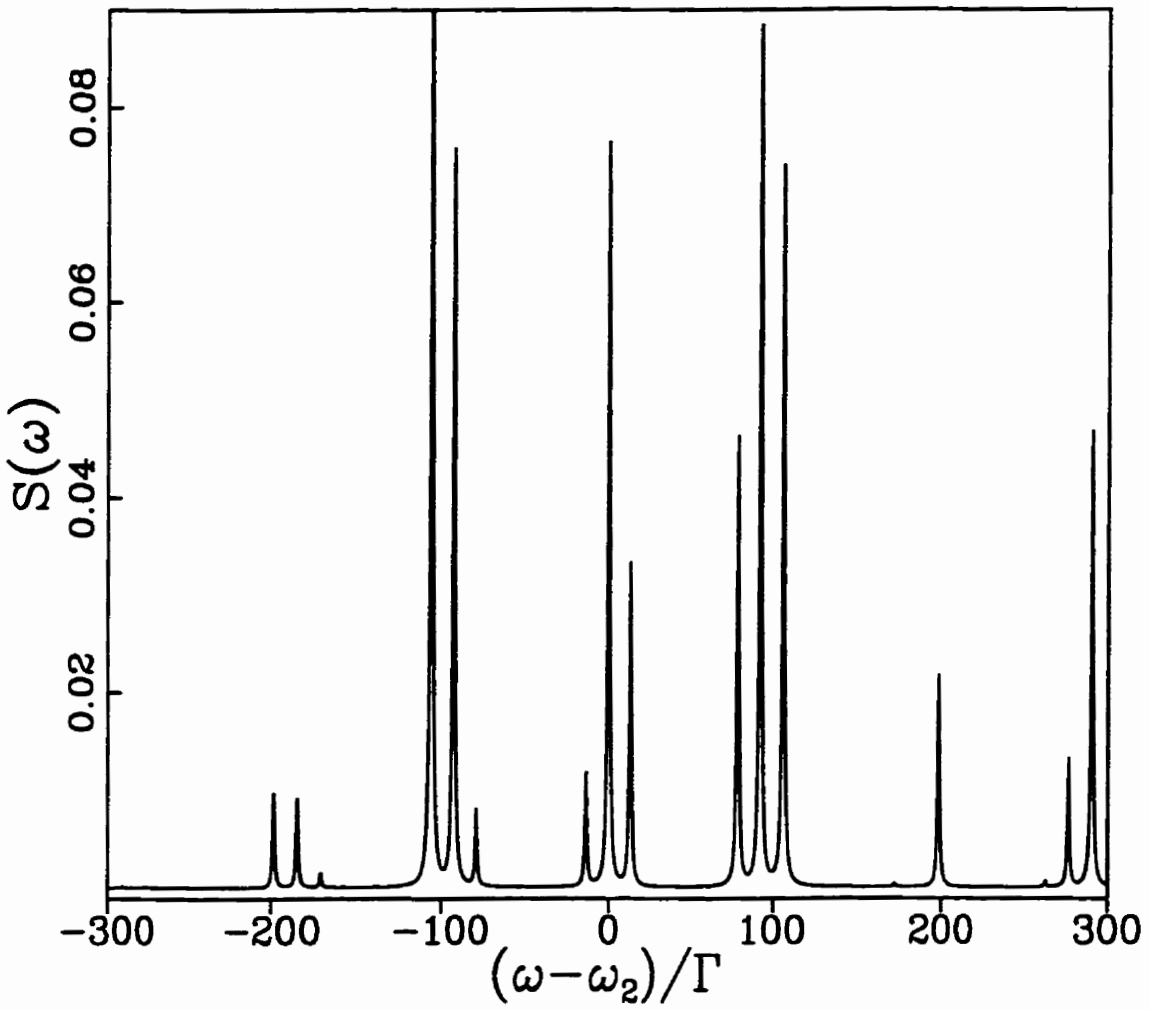

Figure 3.8 The k=2 fluorescence spectrum for $\omega_1 = \omega_0$, $\omega_2 = \omega_0 + \Delta_2$, with with $\Delta_2 = 160/\sqrt{3}$, $2\Omega_1 = 160\Gamma$ and $\beta = 0.35$.

given by

$$\begin{aligned}
\Lambda_{-1}^{+} &= \left(\tfrac{7}{192} - \tfrac{49\sqrt{439}}{42144} + \tfrac{7\sqrt{3}\sqrt{439}}{28096} - \tfrac{\sqrt{3}}{128}\right)\beta^2 \\
\Lambda_{0}^{+} &= \left(\tfrac{\sqrt{3}}{64} + \tfrac{3347069\sqrt{439}}{592038912} + \tfrac{53\sqrt{3}\sqrt{439}}{56192} - \tfrac{52394597}{296019456}\right)\beta^2 - \tfrac{7\sqrt{439}}{878} + \tfrac{1}{4} \\
\Lambda_{1}^{+} &= \left(\tfrac{9}{32} + \tfrac{45\sqrt{3}\sqrt{439}}{28096}\right)\beta^2 \\
\Lambda_{2}^{+} &= \left(\tfrac{53\sqrt{3}\sqrt{439}}{56192} - \tfrac{\sqrt{3}}{64} - \tfrac{52445627}{296019456} - \tfrac{3347069\sqrt{439}}{592038912}\right)\beta^2 + \tfrac{7\sqrt{439}}{878} + \tfrac{1}{4} \\
\Lambda_{3}^{+} &= \left(\tfrac{7}{192} + \tfrac{49\sqrt{439}}{42144} + \tfrac{7\sqrt{3}\sqrt{439}}{28096} + \tfrac{\sqrt{3}}{128}\right)\beta^2,
\end{aligned} \tag{3.67}$$

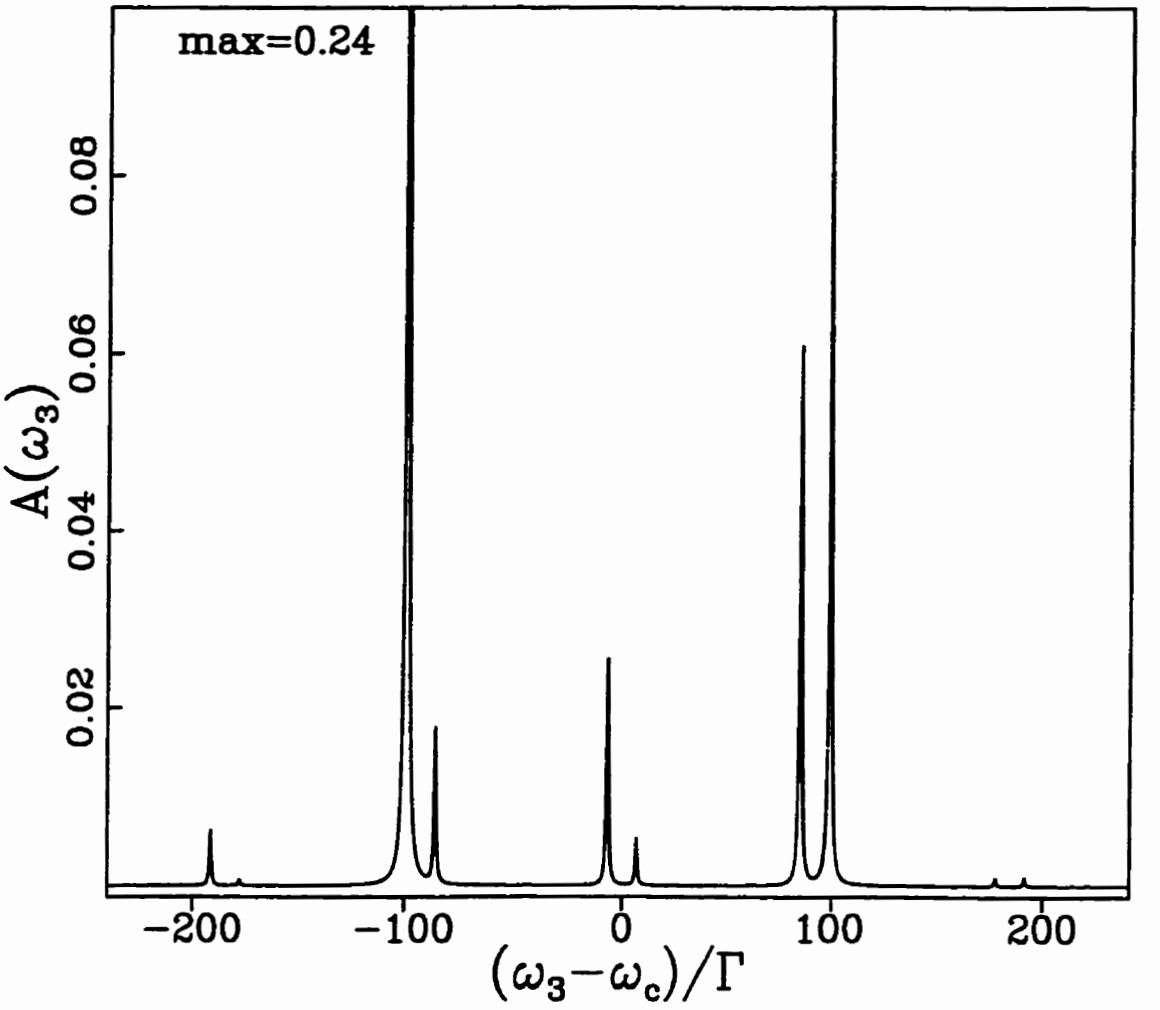

Figure 3.9 The k=2 Autler Townes absorption spectrum for $\omega_1 = \omega_0$, $\omega_2 = \omega_0 + \Delta_2$, with $\Delta_2 = 160/\sqrt{3}$, $2\Omega_1 = 160\Gamma$, $\beta = 0.35$ and $\Gamma_3 = \Gamma/3$.

and

$$
\begin{aligned}
\Lambda_{-1}^{-} &= \left(\tfrac{49\sqrt{439}}{42144} - \tfrac{7\sqrt{3}\sqrt{439}}{28096} - \tfrac{\sqrt{3}}{128} + \tfrac{7}{192}\right)\beta^2 \\
\Lambda_{0}^{-} &= \left(-\tfrac{3354359\sqrt{439}}{592038912} - \tfrac{53\sqrt{3}\sqrt{439}}{56192} + \tfrac{\sqrt{3}}{64} - \tfrac{52445627}{296019456}\right)\beta^2 + \tfrac{7\sqrt{439}}{878} + \tfrac{1}{4} \\
\Lambda_{1}^{-} &= \left(\tfrac{9}{32} - \tfrac{45\sqrt{3}\sqrt{439}}{28096}\right)\beta^2 \\
\Lambda_{2}^{-} &= \left(-\tfrac{53\sqrt{3}\sqrt{439}}{56192} - \tfrac{\sqrt{3}}{64} - \tfrac{52394597}{296019456} + \tfrac{3339779\sqrt{439}}{592038912}\right)\beta^2 - \tfrac{7\sqrt{439}}{878} + \tfrac{1}{4} \\
\Lambda_{3}^{-} &= \left(-\tfrac{49\sqrt{439}}{42144} - \tfrac{7\sqrt{3}\sqrt{439}}{28096} + \tfrac{\sqrt{3}}{128} + \tfrac{7}{192}\right)\beta^2.
\end{aligned}
\tag{3.68}
$$

The Autler-Townes spectrum is plotted in Figure 3.9, and can be compared to Figure 3.5(a).

3.6 Conclusions

In this chapter we have first studied the effect of bichromatic excitation on the radiative and absorptive properties of a two-level atom under the condition that one of the excitation fields is strong and exactly resonant with the atomic transition, while the other is weaker and detuned by a subharmonic of the Rabi frequency of the strong field. The energy levels of this system have been found and the radiative and absorptive properties interpreted in terms of the transitions between them. We have seen that this system, despite the one-photon coupling between the atom and driving fields, exhibits a multiphoton AC Stark effect. As such the fluorescence, absorption and Autler-Townes spectra exhibit spectral features at subharmonics as well as harmonics of the Rabi frequency of the strong field, with the number of features dependent on the order n of the resonance. The presence of the multiphoton AC Stark effect leads to a splitting of these features into a triplet (fluorescence spectrum) or a doublet (weak probe and Autler-Townes spectra).

We also briefly considered the situation that arises when the stronger field is detuned and the weaker field is on resonance, and showed that a multiphoton coupling between the dressed states is once again possible.

Finally, it should be noted that the multi-photon splitting and the Autler-Townes spectra of a system similar to that considered here, have recently been

observed experimentally [23] and our theoretical predictions agree with these observations.

References

[1] B.R. Mollow, Phys. Rev. **188**, 1969 (1969).

[2] F. Schuda, C.R. Stroud, Jr., and M. Hercher, J. Phys. B **7**, L198 (1974); F.Y. Wu, R.E. Grove and S. Ezekiel, Phys. Rev. Lett. **35**, 1426 (1975).

[3] B.R. Mollow, Phys. Rev. A **5**, 2217 (1972); F.Y. Wu, S. Ezekiel, M. Ducloy and B.R. Mollow, Phys. Rev. Lett. **38**, 1077 (1977); C. Wei and N.B. Manson, Phys. Rev. A **49**, 4751 (1994); A.D. Wilson-Gordon and H. Friedmann, Optics Comm. **94**, 238 (1992); Tran Quang and Helen Freedhoff, Phys. Rev. A **48**, 3216 (1993).

[4] S.H. Autler and C.H. Townes, Phys. Rev. **100**, 703 (1955); C. Wei, N.B. Manson and J.P.D. Martin, Phys. Rev. A **51**, 1438 (1995).

[5] Y. Zhu, A. Lezama, D.J. Gauthier and T.W. Mossberg, Phys. Rev. A **41**, 6574 (1990).

[6] H.S. Freedhoff and Z. Chen, Phys. Rev. A **41**, 6013 (1990); **46** 7328(E) (1992).

[7] G. Kryuchkov, Optics Commun. **54**, 19 (1985); S.P. Tewari and M.K. Kumari, Phys. Rev. A **41**, 5273 (1990); G.S. Agarwal, Y. Zhu, D.J. Gauthier and T.W. Mossberg, J. Opt. Soc. Am. B **8**, 1163 (1991).

[8] Z.Ficek and H.S. Freedhoff, Phys. Rev. A **48**, 3092 (1993) and references therein.

[9] M.F. Van Leeuwen, S. Papademetriou and C.R. Stroud, Jr., Phys. Rev. A **53**, 990 (1996); S. Papademetriou, M.F. Van Leeuwen and C.R. Stroud, Jr., Phys. Rev. A **53**, 997 (1996).

[10] N.B. Manson, C. Wei, and J.P.D. Martin, Phys. Rev. Lett. **76**, 3943 (1996) and references therein.

[11] S. Feneuille, M.G. Scheighofer and G. Oliver, J. Phys. B**9**, 2003 (1976); A.M. Bonch-Bruevich, T.A. Vartanyan and N.A. Chigir, Sov. Phys. JETP**50**, 901 (1979); P. Thomann, J. Phys. B**13**, 1111 (1980); G.S. Agarwal and N. Nayak, J. Opt. Soc. Am. B **1**, 164 (1984); H. Friedmann and A.D. Wilson-Gordon, Phys. Rev. A**36**, 1333 (1987); S. Chakmakjian, K. Koch and C.R. Stroud Jr., J. Opt. Soc. Am. B**5**, 2015 (1988).

[12] S.Papademetriou, S.M. Chakmakjian, and C.R. Stroud, Jr., J. Opt. Soc. Am. B**9**, 1182 (1992).

[13] B. Lounis, F. Jelezko and M. Orrit, Phys. Rev. Lett. **78**, 3673 (1997).

[14] Y. Zhu, Q. Wu, S. Morin and T. Mossberg, Phys. Rev. Lett. **65**, 1200 (1990).

[15] D.J. Gauthier, Q. Wu, S. Morin and T.W. Mossberg, Phys. Rev. Lett. **65**, 1200 (1990)

[16] J.R. Ackerhalt and B.W. Shore, Phys. Rev. A **16**, 277 (1977); R.M. Whitley and C.R. Stroud, Jr., Phys. Rev. A **14**, 1498 (1976); R. Salomaa, J. Phys. B **10**, 3005 (1977); L. Allen and C.R. Stroud, Jr., Phys. Rep. **91**, 1 (1982).

[17] G. Grynberg and C. Cohen-Tannoudji, Optics. Commun. **96**, 150 (1993).

[18] P.B. Sellin, C.C. Yu, J.R. Bochinski and T.W. Mossberg, Phys. Rev. Lett., **78**, 1432 (1997).

[19] C. Cohen-Tannoudji and S. Reynaud, J. Phys. B **10**, 345 (1977); C. Cohen-Tannoudji, J. Dupont-Roc, and G. Grynberg *Atom-Photon Interactions* (Wiley, New York, 1992).

[20] G.S. Agarwal in *Quantum Optics*, edited by G. Höhler, Springer Tracts in Modern Physics Vol. 70 (Springer, Berlin, 1974) p. 25.

[21] Z.Ficek and H.S. Freedhoff, Phys. Rev. A **53**, 4275 (1996).

[22] C.C. Yu, J.R. Bochinski, T.M.V. Kordich, T.W. Mossberg and Z. Ficek, Phys. Rev. A**56**, R4381 (1997).

[23] K.Catchpole, A. Greentree, C. Wei, S. Holstrom, N. Manson and J. Martin, in *Proceedings of the International Quantum Electronics Conference, 1996,* (Optical Society of America, Washington, D.C., 1996) p. 203.

[24] M. Lax, Phys. Rev. **172**, 350 (1968).

[25] M.O. Scully, Phys. Rev. Lett. **67**, 1855 (1991); M.O. Scully and M. Fleischhauer, Phys. Rev. Lett. **69**, 1360 (1992); A.D. Wilson-Gordon and H. Friedmann, Optics Commun. **94**, 238 (1992); T. Quang and H.S. Freedhoff, Phys. Rev. A **48**, 3216 (1993); C. Szymanowski and C.H Keitel, J.Phys. B **27**, 5795 (1994).

4. Subharmonic resonance shifts and suppression of fluorescence in a two-level atom driven by a bichromatic field

4.1 Introduction

The purpose of the present chapter is to apply the treatment of the resonance fluorescence from a two-level atom driven by a bichromatic field discussed in Chapter 3, to a (practical) scenario in which one can suppress fluorescence at the frequency ω_1 *without* population trapping. In the case of interest, the stronger field component is kept exactly resonant with the atomic transition frequency while the weaker field is detuned. We analyse the problem both by a numerical integration of the optical Bloch equations of the system and by the dressed-atom model, which provides a simple explanation of the numerical results. We find the interesting result that under certain conditions the system does not fluoresce at either the frequency ω_1 of the strong component or the three-wave mixing frequency $2\omega_1 - \omega_2$, where ω_2 is the frequency of the tunable component. This occurs whenever the weaker component is detuned from the atomic resonance by an amount δ close to either the Rabi frequency $2\Omega_1$ of the strong component or one of its subharmonics $2\Omega_1/n$, $n = 1, 2, ...$ However, suppression does not appear for detunings exactly equal to a subharmonic frequency; rather, it appears for detunings slightly shifted from them. We interpret the shifts as arising from the

interaction of the weaker field with the strongly driven system and attribute this effect to a dynamic Stark shift.

A suppression of fluorescence at some frequencies has been predicted previously for other systems [8]. For example, in three-level atoms fluorescence can be eliminated between some of the levels or even completely suppressed if the atoms are excited to a certain coherent superposition of the levels. Furthermore, in multi-level atoms it can be suppressed by quantum interference of transition amplitudes from two closely lying atomic levels [8] or even well separated levels [9] to a third level. Two-level atoms driven by a strong laser field can also exhibit a suppression of fluorescence when the atoms are damped by a squeezed vacuum [10], or are placed in a narrow bandwidth cavity [11].

The suppression effects listed above all have a common origin: the trapping of the atomic population in certain atomic or dressed states. The cancellation of fluorescence discussed here is different in that it can occur at some frequencies without population trapping. These studies suggest then that one can, in principle, eliminate fluorescence without trapping or destroying the population of the upper levels.

The chapter is organised as follows: In section 4.1, we study the fluorescence spectrum of a bichromatically driven two-level atom by solving numerically the optical Bloch equations of the system. In section 4.2, we provide a simple explanation of the shift of the subharmonic resonances and the suppression of fluorescence

using the dressed atom model of the system. We summarise the results in section 4.3.

4.2. Optical Bloch equations

As in the previous chapter, we consider a two-level atom with excited state $|e\rangle$ and ground state $|g\rangle$, connected by a transition dipole moment $\vec{\mu}$ and separated by a transition frequency ω_0. The atom is driven by a bichromatic field whose stronger component is resonant with ω_0 while the weaker is detuned. We calculate the steady-state fluorescence spectrum of the system, defined as

$$S(\omega) = \Re \int_0^\infty d\tau\, e^{i\omega\tau} \lim_{t\to\infty} \langle S^+(t) S^-(t+\tau)\rangle, \tag{4.1}$$

where $\Re$ is the real part of the integral and $S^+ = |e\rangle\langle g|$ ($S^- = |g\rangle\langle e|$) is the atomic raising (lowering) operator. In this section we compute the fluorescence spectrum by solving the equation of motion for the two-time correlation function of (4.1) numerically[†]. The average values of the atomic operators satisfy the following set of (optical Bloch) equations [3],[7]:

$$\begin{aligned}
\frac{d}{dt}\langle \tilde{S}^-(t)\rangle &= -\frac{1}{2}\Gamma\langle \tilde{S}^-(t)\rangle + 2\Omega_1(1+\alpha e^{-i\delta t})\langle S^z(t)\rangle,\\
\frac{d}{dt}\langle \tilde{S}^+(t)\rangle &= -\frac{1}{2}\Gamma\langle \tilde{S}^+(t)\rangle + 2\Omega_1(1+\alpha e^{i\delta t})\langle S^z(t)\rangle,\\
\frac{d}{dt}\langle S^z(t)\rangle &= -\frac{1}{2}\Gamma - \Gamma\langle S^z(t)\rangle - \Omega_1(1+\alpha e^{i\delta t})\langle \tilde{S}^-(t)\rangle - \Omega_1(1+\alpha e^{-i\delta t})\langle \tilde{S}^+(t)\rangle,
\end{aligned} \tag{4.2}$$

where

$$\langle \tilde{S}^\pm(t)\rangle = \langle S^\pm\rangle e^{\mp i\omega_0 t},$$

[†] The numerical simulation of the Bloch equations is due to Dr. Z. Ficek.

are the slowly varying parts of the atomic operators, S^z is the average value of the inversion operator, and Γ is the spontaneous emission rate. In equation (4.2), $\alpha = \Omega_2/\Omega_1$ is the ratio between the "on resonance" Rabi frequencies of the weak ($2\Omega_2$) and the strong ($2\Omega_1$) components, and $\delta = \omega_2 - \omega_0$ is the detuning of the weaker component of frequency ω_2.

Applying the quantum regression theorem [12] and the Floquet method [13] to equation (4.2), we can find numerically the steady-state fluorescence spectrum. For a more detailed description of the method, we refer the reader to [7]. In Figure 4.1, we present the spectrum for $2\Omega_1 = 40\Gamma$, $\alpha = 0.4$ and detuning $\delta = 2\Omega_1/n$, $n = 1, 2, 3$. All the spectral features are composed of triplets centred at ω_0, $\omega_0 \pm 2\Omega_1$ and $\omega_0 \pm m(2\Omega_1/n)$ (m=1,2,..), the harmonics and subharmonics of $2\Omega_1$. The figures indicate that there is no suppression at ω_0 when the weaker field is exactly tuned to a subharmonic resonance[†]. However, a careful analysis shows that the central components of the triplets centred at ω_0 and $2\omega_0 - \omega_2$ can be made to vanish, but for detunings δ slightly shifted from the exact resonance. At these special detunings the splitting of the remaining doublet is seen to be a minimum. In Figure 4.2, we display the amplitude of the fluorescence spectrum at ω_0 as a function of the detuning δ for $2\Omega_1 = 40\Gamma$ and $\alpha = 0.4$. We see that the central line of the spectrum vanishes for values close but not exactly equal to the subharmonic resonances of $2\Omega_1$, indicating that the multi-photon resonances to which the weaker field couples are slightly shifted from $2\Omega_1/n$.

[†] In the case of n=1, shown in Figure 4.1(a), there *is* in fact a small "bump" at the central frequency indicating that even for n=1 the central component appears in the spectrum. The line is more visible for higher values of α [7].

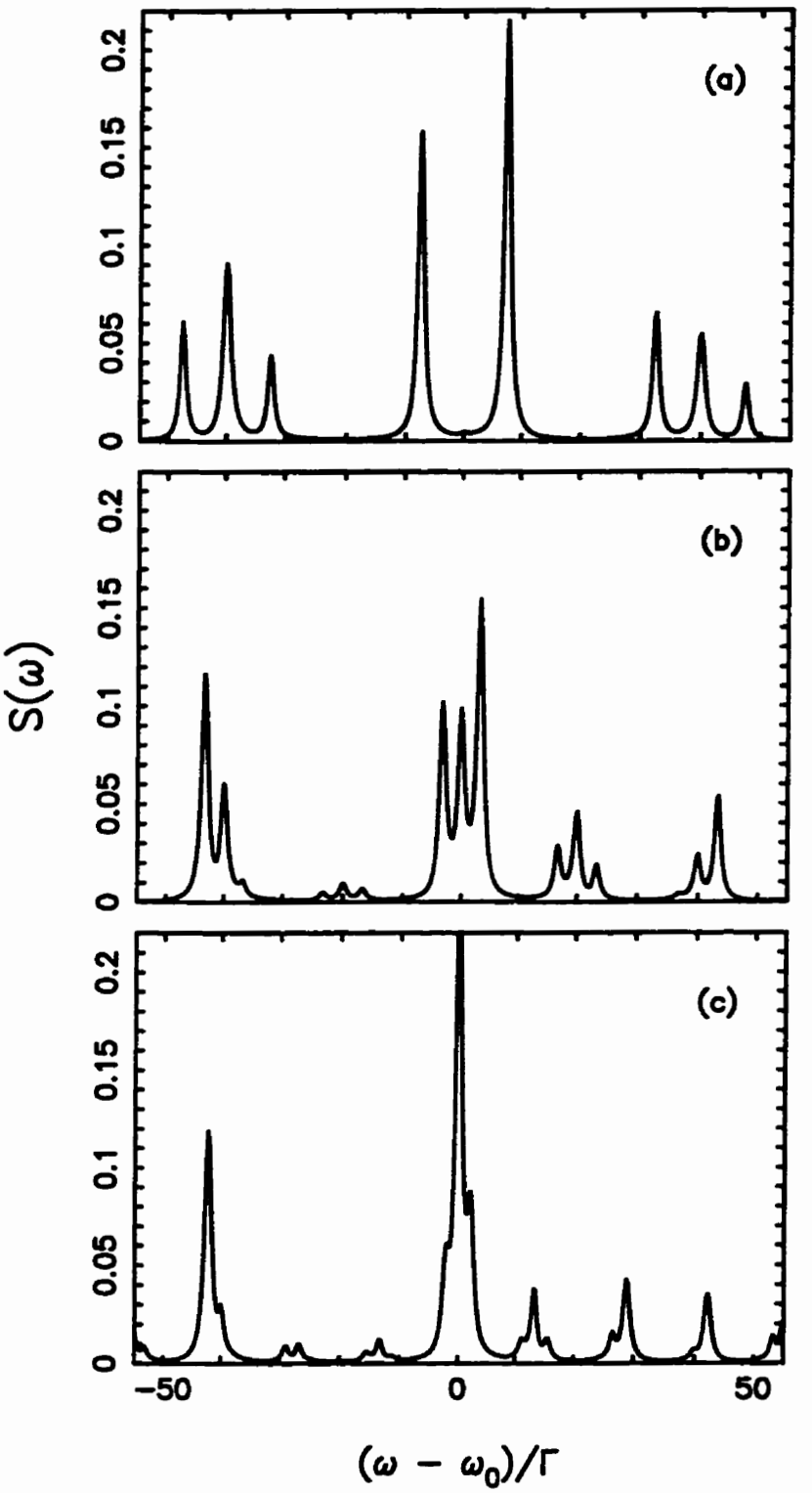

Figure 4.1 The steady-state fluorescence spectrum for $2\Omega_1 = 40\Gamma$, $\alpha = 0.4$, and different $n = 2\Omega_1/\delta$: (a) n=1, (b) n=2, (c) n=3. ω_2 is tuned exactly to the subharmonic resonance. *Figure courtesy of Dr. Z. Ficek*

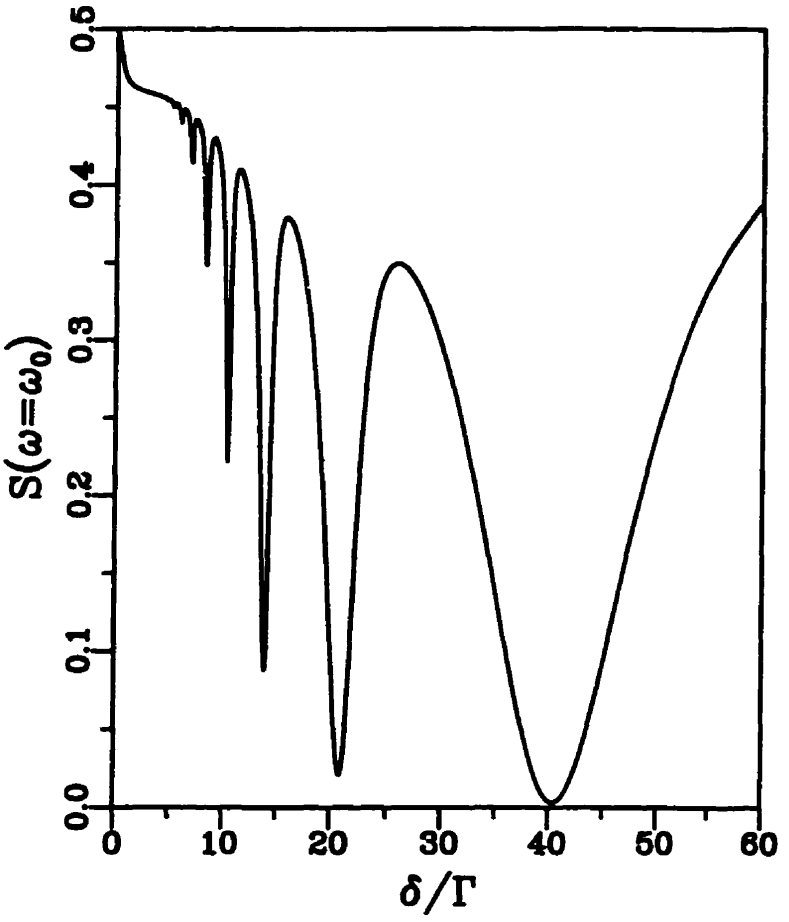

Figure 4.2 The amplitude of the fluorescence spectrum at $\omega = \omega_0$ as a function of δ/Γ for $2\Omega_1 = 40\Gamma$ and $\alpha = 0.4$.

In Figure 4.3, we plot the fluorescence spectrum for $2\Omega_1 = 40\Gamma$, $\alpha = 0.4$, and the detunings δ corresponding to the vanishing central line at ω_0. For n=1,2 and 3, the central line vanishes when $\delta_1 = 40.4\Gamma$, $\delta_2 = 21.06\Gamma$ and $\delta_3 = 13.93\Gamma$ respectively. This corresponds to the weaker field frequency shifted from the n=1 resonance by $\Delta_1 = 0.4\Gamma$ and from the n=2 (3) subharmonic resonance by $\Delta_2 = 1.06\Gamma$ ($\Delta_3 = 0.60\Gamma$). Apparently, at these frequencies not only does the line at ω_0 vanish, but for $n > 1$ so too does the central line of the lowest frequency red triplet. This line corresponds to three-wave mixing at the frequency $2\omega_0 - \omega_2$.

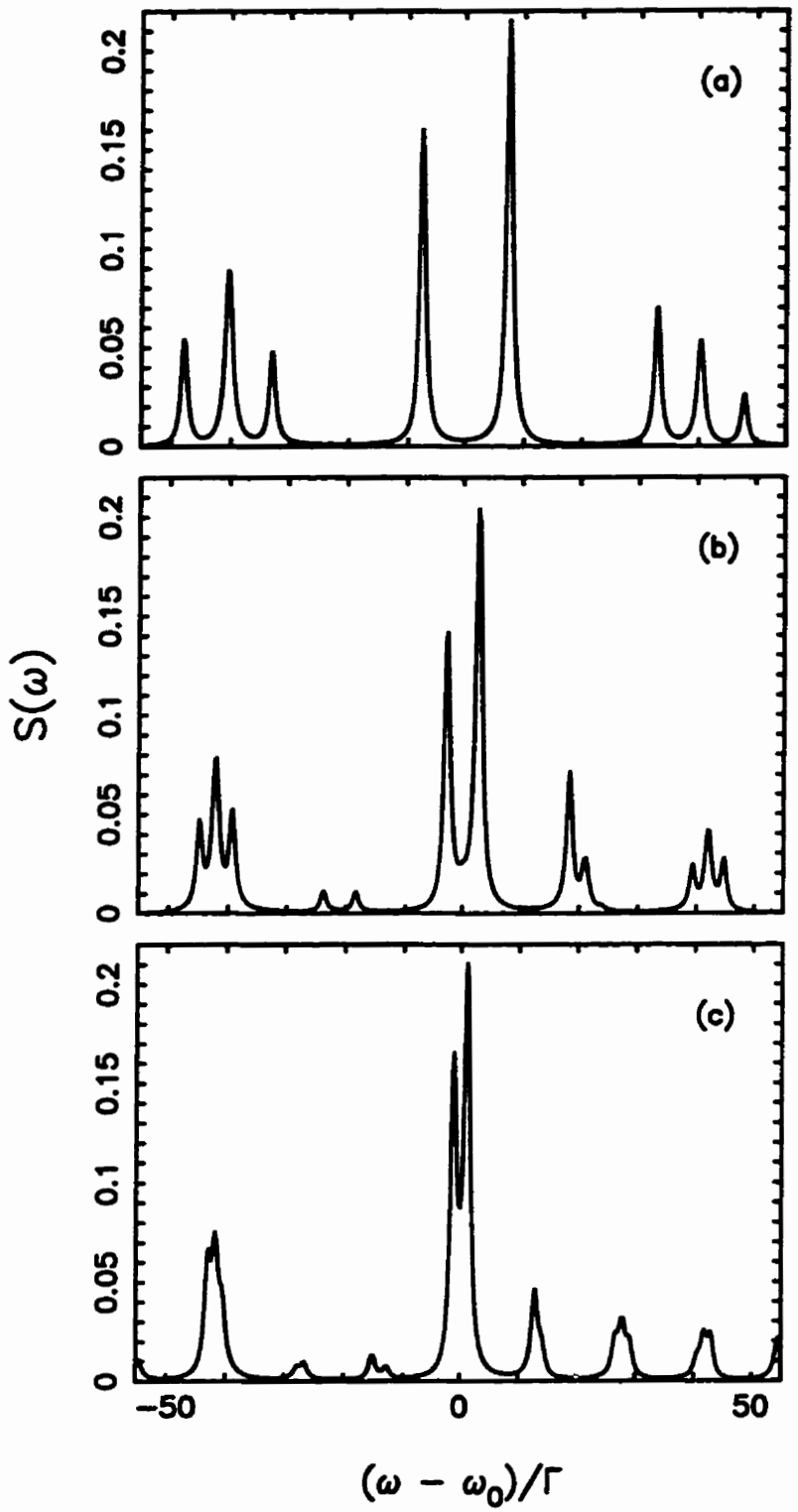

Figure 4.3 The fluorescence spectrum for $2\Omega_1 = 40\Gamma$, $\alpha = 0.4$ and different δ: (a) $\delta = 40.4\Gamma$ (b) $\delta = 21.06\Gamma$, (c) $\delta = 13.93\Gamma$. *Figure courtesy of Dr. Z. Ficek*

In the next section, we use the dressed-atom model to derive a simple formula for the shifts of the subharmonic resonances and to give a simple explanation for the disappearance of the spectral lines at ω_0 .

4.3 Dressed atom analysis

In this section, we apply the dressed-atom model [14] to study the system. This analysis provides simple analytical formulae for the positions of the resonances and explains the vanishing fluorescence in terms of the spontaneous emission transition rates and populations. The dressed-atom treatment is valid in the limits

$$\omega_0, \omega_2 \gg \Omega_1 > \Omega_2, \delta,$$

which correspond to the approximations made in the Bloch equations of section 4.2 as well.

We first find the dressed states of the system and their energies by applying the double-dressing procedure, described in detail in [4]. In this technique, we first dress the atom with the strong resonant component of the bichromatic field, which results in the singly dressed states [14]

$$|N\pm\rangle = \frac{1}{\sqrt{2}}(|g, N\rangle \pm |e, N-1\rangle), \tag{4.3}$$

where $|i, N\rangle$ (i=g,e) is the state in which the atom is in state $|i\rangle$ and N photons are present in the strong driving mode. Next, we couple the resulting singly dressed atom to the weaker component at frequency $\omega_2 = \omega_0 + 2\Omega_1/n + \Delta_n$.

The eigenstates of the combined (uncoupled) system of singly dressed atom plus weaker field are (nearly-degenerate) doublets (see Figure 4.4(a))

$$\begin{aligned} |(N+n-m)+, M-n+m\rangle &\equiv |a_m^n\rangle, \\ |(N-m)-, M+m\rangle &\equiv |b_m^n\rangle, \end{aligned} \tag{4.4}$$

with energies

$$\begin{aligned} E_{am}^n &= \bar{N}\omega_0 - \Omega_1 + m(\frac{2\Omega_1}{n} + \Delta_n) - n\Delta_n, \\ E_{bm}^n &= \bar{N}\omega_0 - \Omega_1 + m(\frac{2\Omega_1}{n} + \Delta_n), \end{aligned} \tag{4.5}$$

where $\bar{N} = N + M$ is the total number of photons. In state $|b_m^n\rangle$, for example, the (singly-dressed) atom is in state $|(N-m)-\rangle$, and there are $M+m$ photons in the weaker field.

The combined dressed states (4.4) form doublets with intradoublet separation $n\Delta_n$ and interdoublet spacing $2\Omega_1/n > n\Delta_n$. We treat the states (4.4) as basis states, and calculate the effect on them of the interaction V_2 between the singly dressed atom and the weaker field given in the rotating-wave approximation by

$$V_2 = g_2(a_2^\dagger S^- + S^+ a_2), \tag{4.6}$$

where g_2 is the coupling constant between the atom and field, and $a_2^\dagger(a_2)$ the creation (annihilation) operator of the field mode. Applying the interaction (4.6) to the states (4.4), we find

$$\begin{aligned} V_2|a_m^n\rangle &= \frac{1}{2}\alpha\Omega_1(|a_{m+1}^n\rangle + |a_{m-1}^n\rangle + |b_{m+1-n}^n\rangle - |b_{m-1-n}^n\rangle), \\ V_2|b_m^n\rangle &= \frac{1}{2}\alpha\Omega_1(-|b_{m+1}^n\rangle - |b_{m-1}^n\rangle - |a_{m+1+n}^n\rangle + |a_{m-1+n}^n\rangle), \end{aligned} \tag{4.7}$$

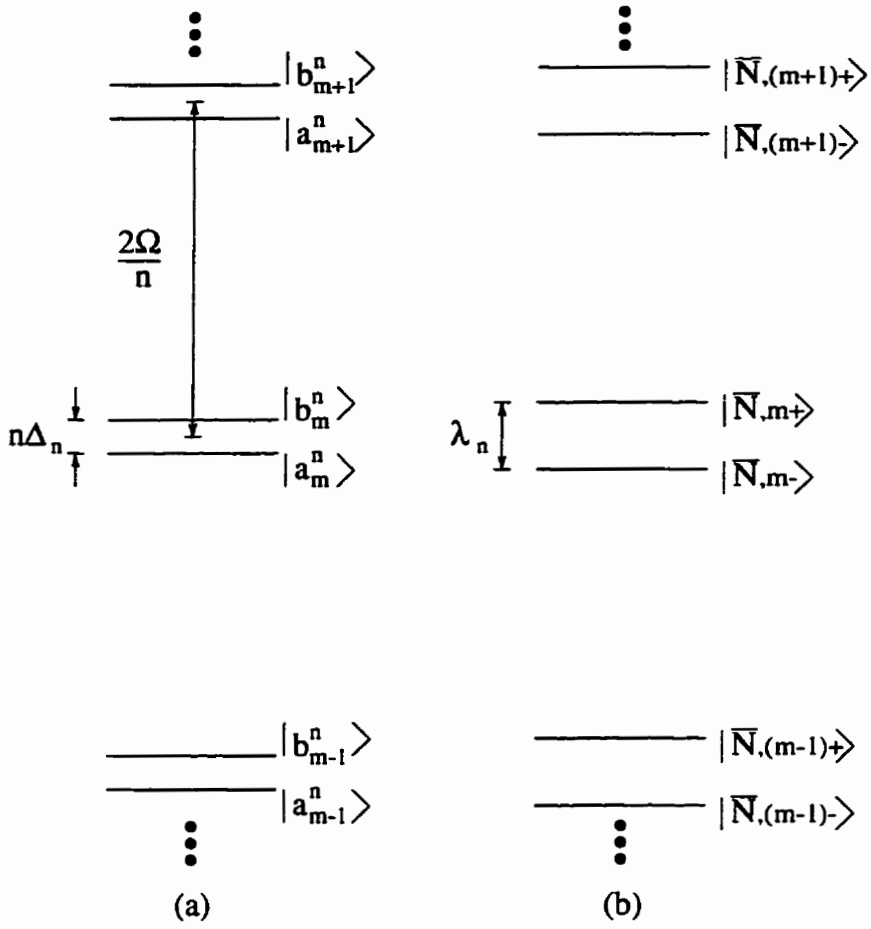

Figure 4.4 Energy level diagrams of: (a) the combined (uncoupled) system of singly-dressed atom plus weaker field, and: (b) the doubly-dressed system.

indicating that for $n > 1$ the states $|a^n_m\rangle$ and $|b^n_m\rangle$ are not directly coupled to each other by the interaction V_2. Therefore, we must go to higher order perturbation theory to find the perturbed states and their energies.

It turns out useful to first take into account the effect on $|a^n_m\rangle$ and $|b^n_m\rangle$ of all doublets *other* than m; these states induce shifts of the energies of $|a^n_m\rangle$ and $|b^n_m\rangle$. Using perturbation theory, which for $n \geq 2$ requires going to at least second

order, we find that to lowest nonvanishing order in α these shifts are

$$R^1_{aa} = -R^1_{bb} = \frac{\alpha^2}{8(2+\Delta_1/\Omega_1)}\Omega_1, \quad \text{for } n=1, \tag{4.8}$$

and

$$R^n_{aa} = -R^n_{bb} = \frac{n^2}{2(n^2-1)}\frac{\alpha^2}{(2+n\Delta_n/\Omega_1)}\Omega_1, \quad \text{for } n>1, \tag{4.9}$$

where R^n_{aa} and R^n_{bb} are the diagonal elements of the operator [14,15]

$$R^n = \sum_{\substack{s\neq m \\ i=a,b}} \frac{V_2|i^n_s\rangle\langle i^n_s|V_2}{E^n_{am}-E^n_{is}}. \tag{4.10}$$

These diagonal elements cause the anticrossing point of the doublet energies, $E^n_a + R^n_{aa} = E^n_b + R^n_{bb}$, to shift by the amount

$$\Delta^{min}_n = \frac{2}{n}R^n_{aa}, \tag{4.11}$$

or (to lowest order in alpha)

$$\Delta^{min}_1 = \frac{1}{8}\alpha^2\Omega_1, \quad \text{for } n=1, \tag{4.12}$$

and

$$\Delta^{min}_n = \frac{n\alpha^2}{2(n^2-1)}\Omega_1, \quad \text{for } n>1. \tag{4.13}$$

It follows that the anticrossing point of the eigenstates (4.4) appears not at Δ_n=0, but rather at small detunings from the subharmonic resonances $\Delta_n = \Delta^{min}_n$. For the parameters used in Figure 4.3, the shifts given by equations (4.12) and (4.13) are $\Delta^{min}_1 = 0.4\Gamma$, $\Delta^{min}_2 = 1.066\Gamma$ and $\Delta^{min}_3 = 0.60\Gamma$, in perfect agreement with the detunings found in the previous section.

We now include the coupling by V_2 *between* the states $|a_m^n\rangle$ and $|b_m^n\rangle$, which leads to the doubly dressed eigenstates (Figure 4.4(b)) and energies of the system. For $n = 1$ the states are coupled directly by V_2 [7]. For n=2 the lowest nonvanishing coupling is given by the off-diagonal elements of the operator R^2 in equation (4.10), while for n=3 we must compute the off diagonal elements of the operator [15]

$$T^3 = \sum_{\substack{r,s\neq m \\ i,j=a,b}} \frac{V_2|j_r^3\rangle\langle j_r^3|V_2|i_s^3\rangle\langle i_s^3|V_2}{(E_{am}^3 - E_{is}^3)(E_{am}^3 - E_{jr}^3)}. \tag{4.14}$$

Higher values of n involve operators with more intermediate couplings. For n=1,2 and 3, we obtain the following expressions for the shifts of the doublet energies from E_{am}^n:

$$\begin{aligned}
\lambda_1 &= \pm\frac{1}{2}\Omega_1\left[\left(\frac{\Delta_1}{\Omega_1} - \frac{\alpha^2}{8}\right)^2 + \alpha^2\right]^{\frac{1}{2}}, \\
\lambda_2 &= \pm\Omega_1\left[\left(\frac{\Delta_2}{\Omega_1} - \frac{\alpha^2}{3}\right)^2 + \left(\frac{\alpha^2}{2}\right)^2\right]^{\frac{1}{2}}, \\
\lambda_3 &= \pm\frac{3}{2}\Omega_1\left[\left(\frac{\Delta_3}{\Omega_1} - \frac{3\alpha^2}{16}\right)^2 + \left(\frac{27\alpha^3}{64}\right)^2\right]^{\frac{1}{2}}.
\end{aligned} \tag{4.15}$$

In Figure 4.5, we plot the intradoublet splittings $2\lambda_n$ as a function of Δ_n for $n = 2$ and 3 and for the same parameters as in Figure 4.3. The figure indicates a clear minimum at $\Delta_n = \Delta_n^{min}$. At these special detunings the intradoublet splittings are given by the simple expressions

$$\begin{aligned}
2\lambda_1^{min} &= \alpha\Omega_1, \\
2\lambda_2^{min} &= \alpha^2\Omega_1, \\
2\lambda_3^{min} &= \frac{81}{64}\alpha^3\Omega_1.
\end{aligned} \tag{4.16}$$

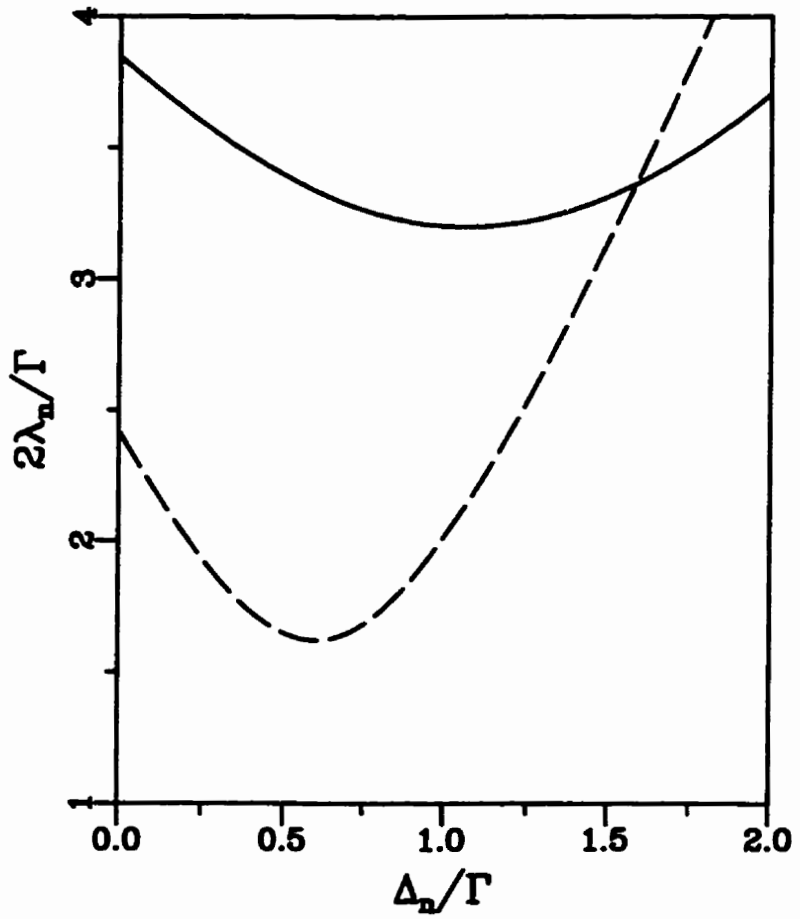

Figure 4.5 The intradoublet splittings $2\lambda_n$ as a function of Δ_n for $2\Omega_1 = 40\Gamma$, $\alpha = 0.4$ and $n = 2$ (solid line), $n = 3$ (dashed line).

Since the diagonal elements of the operators R^n_{aa} and R^n_{bb} vanish at the minimum detunings Δ^{min}_n, we can easily determine that the dressed states are then given by

$$|\bar{N}, m\pm\rangle_{min} = \frac{1}{\sqrt{2}}(|a^n_m\rangle \pm |b^n_m\rangle). \tag{4.17}$$

Having available the dressed states of the system, we can calculate the spontaneous emission rates. The probability of a spontaneous transition between any two dressed states is given by

$$\Gamma_{pi,qj} = \Gamma \left|\langle \bar{N}, ip|S^+|\bar{N}-1, qj\rangle\right|^2, \tag{4.18}$$

where $i, j = +, -$. Using equations (4.17) and (4.4), we find that the transition moments $|\bar{N}, m+\rangle \rightarrow |\bar{N}-1, m+\rangle$ and $|\bar{N}, m-\rangle \rightarrow |\bar{N}-1, m-\rangle$ are equal and opposite, and therefore the transition rates $\Gamma_{m\pm,m\pm}$ corresponding to the central frequency ω_0 vanish. This leads to the suppression of the spectral line at ω_0. Also, since the eigenstates (4.17) contain equal superpositions of the $|a_m^n\rangle$ and $|b_m^n\rangle$ states, the populations $\Pi_\pm$ are equal at the points of minimum splitting. Thus, the suppression of the fluorescence at ω_0 results from destructive interference between the transition amplitudes, and is not accompanied by the trapping or destruction of the population of the dressed states. The suppression of the fluorescence at $2\omega_0 - \omega_2$ is less transparent and occurs in higher order corrections which cannot be determined explicitly from the zeroth-order dressed states (4.17).

It is worthwhile to explain the origin of the shift Δ_n^{min}. Ruyten [16] has noticed that the subharmonic resonances are shifted from the $2\Omega_1/n$ positions and has termed the shifts the "generalised" Bloch-Siegert shifts. The original Bloch-Siegert shift [17] in a driven two-level atom arises from the effect of the *counter-rotating* terms in the atom-laser interaction Hamiltonian, which couple states of a given manifold N with states of the other manifolds $N' \neq N$, separated from N by distances of order ω_0. This coupling results in a (very small) shift of the energy levels of order Ω_1^2/ω_0. In the bichromatically driven atom discussed here, the energy doublets within the manifold $\bar{N}$ are separated by distances of the same order as the Rabi frequency of the strong component (see Figure 4.4(a)), and the *rotating wave* terms of the interaction V_2 couple a given doublet with other doublets within the same manifold, resulting in a shift of order Ω_2^2/Ω_1,

much larger than the Bloch-Siegert shift[†]. Thus, the shift Δ_n^{min} of the spectral lines calculated here represents a dynamic Stark shift of the doublet sublevels due to their coupling by the weaker field to other levels within the same energy manifold.

4.4 Conclusions

In this chapter we have shown that under certain conditions a selective suppression of fluorescence is possible in a two-level atom driven by a bichromatic field. The bichromatic field considered is composed of a strong component resonant with the atomic transition frequency and a weaker component tuned near a subharmonic resonance of the Rabi frequency of the strong component. The weaker field couples the dressed states created by the strong field in an n-photon process which results in a dynamic Stark shift of the states and consequently of their anticrossing. This effectively shifts the position of the resonance. When the weaker field is tuned to this shifted resonance, the system does not fluoresce at either the strong field frequency ω_0 or (for $n \geq 2$) the three-photon mixing frequency $2\omega_0 - \omega_2$, and the doublet energy and spectral feature splittings are a minimum. The fluorescence is suppressed without trapping or destroying the populations of the dressed states. These effects have been explained in terms of the doubly-dressed atom model.

Finally we point out that while the multiphoton AC Stark fluorescence spectrum has not yet been observed experimentally, the Autler-Townes spectrum *has*

[†] Inclusion of the counter-rotating terms into the interaction V_2 couples doublets from different manifolds, and yields additional shifts of order Ω_2^2/ω_0.

been observed [18]. Furthermore a minimum has been seen in the splitting of the Autler-Townes doublets in agreement with the expressions presented here.

References

[1] Y. Zhu, Q. Wu, A. Lezama, D.J. Gauthier and T.W. Mossberg, Phys. Rev. A **41**, 6574 (1990); H.S. Freedhoff and Z. Chen, Phys. Rev. A **41**, 6013 (1990); S.P.Tewari and M.K. Kumari. Phys. Rev. A **41**, 5273 (1990); G.S. Agarwal, Y. Zhu, D.J. Gauthier and T.W. Mossberg, J. Opt. Soc. Am. B **8**, 1163 (1991); G.S. Agarwal and Y. Zhu, Phys. Rev. A **46**, 479 (1992); Z. Ficek and H.S. Freedhoff, Phys, Rev. A **48**, 3092 (1993); M. Elk and P. Lambropoulos, Phys. Rev. A **50**, 1490 (1994); G.S. Agarwal, W. Lange and H. Walther, Phys. Rev. A **51**, 721 (1995); H.S. Freedhoff and Z. Ficek, Phys. Rev. A **55**, 1234 (1997); C.C. Yu, J.R. Bochinski, T.M.V. Kordich, T.W. Mossberg and Z. Ficek, Phys. Rev. A **56**, R4381 (1997).

[2] M.F. Van Leeuwen, S. Papademetriou and C.R. Stroud Jr., Phys. Rev. A **53**, 991 (1996); S. Papademetriou, M.F. Van Leeuwen and C.R. Stroud Jr., Phys. Rev. A **53**, 997 (1996).

[3] G.I. Toptygina and E.E. Fradkin, Zh. Eksp. Teor. Fiz. **82**, 429 (1982) [Sov.Phys. -JEPT **55**, 246 (1982)]; R. Guccione-Gush and H.P.Gush, Phys. Rev. A **10**, 1474 (1974); H. Friedmann and A.D. Wilson-Gordon, Phys. Rev. A **36**, 1333 (1987); G.S. Agarwal and N. Nayak, Phys. Rev. A **33**, 391 (1986); J.H. Eberly and V.D. Popov, Phys. Rev. A **37**, 2012 (1988); Y. Zhu, Q. Wu, S. Morin and T.W. Mossberg, Phys. Rev. Lett. **65**, 1200 (1990); S. Papademetriou, S.M.

Chakmakjian and C.R. Stroud Jr., J. Opt. Soc. Am. B **9**, 1182 (1992); N.B. Manson, C. Wei and J.P.D Martin, Phys. Rev. Lett. **76**, 3943 (1996); B. Lounis, F. Jelezko and M. Orrit, Phys. Rev. Lett. **78**, 3673 (1997).

[4] T.G. Rudolph, H.S. Freedhoff, and Z. Ficek, Optics Commun. (in press); T.G. Rudolph, H.S. Freedhoff and Z. Ficek, Phys. Rev. A (in press).

[5] T.W. Mossberg and M. Lewenstein, Phys. Rev. A **39**, 163 (1989); Q. Wu, D.J. Gauthier and T.W. Mossberg, Phys. Rev. A **49**, R1519 (1994); S.F. Chien, M.R.B. Wahiddin and Z. Ficek, Phys. Rev. A **57**, 1295 (1998).

[6] G.S. Agarwal and W. Harshawardhan, Phys. Rev. A **50**, R4465 (1994).

[7] Z. Ficek and H.S. Freedhoff, Phys. Rev. A **53**, 4275 (1996).

[8] E. Arimondo, in *Progress in Optics* XXXV, edited by E. Wolf (Elsevier, Amsterdam, 1996), p.257; S.Y. Zhu, R.C.F. Chan and C.P. Lee, Phys. Rev. A **52**, 710 (1995); S.E.Harris, Phys. Rev. Lett. **62**, 1033 (1989); P. Zhou and S. Swain, Phys. Rev. A **56**, 3011 (1997).

[9] S.Y. Zhu and M.O. Scully, Phys. Rev. Lett. **76**, 388 (1996); H. Lee, P. Polynkin, M.O. Scully and S.Y. Zhu, Phys. Rev. A **55**, 4454 (1997); G.S. Agarwal, Phys. Rev. A **55**, 2457 (1997).

[10] J.M. Courty and S. Reynaud, Europhys. Lett. **10**, 237 (1989); C. Cabrillo, W.S. Smyth, S. Swain and P. Zhou, Optics Commun. **114**, 344 (1995).

[11] M. Lewenstein, T.W. Mossberg and R.J. Glauber, Phys. Rev. Lett. **59**, 775 (1987); S. Haroche and D. Kleppner, Phys. Today **42**(1), 24 (1989).

[12] M. Lax, Phys. Rev. **172**, 350 (1968).

[13] H. Risken, *The Fokker - Planck Equation* (Springer - Verlag, Berlin, 1984), Chap. 9.

[14] C. Cohen - Tannoudji and S. Reynaud, J. Phys. B **10**, 345 (1997); C. Cohen-Tannoudji, J. Dupont-Roc and G. Grynberg, *Atom-Photon Interactions* (Wiley, New York, 1992).

[15] L. Ballentine, *Quantum Mechanics* (Englewood Cliffs NJ: Prentice Hall, 1990).

[16] W.M. Ruyten, J.Opt.Soc. Am. B **6**, 1796 (1989); Phys. Rev. A **40**, 1447 (1989); J. Opt. Soc. Am. B **9**, 1892 (1992); Phys. Rev. A **46**, 4077 (1992).

[17] F. Bloch and A. Siegert, Phys. Rev. **57**, 522 (1940).

[18] A. Greentree, C. Wei and N. Manson, *private communication.*

5. Dressing the Atom in Fields of Three Different Frequencies

5.1 Introduction

In the previous two chapters we considered the case of bichromatic driving; in particular we concentrated on the multiphoton AC Stark and associated effects. We saw that the spectra could be very different and much more intricate than the spectra associated with monochromatic driving. In this chapter, the case of trichromatic driving will be considered, and we will see that the results are in fact quite different again to those of bichromatic driving.

The case of trichromatic driving on which we will focus is that which corresponds to driving the atom with an amplitude modulated (AM) field. An AM field is characterised by a central (carrier) component of frequency $\omega_1 = \omega_0 + \Delta$, where ω_0 is the atomic transition frequency, and modulation frequency δ, which corresponds to two sideband frequencies equally detuned from ω_1: $\omega_\pm = \omega_1 \pm \delta$. A 100% AM field (with carrier suppressed) is a bichromatic field consisting only of the frequencies $\omega_\pm$ and has been studied previously [1-3].

The limited number of previous studies of an atom driven by an AM field have mainly used numerical techniques, such as solving the Bloch equations [4], or occasionally techniques using semi-classical dressed states in addition to numerical work [5]. In this chapter we will use the fully quantum dressed states to explain a few of the many possible phenomena associated with trichromatic driving.

In particular we will focus in this chapter on obtaining results in as physical a manner as possible. The "derivation" (limited as it was) of the fluorescence spectrum given in Chapters 2 and 3 is actually there to persuade the reader that a rigorous derivation is *possible*. Certainly it is often unnecessary. Expressions such as (3.39) for the fluorescence spectrum follow intuitively from an understanding of the dressed atom dynamics. In the last section of this Chapter, we will briefly describe an interesting exception to this which has still not been completely resolved.

In this chapter we consider an atom with excited (ground) state $|e\rangle$ ($|g\rangle$), transition frequency ω_0 and transition dipole moment $\vec{\mu}$, that is driven by an AM field. The central component of the field, ω_1, has (on resonance) Rabi frequency $2\Omega_1$. The two sideband fields of frequencies $\omega_\pm$ have the same (on resonance) Rabi frequency $2\Omega_2$.

The chapter is organised as follows: In section 5.2 we consider the case of weak amplitude modulation ($\Omega_2 < \Omega_1$) and a small detuning ($\delta < \Omega_1$) of the sideband fields. In the next section we describe the reverse situation, in which the modulation is strong and the central field component weak ($\Omega_1 < \Omega_2$). In the last section we briefly consider the special case that the detuning of the two sideband fields is at the Rabi frequency of the central component ($\delta = 2\Omega_1$).

5.2 Weak amplitude modulation, small detuning

In this section we consider the situation in which our atom is driven by a weakly amplitude modulated field, whose modulation frequency is also small compared to Ω_1, *i.e.* δ, $\Omega_2 < \Omega_1$.

Since the central field is strong, we dress around it first to obtain the familiar singly-dressed states

$$\begin{aligned} |N+\rangle &= \sin\theta|g,N\rangle + \cos\theta|e,N-1\rangle \\ |N-\rangle &= \cos\theta|g,N\rangle - \sin\theta|e,N-1\rangle, \end{aligned} \tag{5.1}$$

where

$$\sin^2\theta = \frac{1}{2} + \frac{\Delta}{4G},$$

and the generalised Rabi frequency is given by

$$2G = \sqrt{4\Omega_1^2 + \Delta^2}. \tag{5.2}$$

Next we include the two sideband fields. In particular, we consider the two states

$$|n_N^{\pm}\rangle \equiv |(N-2M-n)\pm, M+n, M\rangle, \tag{5.3}$$

where the second (third) term in the tensor product is that of the number of photons in the ω_+ (ω_-) mode, and n is an integer ($N > M > n$). These states have energies (before interaction) of $N\omega_1 \pm G + n\delta$. Thus on manifold $\epsilon(N)$ they form two submanifolds of states which are separated by $2G$. Each submanifold in

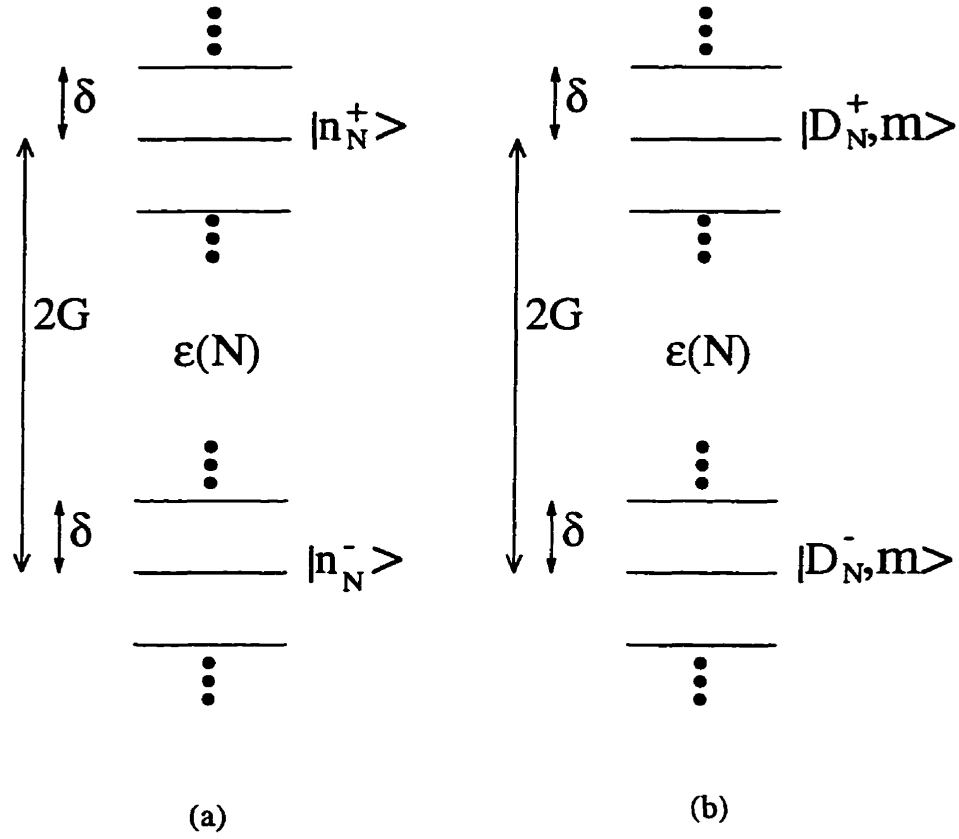

(a) (b)

Figure 5.1 (a) The energy structure of a singly-dressed atom driven by a weakly modulated field, before interaction. (b) The energy structure of the doubly-dressed states, which is identical to that of the singly-dressed states. Notice that the *single* manifold $\epsilon(N)$ is split into two submanifolds separated by $2G$, with each submanifold consisting of states separated by δ.

turn contains an infinite set of states separated by δ, as shown in Figure 5.1(a). At this stage we should point out that the state $|n_N^{\pm}\rangle$ is not the most general possible; it is just one of the more general set of states $|(N-2M-p-m)\pm, M+p, M+m\rangle$ which have the same energy for a fixed value of $p-m$. In some sense then, we are assuming that all such states are equivalent as far as the interaction operators $V_{\pm}$ are concerned. This can only be justified *a posteriori*, when we see what sort of agreement we obtain with numerical and experimental results.

It is not difficult to show that the action of the total Hamiltonian ($H = H_0 + V_+ + V_-$) on the state $|n_N^{\pm}\rangle$ is

$$H|n_N^{\pm}\rangle \approx (N\omega_1 \pm G + n\delta)\,|n_N^{\pm}\rangle \pm 2\Omega_2 \sin\theta\cos\theta\left(|(n+1)_N^{\pm}\rangle + |n-1_N^{\pm}\rangle\right) \quad (5.4).$$

By "approximately equals" in (5.4) we mean two things. Firstly the states on the right are the only states which lie on the same energy submanifold as the state on the left (as is standard within perturbation theory). Secondly it indicates that in fact we have approximated $M + 1 \approx M$ for some of the states. This can be justified by saying that ultimately we will be interested in the reduced populations and coherences, for which this approximation is made explicitly.

We now assume that the eigenstates take the form of an infinite sum over all possible connected states, *i.e.*

$$|D_N\pm, m\rangle = \sum_{n=-\infty}^{\infty} a_n^{N\pm}|n_N^{\pm}\rangle. \quad (5.5)$$

Here D labels a doubly-dressed state, while m labels the eigenvalues of H -which we are yet to determine. However (5.4) and (5.5) are analogous to equations in [1], and we can invoke the same symmetry arguments to show that the eigenvalues of H are $m\delta$ with m any integer.

Applying H to the dressed state $|D_N\pm, m\rangle$ and then multiplying on the left by $\langle n_N^{\pm}|$ produces the recursion relation

$$\delta(n-m)a_n^{N\pm} \pm 2\Omega_2 \sin\theta\cos\theta(a_{n+1}^{N\pm} + a_{n-1}^{N\pm}) = 0. \quad (5.6)$$

This recursion relation has the solution

$$a_n^{N\pm} = J_{n-m}(\mp x), \tag{5.7}$$

where $x = (4\Omega_2 \sin\theta\cos\theta)/\delta$, and $J_{n-m}(x)$ is the Bessel function of the first kind. Thus the doubly-dressed states on $\epsilon(N)$ (shown in Figure 5.1(b)) have exactly the same energy structure as the singly-dressed states (Figure 5.1(a)). This is a result of the high degree of symmetry in the driving fields, and can be thought of as equal "pushes" up and down on each state by the sideband fields.

Following the (by now hopefully familiar!) standard procedure, we next compute the transition rates. The transition from $|D_{N+1}\pm, l\rangle$ to $|D_N\pm, m\rangle$, which occurs with transition frequency $\omega_{l-m}^{\pm\pm} = \omega_1 + (l-m)\,\delta$, is governed by the transition rate

$$\begin{aligned}\Gamma_{l-m}^{\pm\pm} &= \Gamma|\langle D_{N+1}\pm, l|S^+|D_N\pm, m\rangle|^2 \\ &= \Gamma|\pm\sum_n J_{n-l}(\mp x)J_{n-m}(\mp x)\sin\theta\cos\theta|^2 \\ &= \Gamma\sin^2\theta\cos^2\theta\,\delta_{lm},\end{aligned} \tag{5.8}$$

where we have used a well known Bessel function summation relation [6], and $\Gamma = |\vec{\mu}|^2$ is the natural linewidth. For transitions from $|D_N\pm, m\rangle$ to $|D_{N+1}\mp, l\rangle$, which occur with transition frequency $\omega_{l-m}^{\pm\mp} = \omega_1 \pm 2G + (l-m)\delta$, we find the transition rates

$$\begin{aligned}\Gamma_{lm}^{+-} &= \Gamma|\langle D_{N+1}+, l|S^+|D_N-, m\rangle|^2 \\ &= \Gamma|\sum_n J_{n-l}(-x)J_{n-m}(x)\cos^2\theta|^2 \\ &= \Gamma\cos^4\theta J_{l-m}^2(2x),\end{aligned} \tag{5.9}$$

and

$$\begin{aligned}\Gamma^{-+}_{l-m} &= \Gamma|\langle D_{N+1}-, l|S^+|D_N+, m\rangle|^2 \\ &= \Gamma|-\sum_n J_{n-l}(x)J_{n-m}(-x)\sin^2\theta|^2 \\ &= \Gamma\sin^4\theta J^2_{l-m}(2x).\end{aligned} \tag{5.10}$$

Thus we expect the Mollow sidebands to be split into an infinite number of components, with intensities of the split components proportional to $J^2_{l-m}(2x)$.

At this stage we have a good idea of what the spectrum will look like. In fact all we need are the linewidths and steady state populations. These are found by projecting the master equation

$$\frac{\partial\rho}{\partial t} = -i[H,\rho] - \frac{\Gamma}{2}(S^+S^-\rho + \rho S^+S^- - 2S^-\rho S^+), \tag{5.11}$$

onto the dressed states, and finding equations of motion for the populations and coherences. When we do so (employing the secular approximation), we find for the populations

$$\dot{\rho}^{\pm}_{mm} = -\Gamma^{\pm\mp}_0\rho^{\pm}_{mm} + \Gamma^{\mp\pm}_0\rho^{\mp}_{mm}. \tag{5.12}$$

where $\rho^{\pm}_{mm} = \langle D_N\pm, m|\rho|D_N\pm, m\rangle$. Thus the reduced populations $\Pi^{\pm} = \sum_m \rho^{\pm}_{mm}$ have steady state solutions

$$\begin{aligned}\Pi^+_{ss} &= \frac{\sin^4\theta}{\cos^4\theta+\sin^4\theta} \\ \Pi^-_{ss} &= \frac{\cos^4\theta}{\cos^4\theta+\sin^4\theta}.\end{aligned} \tag{5.13}$$

From equation (5.12) we deduce that the linewidth of the central component of our spectrum is $\Gamma_c = \cos^4\theta + \sin^4\theta$.

The coherences $\varrho_{lm}^{\pm\mp} = \langle D_{N+1}\pm, l|\rho|D_N\mp, m\rangle$ are found to obey the equations of motion

$$\dot{\varrho}_{lm}^{+-} = \left(i\omega_{l-m}^{\pm\mp} - \Gamma_s\right)\varrho_{lm}^{+-}. \tag{5.14}$$

In (5.14) $\Gamma_s = \Gamma(\frac{1}{2} + \cos^2\theta\sin^2\theta)$ will be the linewidth of the sideband spectral components.

It is now a simple matter to write down the fluorescence spectrum. It is given by

$$\begin{aligned} S(\omega) = & \frac{(\Gamma_0^{++}\Pi_{ss}^{+} + \Gamma_0^{--}\Pi_{ss}^{-})\Gamma_c}{(\omega-\omega_1)^2+\Gamma_c^2} \\ & + \sum_k J_k^2(2x)\left(\frac{\Pi_{ss}^{+}\cos^4\theta\Gamma_s}{(\omega-\omega_k^{+-})^2+\Gamma_s^2} + \frac{\Pi_{ss}^{-}\sin^4\theta\Gamma_s}{(\omega-\omega_k^{-+})^2+\Gamma_s^2}\right) \end{aligned} \tag{5.15}$$

The fluorescence spectrum is plotted in Figure 5.2, for the case of an on-resonance carrier field of Rabi frequency $2\Omega_1 = 40\Gamma$, sideband fields detuned by $\delta = 5\Gamma$ and different values of $2\Omega_2$. We see that the weak (modulation) bichromatic field modifies the sidebands of the Mollow triplet dramatically, while leaving the central feature unaffected.

The weak probe absorption spectrum can now also be simply written down. It is given by

$$W(\omega_p) = \sum_k J_k^2(2x)\left(\frac{(\Pi_{ss}^{-}-\Pi_{ss}^{+})\cos^4\theta\Gamma_s}{(\omega_p-\omega_k^{+-})^2+\Gamma_s^2} + \frac{(\Pi_{ss}^{+}-\Pi_{ss}^{-})\sin^4\theta\Gamma_s}{(\omega_p-\omega_k^{-+})^2+\Gamma_s^2}\right) \tag{5.16}$$

This expression is plotted in Figure 5.3 for parameter values $\Delta = 2\Gamma$, $\delta = 5\Gamma$, $2\Omega_1 = 40\Gamma$ and $2\Omega_2 = 12\Gamma$. Notice that since the absorption spectrum depends on the population difference between dressed states, we must have a detuned central

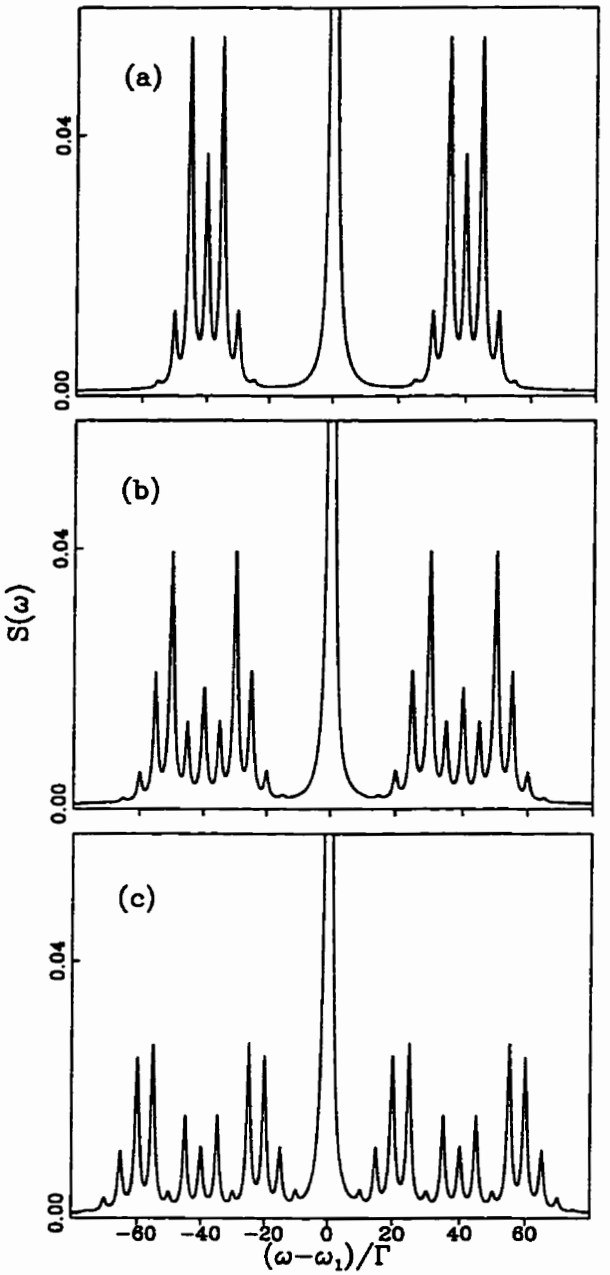

Figure 5.2 The fluorescence spectrum of a two-level atom driven by a weakly modulated field. The spectrum is shown for $\Delta = 0$ (central field exactly on resonance), $\delta = 5\Gamma$, $2\Omega_1 = 40\Gamma$ and (a) $2\Omega_2 = 4\Gamma$, (b) $2\Omega_2 = 8\Gamma$, (c) $2\Omega_2 = 12\Gamma$. The central peak has a maximum at 0.5.

field $\Delta \neq 0$) to obtain a non-vanishing spectrum (within the secular approximation).

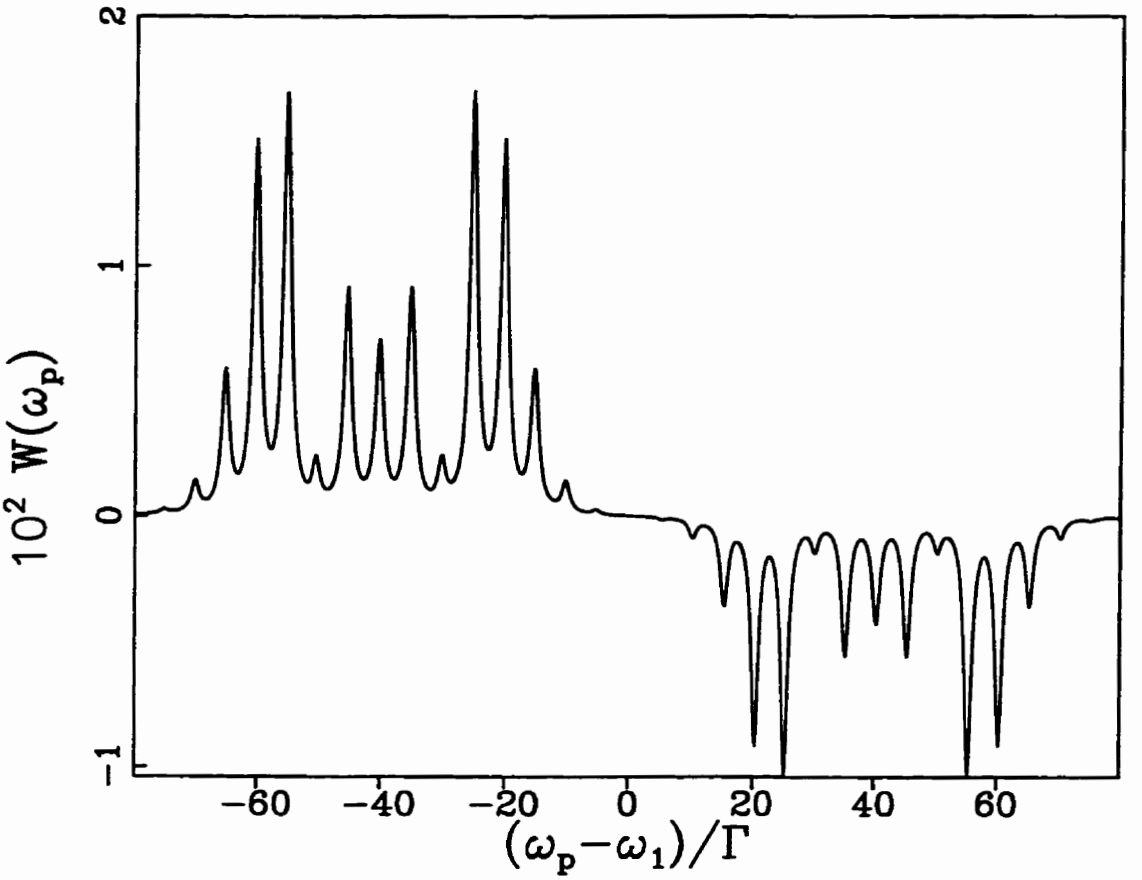

Figure 5.3 The weak probe absorption spectrum of an atom driven by a weakly modulated field. The spectrum is shown for $\Delta = 2\Gamma$, $\delta = 5\Gamma$, $2\Omega_1 = 40\Gamma$ and $2\Omega_2 = 12\Gamma$.

The last spectrum we will consider in this section is the Autler-Townes spectrum. As before, we consider the transition from $|g\rangle$ to a third atomic level $|c\rangle$ of energy (measured from $|g\rangle$) ω_c, which is probed by a weak field of frequency ω_3. The intensities of the lines in the Autler Townes doublets are given by

$$\begin{aligned}\Lambda_m^+ &= |\langle D_N\pm, m|g, N-2M, M, M\rangle|^2 \\ &= |\sin\theta J_{-m}(\mp x)|^2 \\ &= \sin^2\theta J_m^2(x),\end{aligned} \tag{5.17}$$

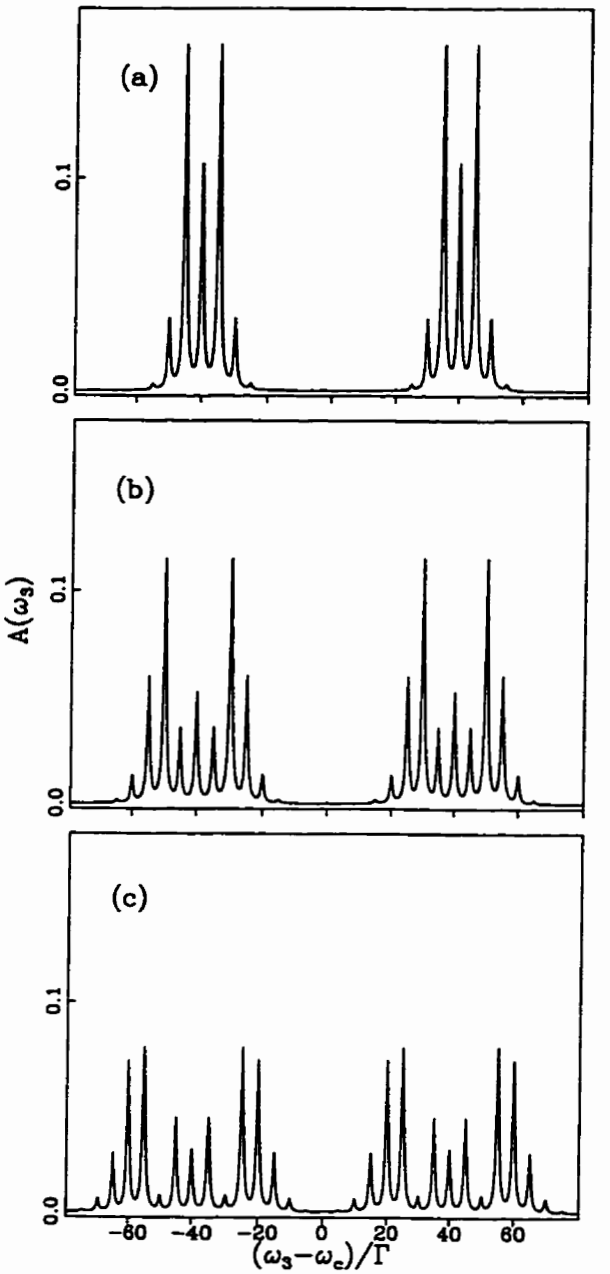

Figure 5.4 The Autler-Townes absorption spectrum of an atom in a weakly modulated field. The spectrum is shown for $\Delta = 0$ (central field exactly on resonance), $\delta = 5\Gamma$, $2\Omega_1 = 40\Gamma$, $\Gamma_3 = \Gamma$ and (a) $2\Omega_2 = 8\Gamma$, (b) $2\Omega_2 = 16\Gamma$, (c) $2\Omega_2 = 24\Gamma$.

and similarly

$$\Lambda_m^- = \cos^2\theta J_m^2(x). \tag{5.18}$$

The linewidths of the Autler-Townes peaks are given by

$$\Gamma_a = \frac{1}{2}(\Gamma_s + \Gamma_3), \tag{5.19}$$

where Γ_3 is the natural linewidth of the third level. Accordingly the Autler-Townes spectrum is given by the expression

$$A(\omega_3) = \sum_k \frac{1}{4} J_k^2(x) \Big(\frac{\Pi_{ss}^+ \sin^2\theta \Gamma_a}{(\omega_3 - \omega_c + G + k\delta)^2 + \Gamma_a^2} + \frac{\Pi_{ss}^- \cos^2\theta \Gamma_a}{(\omega_3 - \omega_c - G + k\delta)^2 + \Gamma_a^2} \Big). \tag{5.20}$$

The spectrum (5.20) is plotted in Figure 5.4, for $\Delta = 0$ (central field exactly on resonance), $\delta = 5\Gamma$, $2\Omega_1 = 40\Gamma$, $\Gamma_3 = \Gamma$ and different values of $2\Omega_2$.

5.3 Strong amplitude modulation

In this section we consider the case that the amplitude modulation is strong ($\Omega_1 < \Omega_2$). The atom is therefore seeing a strong, symmetrically detuned bichromatic field, and a weaker, near resonance, central field. Consider the pairs of states on $\epsilon(2M + N)$:

$$|(2M + N)(2n)\pm\rangle \equiv |N\pm, M + n, M - n\rangle \tag{5.21a}$$

and

$$|(2M + N)(2n + 1)\pm\rangle \equiv |(N - 1)\pm, M + n, M - n\rangle, \tag{5.21b}$$

where, as before, the first state in the tensor product corresponds to the atom and ω_1 (the central component) and the other two states to ω_+ and ω_- respectively. Note that we have used the $|N\pm\rangle$ states for the atom+central component of

the field. This does not mean we have included the interaction yet with this component (it is after all weaker than the other two); rather it reflects the freedom we have in choosing an undressed basis. Hopefully we have made an intelligent choice; that of course can be seen only when we attempt the second dressing. These states have energies $(N+2M)\omega_0 + N\Delta + 2n\delta$ and $(N+2M)\omega_0 + N\Delta + (2n+1)\delta$ respectively. In this section we will consider only the case $\Delta = 0$, that is the weak central component is exactly on resonance.

Since the $\omega_\pm$ modes are now the strongest, we dress first around them. We should expect that such a diagonalisation would be a nontrivial mathematical exercise. We are helped, however, by having the solution to the case of pure (symmetrically detuned) bichromatic driving [1], and so we make the (educated?) guess that the singly dressed states are the following superpositions of the states (5.21):

$$|m\pm; 2M+N\rangle = \sum_{n=-\infty}^{\infty} J_{n-m}(\mp x)|(2M+N)n\pm\rangle \qquad (5.22),$$

where $x = 2\Omega_2/\delta$. To verify that the states (5.22) *are* actually the eigenstates requires some algebra, and is left as an exercise for the interested reader. In particular, since the states $|m+; 2M+N\rangle$ and $|m-; 2M+N\rangle$ are degenerate with energies $(2M+N)\omega_0 + m\delta$, we must examine $\langle m-; 2M+N|(V_+ + V_-)|m+; 2M+N\rangle$, where $V_\pm$ are the interaction terms for the $\omega_\pm$ modes. It turns out that the

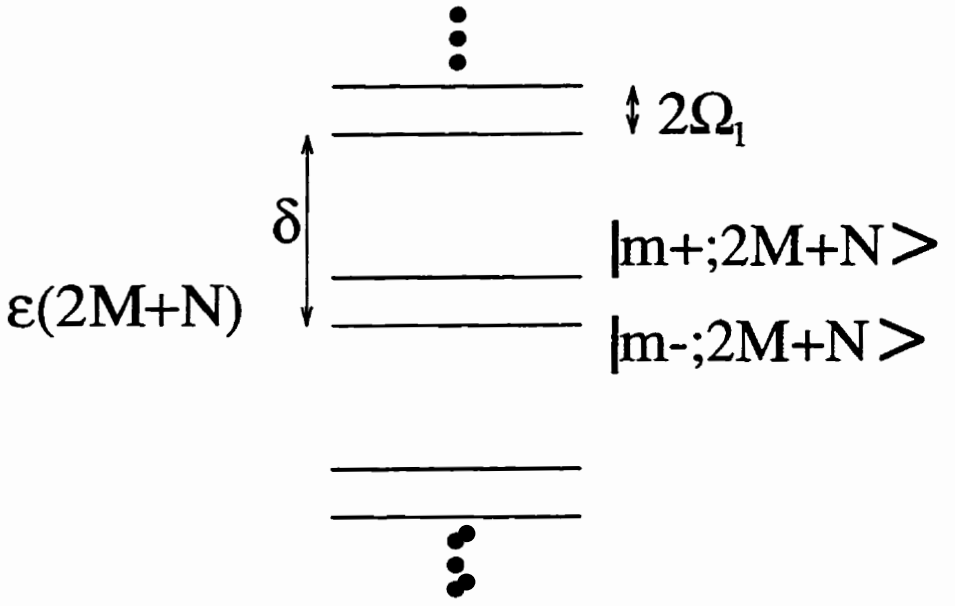

Figure 5.5 The dressed state energy structure for an atom in a strongly modulated field. The manifold consists of an infinite number of doublets, with an intra-doublet separation $2\Omega_1$ and an inter-doublet separation δ.

plus and minus states *are* decoupled; we find

$$\begin{aligned}
&\langle m-;2M+N|(V_+ + V_-)|m+;2M+N\rangle \\
&= \frac{1}{2}\sqrt{M}(-1)^m \sum_n \Big(J_{2n-m}(x)J_{2n+1-m}(x) + J_{2n+1-m}(x)J_{2n+2-m}(x) \\
&+ J_{2n-1-m}(x)J_{2n-m}(x) + J_{2n-m}(x)J_{2n+1-m}(x) \Big) \qquad (5.23) \\
&= \sqrt{M}(-1)^m \sum_n \Big(J_{2n}(x)J_{2n+1}(x) + J_{2n+1}(x)J_{2n+2}(x) \Big) \\
&= 0.
\end{aligned}$$

We must now include the weak central field to find the correct doubly - dressed states. This involves diagonalising V_0 (the central mode interaction term) on the degenerate subspace spanned by the $|m\pm;2M+N\rangle$ states. By lucky coincidence† the states $|m\pm;2M+N\rangle$ can easily be shown to already be diagonal on V_0, and

† Well maybe not so lucky - you will see now why we chose the states (5.21) as we did!

so they are not mixed (to zeroth order in perturbation theory). We therefore find that the first-order corrections to the energies of the states $|m+;2M+N\rangle$ and $|m-;2M+N\rangle$ are $\pm\Omega_1$, respectively. Thus the dressed states on $\epsilon(2M+N)$ consist of an infinite series of doublets separated by δ, with intradoublet splitting $2\Omega_1$; the energy structure is shown in Figure 5.5.

One does not have to have been more than barely awake while reading this thesis to know that the next step in our calculations is computation of the transition rates between the dressed states. At this stage, if only by simple analogy with the energy structure of the dressed states of Chapter 3, one might expect the spectrum to consist of a series of triplets, with inter-triplet spacing δ and intra-triplet splitting $2\Omega_1$. It turns out, however, that the transition from $|l\pm;2M+N\rangle$ to $|m\pm;2M+N-1\rangle$, which occurs with transition frequency $\omega_{l-m}^{\pm\pm}=\omega_0+(l-m)\delta$, is governed by the transition rate

$$\begin{aligned}\Gamma_{l-m}^{\pm\pm} &= |\langle l\pm;2M+N|S^+|m\pm;2M+N-1\rangle|^2 \\ &= \frac{1}{4}\Gamma\delta_{lm}.\end{aligned} \tag{5.24}$$

From this we see that the only central component in the spectrum which will be nonvanishing is the one at ω_0. For transitions from $|l\pm,2M+N\rangle$ to $|m\mp;2M+N-1\rangle$, which occur with transition frequency $\omega_{l-m}^{\pm\mp}=\omega_0\pm 2\Omega_1+(l-m)\delta$, we find the transition rates

$$\begin{aligned}\Gamma_{l-m}^{\pm\mp} &= |\langle l\pm;2M+N|S^+|m\mp;2M+N-1\rangle|^2 \\ &= \frac{1}{4}\Gamma J_{l-m}^2(2x),\end{aligned} \tag{5.25}$$

Thus we expect the spectral features (apart from the central triplet) to consist of a series of doublets, centred at $k\delta$ (where k is an integer), with doublet intensities proportional to $J_k^2(2x)$.

We now require the steady state populations and the linewidths. These are easily obtained, in the usual manner, by projecting the master equation onto the dressed states and employing the secular approximation. We find that the steady state populations are equal, *i.e.*

$$\Pi_{ss}^{\pm} = \frac{1}{2}, \tag{5.26}$$

and that the central component linewidth is given by

$$\Gamma_c = \frac{\Gamma}{2}, \tag{5.27}$$

while the sideband linewidths are

$$\Gamma_s = \frac{3\Gamma}{4}. \tag{5.28}$$

These widths are surprising: they are exactly the values obtained for monochromatic, on-resonance, driving. It was found previously [1] for the case of symmetrically detuned bichromatic driving, that the linewidths are different for the even or odd sidebands. Thus it appears that in the limit of $\Omega_1 \to 0$, our spectrum will not go to that of [1]. The resolution of this apparent paradox lies in the assumptions which are made when performing dressed atom calculations. In order to compute a spectrum for this system we have to employ the secular approximation, which in turn requires that $\Omega_1 \gg \Gamma$. If this is true (as we have assumed it to be), then

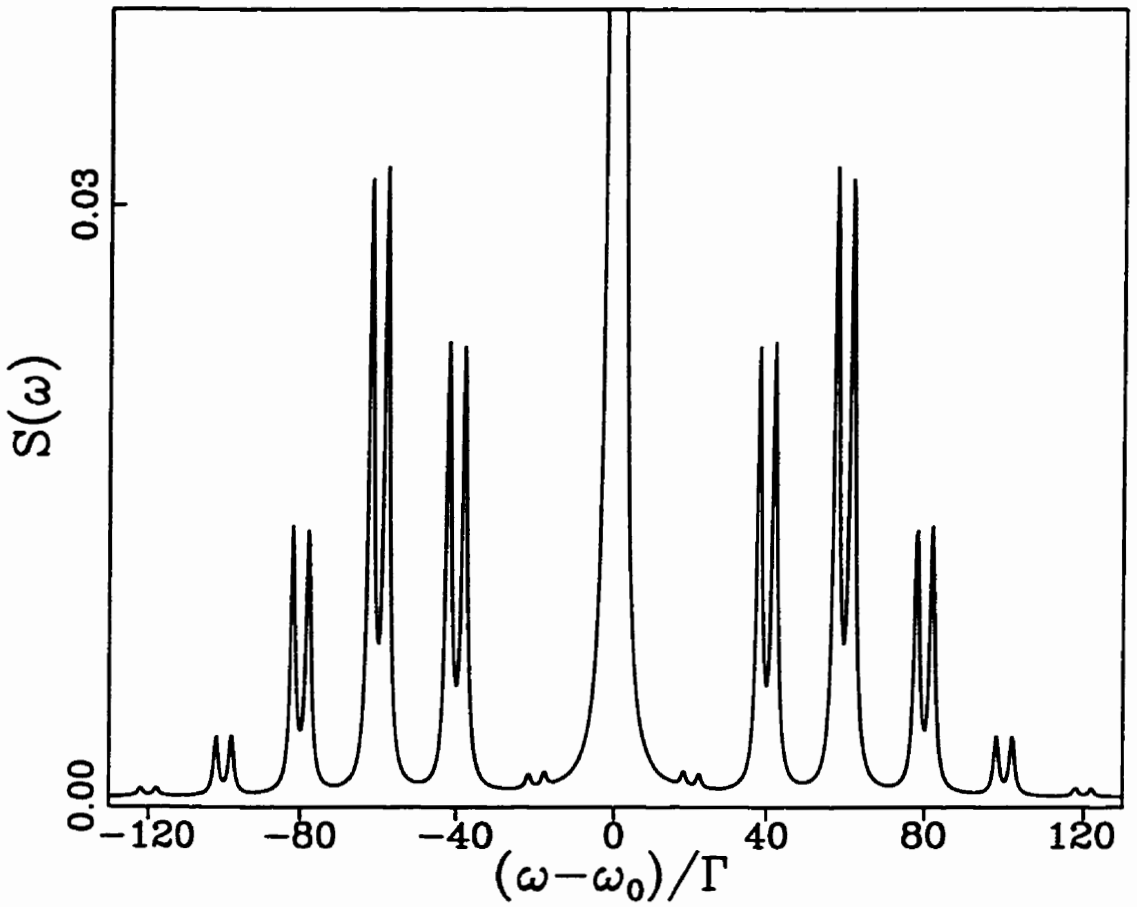

Figure 5.6 The fluorescence spectrum of an atom in a strongly modulated field. The spectrum is shown for $2\Omega_2 = 40\Gamma$, $\delta = 20\Gamma$ and $2\Omega_1 = 2\Gamma$. For larger values of $2\Omega_1$, the central component of the spectrum can be seen to split into a triplet.

we make the approximation $\sqrt{N} \approx \sqrt{N \pm 1} \approx \sqrt{N \pm 2} \approx \ldots$, and this effectively "smears" away the $N \to 0$ limit of our model.

The fluorescence spectrum is given by

$$S(\omega) = \frac{(\Gamma_0^{++}\Pi_{ss}^{+} + \Gamma_0^{--}\Pi_{ss}^{-})\Gamma_c}{(\omega - \omega_0)^2 + \Gamma_c^2} + \sum_k \frac{1}{4} J_k^2(2x) \left(\frac{\Pi_{ss}^{+}\Gamma_s}{(\omega - 2\Omega_1 - k\delta)^2 + \Gamma_s^2} + \frac{\Pi_{ss}^{-}\Gamma_s}{(\omega + 2\Omega_1 - k\delta)^2 + \Gamma_s^2} \right) \tag{5.29}$$

This spectrum is plotted in Figure 5.6 for $2\Omega_2 = 40\Gamma$, $\delta = 20\Gamma$ and $2\Omega_1 = 2\Gamma$. As expected, the spectrum consists of doublets spaced at integer multiples of δ, with an intra-doublet splitting of $4\Omega_1$, and a triplet at $\omega = \omega_0$.

The only other spectrum we will consider is the Autler-Townes absorption spectrum. In the notation of the previous section, we calculate the doublet intensities and find them to be given by

$$\Lambda_m^{\pm} = |\langle g, N, M, M | m\pm; 2M + N\rangle|^2 = \frac{1}{2} J_m^2(x). \tag{5.30}$$

The Autler-Townes spectrum can now be written down:

$$\begin{aligned} A(\omega_3) = \sum_k J_k^2(x) \Big(& \frac{\Pi_{ss}^{+} \Lambda_0^{+} \Gamma_a}{(\omega_3 - \omega_c + \Omega_1 + k\delta)^2 + \Gamma_a^2} \\ & + \frac{\Pi_{ss}^{-} \Lambda_0^{-} \Gamma_a}{(\omega_3 - \omega_c - \Omega_1 + k\delta)^2 + \Gamma_a^2} \Big). \end{aligned} \tag{5.30}$$

This spectrum is plotted in Figure 5.7, for $2\Omega_2 = 40\Gamma$, $\delta = 20\Gamma$, $\Gamma_3 = \Gamma$ and $2\Omega_1 = 4\Gamma$.

5.4 Sideband fields detuned to the Rabi frequency of the central component

In this section we briefly consider a case of trichromatic driving that is *not* easily solved within the dressed atom model. This is not to say that it *cannot* be, rather I have not been smart enough to do so. The case of interest is that in which we have weak amplitude modulation ($\Omega_2 < \Omega_1$), but the sideband fields are detuned to the Rabi frequency of the central field *i.e.* $\delta = 2\Omega_1$. (Recall that the discussion in Section 5.2 was limited to the case $\delta < \Omega_1$.) This particular choice

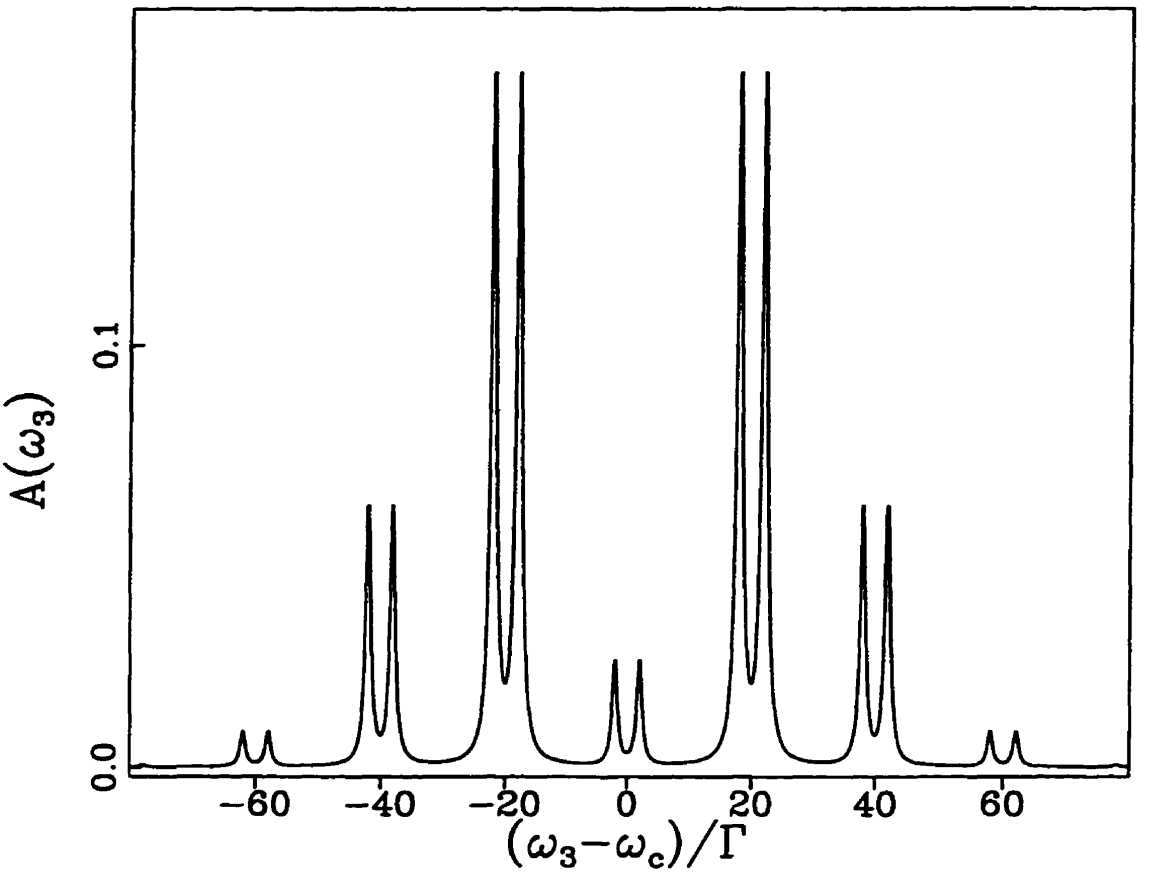

Figure 5.7 The Autler-Townes spectrum of an atom in a strongly modulated field. The spectrum is shown for $2\Omega_2 = 40\Gamma$, $\delta = 20\Gamma$, $\Gamma_3 = \Gamma$ and $2\Omega_1 = 4\Gamma$.

of δ is analogous to an $n = 1$ trichromatic version of the case studied in Chapter 3. The difference is that the two (weak) sideband fields $\omega_\pm$ can couple to the singly dressed states $|N\pm\rangle$ in an infinite "cascade", as shown in Figure 5.8(a).

The system has several unusual features. The first of these relates to performing a numerical simulation. It was found, using the Bloch equations, that the fluorecence spectrum consisted of normal lorentzians; however there was a dependence of some spectral line intensities on the phase difference between one sideband field and the other two fields. At first glance we might have expected

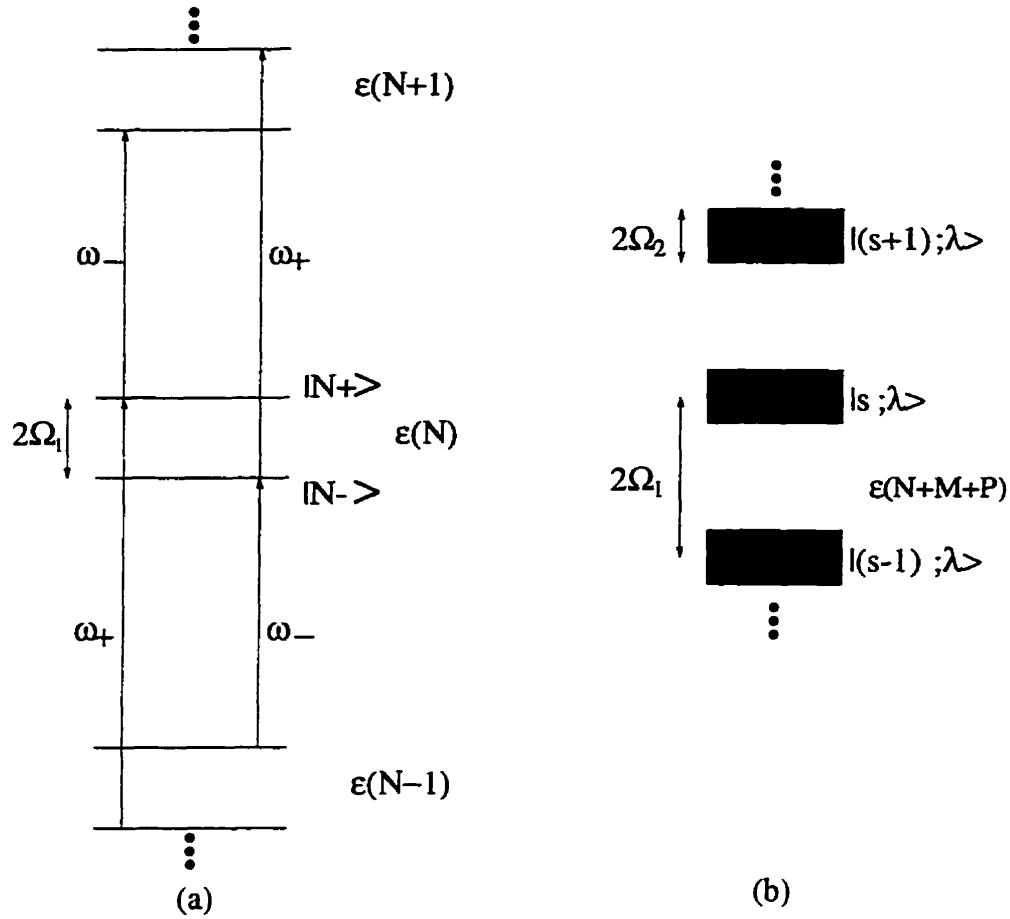

Figure 5.8 The energy structure of an atom in a weakly modulated field with sideband frequencies $\omega_\pm$ detuned to the Rabi frequency of the central field. (a) The singly dressed atom with arrows indicating the absorption of $\omega_\pm$ photons. (b) The energy structure of the doubly dressed atom. The manifold consists of an infinite number of continua of width $2\Omega_2$, with continua separated by $2\Omega_1$.

that since the detuning δ is large compared to Γ, as are the Rabi frequencies involved, any phase dependence would "wash out". Furthermore, this is a concern for those of us who use the dressed atom model because the model is most easily used with number states, and thus cannot easily take phase into consideration.

Another interesting phenomenon was noticed in an experiment on the Autler-Townes spectrum of this system [7]. In the experiment the phase of the fields was

not fixed in any way, and the spectrum appeared to consist of pairs of *continua* centred at $\pm\Omega_1$ of width approximately $2\Omega_2$.

Since the central field is assumed strong (weak modulation), we dress first around it. To find the dressed states for the system correct to zeroth order in perturbation theory, we first recognise that the pairs of states

$$|a_p^s\rangle \equiv |(N-2p-s)+, P+p+s, M+p\rangle \tag{5.31}$$

and

$$|b_p^s\rangle \equiv |(N-2p-s-1)-, P+p+s+1, M+p\rangle, \tag{5.32}$$

are degenerate with energies $E^s_{NMP} = (N+M+P)\omega_0 + (2s+1)\Omega_1$. Here $p = \ldots -2, -1, 0, 1, 2 \ldots$. Thus on manifold $\epsilon(N+M+P)$ there are an infinite number of states (labelled by p) on each degenerate subspace of the manifold (labelled by s). We now include the perturbation

$$W = V_+ + V_-,$$

where V_+ and V_- are the interaction Hamiltonians for ω_+ and ω_- respectively. We assume that our general dressed state will be a linear combination of all the degenerate states, *i.e.*

$$|s_{\bar{N}}; \lambda\rangle = \sum_{p=-\infty}^{\infty} \left(a_p^s |a_p^s\rangle + b_p^s |b_p^s\rangle \right), \tag{5.33}$$

where the coefficients a_p^s and b_p^s are yet to be determined and $\bar{N} = N+M+P$. Here λ labels the expected first-order correction $E^{(1)}$ to the energies; in fact we know $E^{(1)}$ must be proportional to the strength of the perturbation, and so

we write $E^{(1)} = \lambda\Omega_2$. To find the coefficients a_p^s and b_p^s, we follow standard degenerate perturbation theory and diagonalise W on the degenerate subspace. To do so, we let W act on $|s;\lambda\rangle$, then multiply on the left by $\langle a_{p'}^s|$ and $\langle b_{p'}^s|$, to obtain the pair of coupled recurrence relations

$$\begin{aligned} a_p - a_{p+1} &= 2\lambda b_p \\ b_p - b_{p-1} &= 2\lambda a_p, \end{aligned} \tag{5.34}$$

for the dressed state coefficients. Here we have dropped the s in our expressions, it being understood that we are working on a fixed s subspace.

In solving the recurrence relations we are forced into making a choice of boundary conditions. It seems natural to choose $a_{-p} = a_p$ or $b_{-p} = b_p$, since we have no reason to believe that there is anything special about the centre of our manifold. Choosing (arbitrarily) the latter, a little algebra reveals that under this "boundary" condition, one solution to the recurrence relations is

$$a_p(\lambda) = (-1)^p T_{|2p-1|}(\lambda) \tag{5.35}$$

and

$$b_p(\lambda) = (-1)^p T_{|2p|}(\lambda), \tag{5.36}$$

where $T_n(x)$ is the Chebyshev polynomial of the first kind ($T_{|n|}(x) \equiv T_n(x)$), and where we still have to choose an overall normalisation constant.

To determine the allowed values of λ and thereby fix the first-order energy corrections, we examine the normalisation of $|s_{\bar{N}};\lambda\rangle$. We find that

$$\langle s'_{\bar{N}'}, \lambda' | s_{\bar{N}};\lambda\rangle = \delta_{\bar{N}'\bar{N}}\delta_{ss'} \sum_{p=-\infty}^{\infty} [a_p(\lambda')a_p(\lambda) + b_p(\lambda')b_p(\lambda)]. \tag{5.37}$$

It is well known that the Chebyshev polynomials obey the following relation:

$$\frac{1}{\sqrt{1-x^2}}\left(\frac{1}{2}T_0^2(x)+\sum_{n=1}^{\infty}T_n^2(x)\right)=\frac{\pi}{2}\delta(x),\quad -1\leq x\leq 1. \tag{5.38}$$

From this we see that if λ lies in the range $-1\leq\lambda\leq 1$, and we choose our overall normalisation factor so that

$$\begin{aligned} a_p(\lambda) &= \frac{1}{\sqrt{\pi}}(1-\lambda^2)^{-\frac{1}{4}}(-1)^p T_{|2p-1|}(\lambda) \\ b_p(\lambda) &= \frac{1}{\sqrt{\pi}}(1-\lambda^2)^{-\frac{1}{4}}(-1)^p T_{|2p|}(\lambda), \end{aligned} \tag{5.39}$$

then our dressed states obey the orthonormality relation

$$\langle s'_{\bar{N}'};\lambda'|s_{\bar{N}};\lambda\rangle=\delta_{\bar{N}'\bar{N}}\delta_{ss'}\delta(\lambda-\lambda'), \tag{5.40}$$

and the completeness relation

$$\sum_{\bar{N},s}\int_{-1}^{1}d\lambda|s_{\bar{N}};\lambda\rangle\langle s_{\bar{N}};\lambda|=1. \tag{5.41}$$

We see that the dressed states on $\epsilon(\bar{N})$ consist of an infinite number of continua of width $2\Omega_2$, separated by $2\Omega_1$, as shown in Figure 5.8(b). Having these dressed states, we can qualitatively see how the spectrum may consist of continua. Unfortunately however, it proves a little harder to obtain quantitative expressions for the spectra. The general procedure of computing transition rates then populations etc. seems to fail us: certainly the most naive application does. This is because the transition rates all turn out to be Dirac delta functions or combinations of the same, and it becomes unclear whether we can make the secular approximation in a consistent manner. Remember that the secular approximation involved dropping from our population and coherence equations those density

matrix terms which corresponded to transitions at a different frequency. This is justified when the difference between the frequencies involved is large compared to Γ. However when continua are involved, we have an infinite number of terms corresponding to the energies infinitesimally close to the particular level in which we are interested. Thus this approximation may need to be modified.

In fact a dressed atom problem involving continua *has* been solved previously in [8]; however the techniques used there were not rigorous and do not seem to transfer well to the present problem. From [8] and on intuitive grounds however, we can expect that our spectrum will look like a convolution of lorentzians at the positions of the associated Mollow spectra with some population distribution across the continuum. It is making this statement quantitative which proves to be a problem. The exercise is not without merit however, since it is only by looking at such problems that we may gain a better understanding of the dressed atom model's strengths and weaknesses.

5.5 Conclusions

In this chapter we have examined a few of the phenomena which occur when a two-level atom is driven by an amplitude modulated field. We saw that both extremes of strong and weak modulation are nicely explained by the dressed atom model. In particular we found that the case of weak modulation resembles closely that of monochromatic driving, with the Rabi sidebands split into multiplets by the weak bichromatic field. The case of strong amplitude modulation was also easily understood in the context of a strong bichromatic field with a weak central

field acting as a perturber. The spectra in this case consisted mainly of an infinite series of doublets. For both cases the positions of the spectral lines depended only on the detuning of the sideband fields δ, and the strength of the central field. The strength of the sideband fields affected only the intensities of the spectral lines. Finally we examined a case which has not been completely solved within the dressed atom model, namely the case of weak sideband fields detuned to the Rabi sidebands of the central field.

References

[1] H.S. Freedhoff and Z. Chen, Phys. Rev. A **41**, 6013 (1990).

[2] Z. Ficek and H.S. Freedhoff, Phys. Rev. A **48**, 3092 (1993) *and references therein.*

[3] M.F. Van Leeuwen, S. Papademetriou and C.R. Stroud, Jr., Phys. Rev. A **53**, 990 (1996); S. Papademetriou, M.F. Van Leeuwen and C.R. Stroud, Jr., Phys. Rev. A **53**, 997 (1996).

[4] S. Feneuille, M. G. Schweighofer, and G. Oliver, J. Phys. B **9**, 2003 (1976); P. Thomann, J. Phys. B **9**, 2411 (1976); P. Thomann, J. Phys. B **13**, 1111 (1980); G. S. Agarwal and N. Nayak, J. Phys. B **19**, 3385 (1986); H. Friedmann and A.D. Wilson-Gordon, Phys. Rev. A **36**, 1336 (1987); W. M. Ruyten, Phys. Rev. A **42**, 4226 (1990), M. Z. Smirnov, J. Opt. Soc. Am. B **11**, 109 (1994);

[5] B. Blind, P. R. Fontana and P. Thomann, J. Phys. B **13**, 2717 (1980)

[6] G.N. Watson, *A Treatise on the Theory of Bessel Functions*, (Cambridge University Press, 1966).

[7] A. Greentree, N. Manson and C. Wei, private communication.

[8] Z. Ficek and H.S. Freedhoff, Phys. Rev. A **55**, 1234 (1997)

6. Summary and conclusions

In this thesis, the dressed atom model has been applied to a variety of (previously unconsidered) problems involving a two-level atom driven by two or three laser fields, and a number of new effects have been predicted and explained. These include: An explanation of the subharmonic resonance phenomenon as a multiphoton effect and the first analytical calculations of the multiphoton AC Stark splitting; an explanation of the minimum splitting which occurs at slight detunings from the subharmonic resonances and the prediction of suppression of fluorescence at these shifted detunings; and the first analytical calculations of the spectra associated with an atom being driven by an amplitude-modulated field.

In Chapter 3 the technique of "doubly-dressing" the atom was used to provide a clear understanding of the subharmonic resonances, observed when an atom is driven by one near-resonance field and one detuned field, in terms of multiphoton transitions between the (singly-) dressed states. This understanding had not been achieved before because previous studies focussed on the absorptive and dispersive response of the second driving field. This field is intricately involved in the dynamics of the system however, and so is better regarded as itself a dressing field. Perturbation calculations were carried out to high order in order to obtain results that agree perfectly with numerical and experimental studies of the system.

The major portion of Chapter 3 focussed on the case of a strong, on-resonance driving field and a weaker driving field detuned to a subharmonic of the first field's Rabi frequency. The dressed states were found to form an infinite set of doublets, and analytic expressions were obtained for the inter- and intra- doublet splittings.

The master equation was then used to calculate evolution equations for the populations and coherences of the dressed states. These were then used to calculate fluorescence, weak probe absorption and dispersion spectra and Autler-Townes absorption and dispersion spectra. All spectra were found to contain features at the harmonics and subharmonics of the Rabi frequency of the strong field, and these features had an intricate dependence on the order n of the subharmonic resonance and on the ratio of the Rabi frequencies of the two fields.

In the last section of Chapter 3 the reversed situation of strong detuned field and weaker on-resonance field was briefly considered and shown to also be capable of exhibiting the multiphoton Stark effect, albeit in a slightly more opaque manner.

In Chapter 4 the double dressing technique was used to explore the subharmonic resonance shifts and the associated vanishing of the central component of the fluorescence spectrum when the splitting of the dressed states is a minimum. A physical explanation and analytical formulae for the points of minimum splitting were derived, and an explanation of the vanishing fluorescence in terms of quantum interference between dressed state transitions provided.

In Chapter 5 the case of three driving fields, in particular an amplitude modulated field, was examined. The two main perturbative regimes of weak modulation (strong carrier) and strong modulation (weak carrier) were considered. Dressed states and associated population and coherence equations were derived.

In the former case the dressed states were found to split into two submanifolds separated by the strong central field's Rabi frequency. Each submanifold consisted

of states separated by the detuning (modulation frequency) of the sideband fields. The presence of the two sideband fields was found to significantly alter the Mollow sidebands; however, they left the central component unaffected. The Autler-Townes absorption and weak probe absorption spectra were also calculated and found to differ from their Mollow counterparts in a related manner.

For the case of strong modulation, the dressed states were found to correspond closely to the case of pure (symmetrically detuned) bichromatic driving, namely an infinite tower of states separated by the sideband detuning (with no energy dependence on the sideband Rabi frequency). However the central component of the field split these dressed states, resulting in an infinite number of doublets, in a picture reminiscent of the dressed states obtained in Chapter 3. The fluorescence and Autler-Townes absorption spectra were calculated and found to consist of an infinite series of doublets (apart from a central triplet component of the fluorescence spectrum), with intensities dependent on the ratio between the sidebands' Rabi frequencies and the sideband detuning.

A major goal of this thesis was to emphasize the many advantages of using the dressed atom model when considering the AC Stark effect. These advantages include a clear physical picture allowing for strong intuition into the system dynamics, and the ease of obtaining analytical results which are extremely rare in Bloch equation or other related approaches. In the last section of Chapter 5 a situation which is not easily solved in the dressed atom context was examined in order to display the essential role of various approximations, in this case the secular approximation, in making the dressed atom dynamics tractable.

Appendix A: Perturbation Theory for 2 degenerate levels

We consider a general perturbation λV of a Hamiltonian H_0 whose eigenvalues $E_1, E_2, ...$ and eigenstates $|1\rangle, |2\rangle, ...$ are known. In particular we consider the case when two of the unperturbed eigenstates $|a\rangle$ and $|b\rangle$ are degenerate with energy $E_a \equiv E_b$. In the standard manner we assume that the perturbed eigenstates and energies can be expanded as a power series in λ of the form

$$|\psi\rangle = |\psi\rangle^{(0)} + \lambda|\psi\rangle^{(1)} + \lambda^2|\psi\rangle^{(2)} + ...$$

$$E = E^0 + \lambda E^{(1)} + \lambda^2 E^{(2)} + ... \quad ,$$

that the wavefunction correct to zero order is given by

$$|\psi\rangle^{(0)} = C_a^{(0)}|a\rangle + C_b^{(0)}|b\rangle$$

and that the mth order correction to the wavefunction can be written as

$$|\psi\rangle^{(m)} = C_a^{(m)}|a\rangle + C_b^{(m)}|b\rangle + \sum_{i \neq a,b} C_i^{(m)}|i\rangle.$$

The inclusion of the states $|a\rangle$ and $|b\rangle$ in the higher order corrections is often omitted in treatments of perturbation theory, but in fact is found to be critical to a correct calculation of the n-photon dynamic Stark effect discussed in this paper.

By substitution of these expressions into the Schrödinger equation, we set up a hierachy of matrix equations of the form

$$G_0\mathbf{C}^{(0)} = E^{(1)}\mathbf{C}^{(0)} \qquad (A.1)$$

$$G_0\mathbf{C}^{(1)} + G_1\mathbf{C}^{(0)} = E^{(1)}\mathbf{C}^{(1)} + E^{(2)}\mathbf{C}^{(0)} \tag{A.2}$$

$$G_0\mathbf{C}^{(2)} + G_1\mathbf{C}^{(1)} + G_2\mathbf{C}^{(0)} = E^{(1)}\mathbf{C}^{(2)} + E^{(2)}\mathbf{C}^{(1)} + E^{(3)}\mathbf{C}^{(0)} \tag{A.3}$$

Here $\mathbf{C}^{(m)}$ is the vector

$$\begin{pmatrix} C_a^{(m)} \\ C_b^{(m)} \end{pmatrix} \tag{A.4}$$

and the $\{G_i\}$ are 2×2 matrices evaluated in the degenerate subspace. More explicitly

$$G_0 = \begin{pmatrix} V_{aa} & V_{ab} \\ V_{ba} & V_{bb} \end{pmatrix} \tag{A.5}$$

while

$$G_1 = \begin{pmatrix} \mathcal{R}^1_{aa} & \mathcal{R}^1_{ab} \\ \mathcal{R}^1_{ba} & \mathcal{R}^1_{bb} \end{pmatrix}, \tag{A.6}$$

where $\mathcal{R}^p_{ij} \equiv \langle i|\mathcal{R}^p|j\rangle$ is the matrix element (i,j) of the operator

$$\mathcal{R}^p = \sum_i{}' \frac{V|i\rangle\langle i|V}{(E_a - E_i)^p}, \tag{A.7}$$

and the prime indicates that the sum excludes the states $|a\rangle, |b\rangle$. In fact it is useful to define the more general operator

$$\mathcal{R}^{pq..r} = \sum_{i,j,..k}{}' \frac{V|i\rangle\langle i|V|j\rangle\langle j|V....V|k\rangle\langle k|V}{(E_a - E_i)^p(E_a - E_j)^q...(E_a - E_k)^r}, \tag{A.8}$$

and the operator $\Xi^m(l)$ as the sum over all the $\mathcal{R}$ operators with l superscripts such that they add up to m. For example

$$\Xi^4(2) = \mathcal{R}^{13} + \mathcal{R}^{31} + \mathcal{R}^{22}, \qquad \Xi^5(3) = \mathcal{R}^{113} + \mathcal{R}^{131} + \mathcal{R}^{311} + \mathcal{R}^{122} + \mathcal{R}^{212} + \mathcal{R}^{221}. \tag{A.9}$$

Further, we define the operator

$$\mathcal{M}_l^m = \Xi^m(l) - \sum_{j=1}^{l-1} E^{(j)} \mathcal{M}_{l-j}^{m+1-j} \quad m, l \geq 2, \tag{A.10}$$

with

$$\mathcal{M}_1^m = \Xi^m(1) = \mathcal{R}^m.$$

For example M_3^3, from which we calculate G_3, is given by

$$\mathcal{M}_3^3 = \mathcal{R}^{111} - E^{(1)}(\mathcal{R}^{12} + \mathcal{R}^{21} - E^{(1)}\mathcal{R}^3) - E^{(2)}\mathcal{R}^2. \tag{A.11}$$

Finally can write the matrices G_m as

$$G_m = \begin{pmatrix} \langle a|\mathcal{M}_m^m|a\rangle & \langle a|\mathcal{M}_m^m|b\rangle \\ \langle b|\mathcal{M}_m^m|a\rangle & \langle b|\mathcal{M}_m^m|b\rangle \end{pmatrix}. \tag{A.12}$$

We can systematically solve the equations (A.1)-(A.3). However, in the problem investigated in this paper we have $V_{aa} = V_{ab} = V_{ba} = V_{bb} \equiv 0$ and thus G_0=0. Hence the first order energy corrections are zero ($E^{(1)} = 0$), and we must use (A.2) to determine the correct zero order eigenstates and the energy corrections $E^{(2)}$. Equation (A.2) is now a 2 dimensional eigenvalue equation whose eigenvectors $\mathbf{C}_\pm^{(0)}$ and eigenvalues $E_\pm^{(2)}$ give the dressed states correct to zero order and second order energy corrections respectively. Having found and normalised the eigenvectors $\mathbf{C}_\pm^{(0)}$, we proceed to solve the equation (A.3).

Because the matrices G_m are Hermitian, we know that the eigenvectors $\mathbf{C}_\pm^{(0)}$ are orthogonal and that they span the 2 dimensional vector space.Therefore, we

can write the vector $\mathbf{C}_+^{(1)} = f_+^+\mathbf{C}_+^{(0)} + f_+^-\mathbf{C}_-^{(0)}$. Substituting this back into (A.3) and multiplying on the left first by $\mathbf{C}_+^{(0)\dagger}$, then by $\mathbf{C}_-^{(0)\dagger}$, we find

$$\begin{aligned} E_+^{(3)} &= \mathbf{C}_+^{(0)\dagger} G_2 \mathbf{C}_+^{(0)}, \\ f_+^- &= \frac{1}{E_+^{(2)} - E_-^{(2)}} (\mathbf{C}_-^{(0)\dagger} G_2 \mathbf{C}_+^{(0)}). \end{aligned} \tag{A.13}$$

The coefficient f_+^+ is found to be arbitrary, and we choose $f_+^+ = 0$ in order to follow the orthogonality convention that

$$^{(0)}\langle\psi|\psi\rangle^{(n)} = 0. \tag{A.14}$$

The previous derivation is symmetric and we can simply interchange plus and minus signs to obtain expressions for $E_-^{(3)}$ and f_-^+. The process can be continued to next order by taking $\mathbf{C}_+^{(2)} = g_+^+\mathbf{C}_+^{(0)} + g_+^-\mathbf{C}_-^{(0)}$, and so on. In this manner the energy corrections and coefficients of the degenerate states $C_a^{(n)}, C_b^{(n)}$ can be found to any accuracy required. The coefficients of the other states which contribute to the eigenvector corrections are found in the usual way, and given by

$$\begin{aligned} C_k^{(1)} &= \frac{1}{E_a - E_k}(C_a^{(0)} V_{ka} + C_b^{(0)} V_{kb}), \\ C_k^{(m)} &= \frac{1}{E_a - E_k}\Big(\sum_j C_j^{(m-1)} V_{kj} - \sum_{i=1}^{m-1} E^{(i)} C_k^{(m-i)}\Big), \end{aligned} \tag{A.15}$$

where we point out that the first sum includes the states $|a\rangle, |b\rangle$.

Appendix B: Sample Maple worksheet for multiphoton AC Stark effect calculations

In this appendix an example of the type of Maple worksheet used for many of the calculations in this thesis is presented. The author makes no claims as to the efficiency of the Maple code. The worksheet grew gradually out of attempts to avoid algebraic errors when calculating 4th order corrections to the doubly-dressed state energies of Chapter 3. It should be pointed out that despite the accompanying explanation, this worksheet is likely unintelligible to all except regular Maple users.

We begin by reading in the "linalg" package to enable us to use matrices easily, and the "rationalize" and "Taylor co-efficient" commands.

```
[> with(linalg):
[> readlib(coeftayl):readlib(rationalize):
```

We now want Maple to realise that α and Ω_1 are real and positive:

```
[> assume(alpha>0):assume(Omega1>0):
```

Now pick value of n,

```
[> n:=2;
```

and define the Kronecker delta function:

```
[> delta:=(x,y)->if x=y then delta(x,y):=1 else delta(x,y):=0 fi:
```

Now two commands to make simplification and computing the modulus of a complex number easier:

```
[> simp:=x->simplify(expand(rationalize(x))):
```

[⟩ **MODD:=x->x*conjugate(x):**

We want to expand many parameters in a Taylor series in α without the $O(\alpha^8)$ or similar term that Maple leaves. Hence the following:

[⟩ **TAYLOR1:=L->convert(taylor(L,alpha=0,2),polynom):** Plus similar expressions up to **TAYLOR6**.

Now we are going to represent states such as $|(N-p)+, M+p\rangle$ as a list of three elements $[-p, 1, p]$. That is, we drop the N, M and use the middle element to represent the "plus" or "minus" states. As another example, the state $|(N+3)-, M-2\rangle$ would be represented in Maple by the list $[3, -1, -2]$. The operator SP below takes in 2 such lists as arguments and computes a scalar product $\langle \cdots | \cdots \rangle$:

[⟩ **SP:=(U,V)->delta(U[1],V[1]) * delta(U[2],V[2]) * delta(U[3],V[3]):**

We now define a function which takes as input two states in the list form described above and computes the matrix element of our perturbation V between them, *i.e.* $\langle \cdots | V | \cdots \rangle$:

[⟩ **VV:=(U,V)->Omega1*alpha/2* (U[2]*delta(U[1]-1,V[1])**

***delta(U[3],V[3]-1)+V[2]*delta(U[1],V[1]-1)*delta(U[3],V[3]+1)):**

The next two functions compute the energy of an input state and the energy difference between two input states respectively.

[⟩ **En:=U->collect(U[1]*omega[o]+U[2]*Omega1+U[3]***

(omega[o]+2*Omega1/n+delta), [omega[o]]):

[⟩ **Endif:=(X,Y)->simplify(En(X)-En(Y)):**

The next three functions compute the matrix elements of the operators S^-, S^+ and S^+S^- respectively, given two input states.

```
[⟩ uSminusv:=(U,V)->V[2]/2* delta(U[1],V[1]-1)*delta(U[3],V[3])
*(delta(U[2],1)+delta(U[2],-1)):
[⟩ uSplusv:=(U,V)->1/2*delta(U[1],V[1]+1)*delta(U[3],V[3])
*(delta(U[2],1)-delta(U[2],-1)):
[⟩ uSplusSminusv:=(U,V)->V[2]/2*delta(U[1],V[1])
* delta(U[3],V[3])*(delta(U[2],1) - delta(U[2],-1)):
```

Up until now we have functions which take in one or two states as a list of three elements for each state. The problem is we will require superpositions of such states. To enable us to do this, we define a convention whereby a state of the form $|\psi\rangle = \frac{1}{\sqrt{3}}|(N-1)+, M+1\rangle - \sqrt{\frac{2}{3}}|(N-3)-, M+3\rangle$, would be represented in Maple by the list of lists:

```
psi:=[ [[-1,1,1],1/sqrt(3)],[[-3,-1,3],sqrt(2)/sqrt(3)] ]
```

Obviously we can extend this to include any number of states with different amplitudes.

We now need to define generalisations of the operators above to incorporate computing the matrix elements of "superposition lists".

The next four functions compute the matrix elements of S^-, S^+, S^+S^- and V respectively.

```
[⟩ SMINUS:=(L1,L2)->collect(expand(sum('sum('conjugate(L1[i][2])
*L2[j][2]*uSminusv(L1[i][1],L2[j][1])','i'=1..nops(L1))',
'j'=1..nops(L2))),alpha):
```

```
[> SPLUS:=(L1,L2)->collect(expand(sum('sum('conjugate(L1[i][2])
*L2[j][2]*uSplusv(L1[i][1],L2[j][1])','i'=1..nops(L1))',
'j'=1..nops(L2))),alpha):
[> SPLUSMINUS:=(L1,L2)->collect(expand(sum('sum('conjugate(L1[i][2])
*L2[j][2]*uSplusSminusv(L1[i][1],L2[j][1])','i'=1..nops(L1))',
'j'=1..nops(L2))),alpha):
[> SVVS:=(L1,L2)->collect(expand(sum('sum('conjugate(L1[i][2])*L2[j][2]
*VV(L1[i][1],L2[j][1])','i'=1..nops(L1))','j'=1..nops(L2))),alpha):
```

The following computes the "overlap", or scalar product of two superposition lists.

```
[> SS:=(L1,L2)->collect(expand(sum('sum('conjugate(L1[i][2])
*L2[j][2]*SP(L1[i][1],L2[j][1])','i'=1..nops(L1))',
'j'=1..nops(L2))),alpha):
```

We know that in perturbation calculations we are required to sum over all states that "connect" to a given one through the perturbation V. The following operator takes in a state and produces a list (superposition!) of all such states, giving each an initial amplitude of zero.

```
[> Pert:=U->op([[[U[1][1]-1,1,U[1][3]+1],0],[[U[1][1]-1,-1,U[1][3]+1],0],
[[U[1][1]+1,-1,U[1][3]-1],0],[[U[1][1]+1,1,U[1][3]-1],0]]):
```

Obviously we need to generalise this to take in a superposition and to produce *all* connecting states, and this is accomplished with the operator **PRT** below:

```
[> PRT:=proc(L);seq( Pert(L[i]),i=1..nops(L));end:
```

There are just two remaining operators of this form that we will find useful. The first takes a single state and "hits" it from the left onto a superposition of states, that is it computes the overlap of the single state with the superposition. The second performs a similar function, but through the perturbation V.

```
[> SL:=(L1,L2)->expand(sum('L2[j][2]*SP(L1[1],L2[j][1])','j'=1..nops(L2))):
[> SVL:=(L1,L2)->expand(sum('L2[j][2]*VV(L1[1],L2[j][1])','j'=1..nops(L2))):
```

We now define our initial pair of degenerate states with which we work. In this example I have chosen the $m = 0$ states on $\epsilon(N + M)$, as defined in Chapter 3.

```
[> a:=[[n,1,-n],0];b:=[[0,-1,0],0];
```

We now define a series of functions which compute the matrix elements of the operator(s) $\mathcal{R}^{pq\cdots r}$, as defined in equation (A.8).

The last two arguments passed to these functions (here called H[i] where i labels the number of energy denominators) are the states which determine which matrix element we are computing. The first i arguments are the powers to which the energy denominators are raised.

```
[> H[0]:=proc(x,y);VV(x[1],y[1]);end:
[> H[1]:=proc(q,x,y);xx:=[op({Pert(y),Pert(x)} minus {a,b})];
sum('VV(x[1],xx[i][1])*VV(xx[i][1],y[1])/Endif(y[1],xx[i][1])^q',
'i'=1..nops(xx));end:
[> H[2]:=proc(q,r,x,y);xx:=[op(Pert(x) minus a,b)];xy:=[op(Pert(y) minus
a,b)];sum('sum('VV(x[1],xx[i][1])*VV(xx[i][1],xy[j][1])
*VV(xy[j][1],y[1])/Endif(y[1],xx[i][1])^q/Endif(y[1],xy[j][1])^r',
'i'=1..nops(xx))','j'=1..nops(xy));end:
```

A series of such functions up to **H[7]** is similarly defined.

We now define some functions which evaluate the **H**'s for the specific degenerate pair **a,b** that we have chosen.

```
[> U.0:=matrix(2,2,[simp(H[0](a,a)),simp(H[0](a,b)),simp(H[0](b,a)),
simp(H[0](b,b))]):
[> U.1:=proc(q);matrix(2,2,[simp(H[1](q,a,a)),simp(H[1](q,a,b)),simp(H[1](q,b,a)),
simp(H[1](q,b,b))]):end:
[> U.2:=proc(q,r);matrix(2,2,[simp(H[2](q,r,a,a)),simp(H[2](q,r,a,b)),
simp(H[2](q,r,b,a)),simp(H[2](q,r,b,b))]):end:
```

A series of functions up to **U.8** is similarly defined.

Finally we actually compute the 2×2 matrices which we will need. Only a small subset of those required are shown below

```
[> M.0:=U.0:M.1:=U1(1);M.2:=U1(2):
M.1.1:=U2(1,1);M.2.1:=U2(2,1):M.1.2:=U2(1,2):M.3.2:=U2(3,2):
M.1.1.1:=U3(1,1,1):M.1.1.2:=U3(1,1,2): M.1.2.1:=U3(1,2,1):
M.1.1.1.1:=U4(1,1,1,1):M.1.1.1.2:=U4(1,1,1,2):
M.1.1.1.1.1:=U5(1,1,1,1,1):M21111:=U5(2,1,1,1,1):M.1.2.1.1.1:=U5(1,2,1,1,1):
```

We now implement a series of procedures to compute the matrices G_m of equation (A.12). To do this we start with a series of procedures **X.i(N)** which evaluate the sum over the **M** matrices with **i** indices that add to **N**:

```
[> X.1:=N->M.N:
[> X.2:=proc(N);sum('M.(N-j).j','j'=1..N-1);end:
```

Plus similar terms until:

[> X.8:=proc(N);sum('sum('sum('sum('sum('sum('M.j.(k-j).(l-k).(p-l).
(o-p).(r-o).(y-r).(N-y)','j'=1..k-1)','k'=1..l-1)','l'=1..p-1)',
'p'=1..o-1)','o'=1..r-1)','r'=1..y-1)','y'=1..N-1);end:

With these in hand we compute the functions corresponding to equation (A.10). Notice that we have to have two such functions depending on whether we are on the "plus" or "minus" subspace, once the degeneracy is lifted. Thus **PP**, **PM** correspond to the "plus" or "minus" subspaces respectively.

[> PP:=proc(i,n); if i=1 then X.1(n) else X.i(n)-sum('ep.j*PP(i-j,n+1-j)','j'=1..i-1);fi;end;

[> PM:=proc(i,n); if i=1 then X.1(n) else X.i(n)-sum('em.j*PM(i-j,n+1-j)','j'=1..i-1);fi;end;

Below we will use the notation **AP(m)**, **AM(m)** for the matrices G_m.

The next function makes finding a transpose a little easier:

[> dag:=x->transpose(x):

We now implement two functions which compute the coefficients f_+^- (and similar to higher order) of equation (A.13).

[> pv:=N-> >simplify(evalm(1/(ep2-em2)*(sum('cp[i]*dag(m0)&*AP(N+1-i)&*m0','i'=0..N-1)+dag(m0)&*AP(N+1)&*p0 -sum('cp[i]*ep.(N+2-i)','i'=0..N-1))));

[> pm:=N-> >simplify(evalm(1/(em2-ep2)*(sum('cm[i]*dag(p0)&*AM(N+1-i)&*p0','i'=0..N-1)+dag(p0)&*AM(N+1)&*m0 -sum('cm[i]*em.(N+2-i)','i'=0..N-1))));

The next two functions compute the energy corrections to the "plus" or "minus" subspaces respectively.

```
[> enp:=N- >simp(evalm(sum('cp[i]*dag(p0)&*AP(N-1-i)&*m0','i'=0..N-
3)+dag(p0)&*AP(N-1)&*p0));
```

```
[> enm:=N- >simp(evalm(sum('cm[i]*dag(m0)&*AM(N-1-i)&*p0','i'=0..N-
3)+dag(m0)&*AM(N-1)&*m0));
```

Having defined all these functions, we can proceed to compute the energy corrections to whichever order we please, and also the quantities $\mathbf{C_n^{(i)}}$, which determine the co-efficients of the 2 degenerate states in the higher order eigenvector corrections.

Since for $n \geq 2$ the degeneracy is not lifted, the zeroth order terms are all 0:

```
[> cp[0]:=0:cm[0]:=0:
```

```
[> AP(0):=M.0:AM(0):=M.0:
```

```
[> ep1:=0:em1:=0:
```

At second order the two matrices **AP(1)** and **AM(1)** are identical (since no degeneracy has been removed), and we diagonalise them to find the second order energy corrections **ep2** and **em2**, and the zeroth order eigenvectors **p.0** and **m.0**

```
[> AP(1):=PP(1,1):AM(1):=PM(1,1);
```

```
[> ep2:=simp(sqrt(AP(1)[1,1]^2+AP(1)[1,2]^2)):
```

```
em2:=simp(-sqrt(AP(1)[1,1]^2+AP(1)[1,2]^2)):
```

```
[> eta:=simp(-AP(1)[1,2]/(AP(1)[1,1]-ep2));
```

```
[> p.0:=vector([eta/sqrt(1+eta^2),1/sqrt(1+eta^2)]):
```

```
m.0:=vector([1/sqrt(1+eta^2),-eta/sqrt(1+eta^2)]):
```

The variables **Cap[i]** and **Cam[i]** are the coefficients of the **a** state in the plus or minus subspace at order **i**. The **Cbp[i]**, **Cbm[i]** terms are the equivalent expressions for the degenerate state **b**.

```
[> Cap[0]:=p0[1]:Cbp[0]:=p0[2]:Cam[0]:=m0[1]:Cbm[0]:=m0[2]:
```

The whole procedure now proceeds recursively, to whichever order we desire (or have the patience to wait for Maple to compute!).

```
[> AP(2):=PP(2,2):AM(2):=PM(2,2);

[>  ep3:=enp(3):em3:=enm(3);

[> cp[1]:=pv(1);cm[1]:=pm(1);

[> Cap[1]:=cp[1]*Cam[0]:Cbp[1]:=cp[1]*Cbm[0]:

Cam[1]:=cm[1]*Cap[0]:Cbm[1]:=cm[1]*Cbp[0]:

[>  AP(3):=PP(3,3):AM(3):=PM(3,3);

[> ep4:=enp(4);em4:=enm(4);

[> cp[2]:=pv(2):cm[2]:=pm(2):

[> Cap[2]:=cp[2]*Cam[0]:Cbp[2]:=cp[2]*Cbm[0]:

Cam[2]:=cm[2]*Cap[0]:Cbm[2]:=cm[2]*Cbp[0]:

[>  AP(4):=PP(4,4):AM(4):=PM(4,4):

[> ep5:=enp(5):em5:=enm(5):

[>  cp[3]:=pv(3):cm[3]:=pm(3):

[>  Cap[3]:=cp[3]*Cam[0]:Cbp[3]:=cp[3]*Cbm[0]:

Cam[3]:=cm[3]*Cap[0]:Cbm[3]:=cm[3]*Cbp[0]:

[>  AP(5):=PP(5,5):AM(5):=PM(5,5):
```

[> ep6:=enp(6);em6:=enm(6);

[> cp[4]:=pv(4):cm[4]:=pm(4):

[> Cap[4]:=cp[4]*Cam[0]:Cbp[4]:=cp[4]*Cbm[0]:

Cam[4]:=cm[4]*Cap[0]:Cbm[4]:=cm[4]*Cbp[0]:

[> AP(6):=PP(6,6):AM(6):=PM(6,6):

[> ep7:=enp(7);em7:=enm(7);

[> cp[5]:=pv(5):cm[5]:=pm(5):

[> Cap[5]:=cp[5]*Cam[0]:Cbp[5]:=cp[5]*Cbm[0]:

Cam[5]:=cm[5]*Cap[0]:Cbm[5]:=cm[5]*Cbp[0]:

Up to this point we posess only the energy corrections and the higher order coefficients of the 2 degenerate states. By this stage I am so confident of no-one ever reading this far into this appendix, that I will offer a Mars Bar to anyone who points out this sentence to me within 5 yrs of my dissertation.

To calculate the full eigenvectors correct to some order, we can now use standard perturbation theory and be careful to make sure that in sums over interconnecting states we exclude the two degenerate states **a,b**.

The eigenvectors correct to zeroth order are:

[> CORR[0]:=convert([a[1],p0[1]],[b[1],p0[2]],'list');

[> MCORR[0]:=convert([a[1],m0[1]],[b[1],m0[2]],'list');

We now define procedures which compute a list of possible interconnecting states, but remove all those which *are* actually the **a** and **b** states:

[> XXX:=p->convert('union'(PRT(XX[p-1]),op(XX[p-1]))minus a, b ,'list'):

[> XX[0]:=[NULL]: XX[1]:=convert(PRT(CORR[0]),'list'):XX[2]:=XXX(2):

```
XX[3]:=XXX(3):XX[4]:=XXX(4):XX[5]:=XXX(5):XX[6]:=XXX(6):
```

The two functions below, **corrn** and **mcorrn** now compute the co-efficient at order **Q** of some input state **k**.

```
[) corrn:=proc(k,Q);EE:=Endif(a[1],k[1]);
LIST:=convert(Pert(k) minus a, b ,'list'):
if Q=1 then (Cap[0]*VV(k[1],a[1])+Cbp[0]*VV(k[1],b[1]))/EE else
1/EE*(Cap[Q-1]*VV(k[1],a[1])+Cbp[Q-1]*VV(k[1],b[1])
+ sum('VV(k[1],LIST[i][1])*corrn(LIST[i],Q-1)','i'=1..nops(LIST))
-sum('ep.i*corrn(k,Q-i)','i'=1..Q-1)):fi;end:
[) mcorrn:=proc(k,Q);EE:=Endif(a[1],k[1]);
LIST:=convert(Pert(k) minus a, b ,'list'):
if Q=1 then (Cam[0]*VV(k[1],a[1])+Cbm[0]*VV(k[1],b[1]))/EE else
1/EE*(Cam[Q-1]*VV(k[1],a[1])+Cbm[Q-1]*VV(k[1],b[1])
+ sum('VV(k[1],LIST[i][1])*mcorrn(LIST[i],Q-1)','i'=1..nops(LIST))
-sum('em.i*mcorrn(k,Q-i)','i'=1..Q-1)):fi;end:
```

The two functions **correction** and **mcorrection** then apply **corrn** and **mcorrn** to the set of possible states which may have non-zero co-efficients at order **Q**:

```
[) correction:=proc(Q);seq(subsop(2=simp(corrn(XX[Q][i],Q)),XX[Q][i]),
i=1..nops(XX[Q])),[[0,-1,0],simp(Cbp[Q])],[[n,1,-n],simp(Cap[Q])];end;
[)  mcorrection:=proc(Q);seq(subsop(2=simp(mcorrn(XX[Q][i],Q)),XX[Q][i]),
i=1..nops(XX[Q])),[[0,-1,0],simp(Cbm[Q])],[[n,1,-n],simp(Cam[Q])];end:
```

Thus our final correct dressed state is the superposition of all the higher order correction states (here shown computing to order α^4). The **minus op(XX[4])** is just to remove extra states which enter with a zero amplitude and which slow down later calculations.

```
[) KP[0]:=convert('union' (op(CORR[0]),correction(1),correction(2),
correction(3)) minus op(XX[4]),'list'):
[) KM[0]:=convert('union'(op(MCORR[0]),mcorrection(1),mcorrection(2),
mcorrection(3),mcorrection(4)) minus op(XX[4]) ,'list'):
```

We now have our pair of $m = 0$ dressed states on $\epsilon(N + M)$, given by the 2 variables **KP[0]** and **KM[0]**. Of course we require the dressed states for different m and on different manifolds. In what follows **J,K,L** denote manifolds $\epsilon(N + M + 1), \epsilon(N + M)$, and $\epsilon(N + M - 1)$ respectively. The function **Jmn(3)**, for example, computes the dressed states on $\epsilon(N + M + 1)$ for $m = 3$.

```
[) Kpl:=m->[seq(subsop(1=[i[1][1]-m,i[1][2],i[1][3]+m],2=i[2],i),i=KP[0])]:
Kmn:=m->[seq(subsop(1=[i[1][1]-m,i[1][2],i[1][3]+m],i),i=KM[0])]:
Lpl:=m->[seq(subsop(1=[i[1][1]-m-1,i[1][2],i[1][3]+m],i),i=KP[0])]:
Jpl:=m->[seq(subsop(1=[i[1][1]-m+1,i[1][2],i[1][3]+m],i),i=KP[0])]:
Jmn:=m->[seq(subsop(1=[i[1][1]-m+1,i[1][2],i[1][3]+m],i),i=KM[0])]:
Lmn:=m->[seq(subsop(1=[i[1][1]-m-1,i[1][2],i[1][3]+m],i),i=KM[0])]:
```

Since we do not want Maple to run off and keep computing these dressed states every time it requires one, we make an array of them all from $m = -13$ to 13.

```
[) A:=array(-13..13,[seq(i,i=-13..13)]):
[) Lp:=map(Lpl,A):Jp:=map(Jpl,A):Jm:=map(Jmn,A):Lm:=map(Lmn,A):
```

```
Kp:=map(Kpl,A):Km:=map(Kmn,A):Hp:=map(Ipl,A):Hm:=map(Imn,A):
```

As yet our dressed states are unnormalised. The variable **F** computed below is the normalisation factor; the variable **F2** truncates this factor to the order we are interested in.

```
[> F:=sqrt(simp(SS(Kp[0],Kp[0])));
[> F2:=TAYLOR4(F^2);
```

Depending on what order of α we are interested in, we may require transition rates from $m = 0$ to $m = 2$ or 4 or 8 etc. The variables **Y** and **Z** give us some flexibility in changing the "depth" of our transition rates.

```
[> Y:=8;
[> Z:=8;
[> AAA:=array(-Z..Z,[seq(i,i=-Z..Z)]):
```

The functions **MUpp(j)** etc defined below compute the transition rates Γ_j^{++}.

```
[> MUpp:=j->MODD(subs(eta=ETA,simp(SPLUS(Kp[0],Lp[j])))):
MUpm:=j->MODD(subs(eta=ETA,simp(SPLUS(Kp[0],Lm[j])))):
[> MUmm:=j->MODD(subs(eta=ETA,simp(SPLUS(Km[0],Lm[j])))):
MUmp:=j->MODD(subs(eta=ETA,simp(SPLUS(Km[0],Lp[j])))):
```

To avoid recalulating these all the time, we define arrays **MUPP** etc of the transition rates:

```
[> MUPP:=map((MUpp),AAA):MUPM:=map((MUpm),AAA):
MUMP:=map((MUmp),AAA):MUMM:=map((MUmm),AAA):
```

The variables below are all required from the master equation for calculation of the linewidths and populations.

```
[> AAAv:=simp(SPLUSMINUS(Km[0],Km[0])/F^2);
AB:=simp(SPLUSMINUS(Kp[0],Kp[0])/F^2);
[> GC:=simp(1/F^4*sum('SMINUS(Kp[0],Jp[i])*SPLUS(Km[i],Lm[0])','i'=-
Y..Y));
[> GP1:=simp(1/F^4*sum('MUPP[i]','i'=-Y..Y));
[> GP2:=simp(1/F^4*sum('MUMP[i]','i'=-Y..Y));
[> GP3:=simp(1/F^4*sum('MUMM[i]','i'=-Y..Y));
[> GP4:=simp(1/F^4*sum('MUPM[i]','i'=-Y..Y));
[> APLUS:=GP4;AMINUS:=GP2;GAMMAc:=1/2*simp(AAAv+AB-2*GC);
[> Aplus:=APLUS:Aminus:=AMINUS:
```

The variables **Pp** and **Pm** are the populations Π_{ss}^{+} and Π_{ss}^{-} respectively, while **Gc** and **Gs** are the limewidths Γ_c and Γ_s respectively.

```
[> Gs:=TAYLOR6(GAMMAc);Pp:=TAYLOR6(Aminus/(Aplus+Aminus));
Pm:=TAYLOR6(Aplus/(Aplus+Aminus));Gc:=TAYLOR6(Aplus+Aminus);
```

We now can compute the fluorescence spectrum (**Sinc**), the near-resonant weak probe absorption spectrum (**Wp**) and the near-resonant weak probe dispersion profile (**Dis**):

```
[> Sinc:=1/F^4*sum('(MUPP[j]*Pp+MUMM[j]*Pm)*Gc
/((x+2*j*Omega1/n)^2+Gc^2)
+MUPM[j]*Pp*Gs/((x+2*j*Omega1/n-2*DeltaE)^2+Gs^2)
+MUMP[j]*Pm*Gs/((x+2*(j)*Omega1/n+2*DeltaE)^2+Gs^2)','j'=-6..6):
[> SINC:=evalf(subs(alpha=.35,Omega1=80,Sinc)):
[> plot(SINC,x=-280..280,numpoints=2000);
```

```
[> Wp:=1/F^4*sum('MUPM[j]*(Pm-Pp)*Gs
/((x+2*j*Omega1/n-2*DeltaE)^2+Gs^2)
+MUMP[j]*(Pp-Pm)*Gs/((x+2*j*Omega1/n+2*DeltaE)^2+Gs^2)','j'=-Z..Z):
[> WP:=evalf(subs(alpha=.35,Omega1=80,Wp)):
[> plot(WP,x=-280..280,numpoints=2000);
[> Dis:=1/F^4*sum('MUPM[j]*(Pm-Pp)*(x+2*j*Omega1/n-2*DeltaE)
/((x+2*j*Omega1/n-2*DeltaE)^2+Gs^2)
+MUMP[j]*(Pp-Pm)*(x+2*j*Omega1/n+2*DeltaE)
/((x+2*j*Omega1/n+2*DeltaE)^2+Gs^2)','j'=-Z..Z):
[> DIS:=evalf(subs(alpha=.35,Omega1=80,Dis)):
[> plot(DIS,x=-280..280,numpoints=2000);
```

Finally to compute the Autler-Townes spectra, we require the weight factors $\Lambda_j^{\pm}$. These are computed by the functions **ATp** and **ATm**:

```
[> ATp:=i->simp(MODD(sum('1/sqrt(2)*conjugate(Kp[i][j][2])*
SP(Kp[i][j][1],[0,1,0])/F+1/sqrt(2)*conjugate(Kp[i][j][2])*
SP(Kp[i][j][1],[0,-1,0])/F','j'=1..nops(Kp[i])))):
[> ATm:=i->simp(MODD(sum('1/sqrt(2)*conjugate(Km[i][j][2])*
SP(Km[i][j][1],[0,1,0])/F+1/sqrt(2)*conjugate(Km[i][j][2])*
SP(Km[i][j][1],[0,-1,0])/F','j'=1..nops(Km[i])))):
[> ATP:=map(ATp,AAA):ATM:=map(ATm,AAA):
[> seq(SIMP(ATP[i]),i=-Z..Z);seq(SIMP(ATM[i]),i=-Z..Z);
```

We can now compute and plot the Autler-Townes absorption spectrum (**Autler**) and the Autler-Townes dispersion profile (**Autdis**):

```
[> Autler:=sum('ATP[j]*Pp*(1/2*(Gs+G3))/
((x-(1-2*j/n)*Omega1+DeltaE)^2+1/4*(Gs+G3)^2)
+ATM[j]*Pm*(1/2*(Gs+G3))/
((x-(1-2*j/n)*Omega1-DeltaE)^2+1/4*(Gs+G3)^2)','j'=-Z..Z):
[> AUTLER:=evalf(subs(alpha=.35,Omega1=80,G3=1/3,Autler)):
[> plot(AUTLER,x=-280..280,numpoints=2000);
[> Autdis:=sum('ATP[j]*Pp*(x-(1-2*j/n)*Omega1+DeltaE)
/((x-(1-2*j/n)*Omega1+DeltaE)^2+1/4*(Gs+G3)^2)
+ATM[j]*Pm*(x-(1-2*j/n)*Omega1-DeltaE)
/((x-(1-2*j/n)*Omega1-DeltaE)^2+1/4*(Gs+G3)^2)','j'=-Z..Z):
[> ADIS:=evalf(subs(alpha=.35,Omega1=80,G3=1/3,Autdis)):
[> plot(ADIS,x=-280..280,numpoints=2000);
```

IMAGE EVALUATION
TEST TARGET (QA-3)

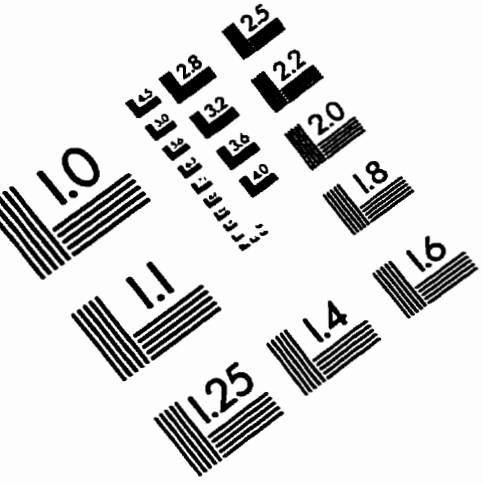

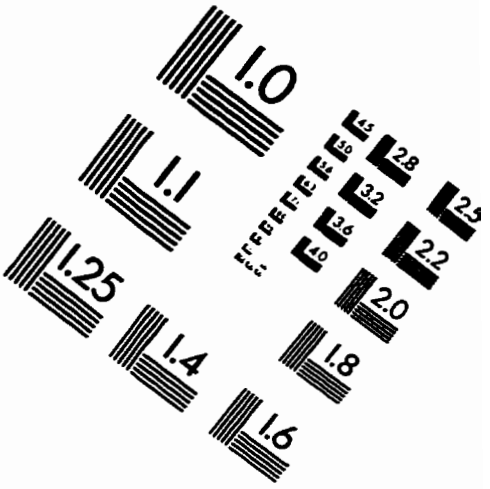

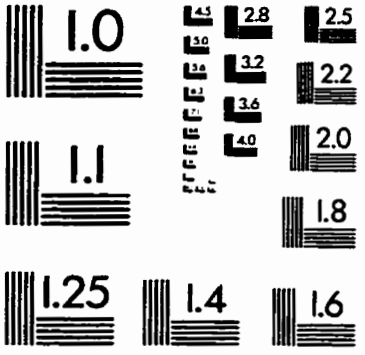

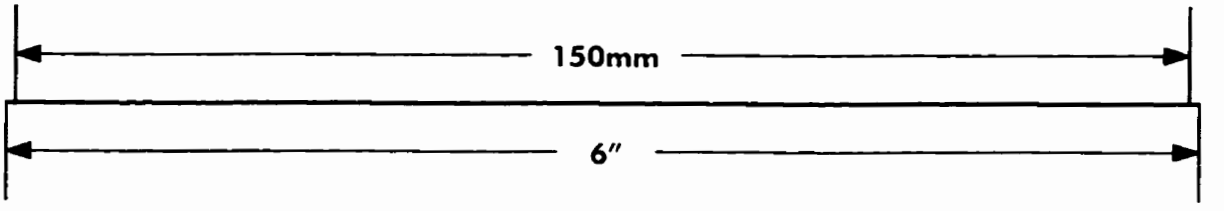

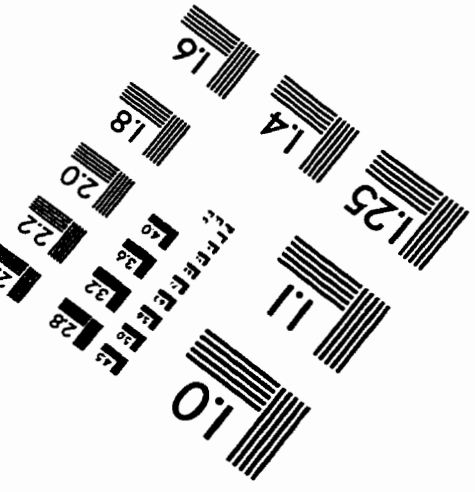

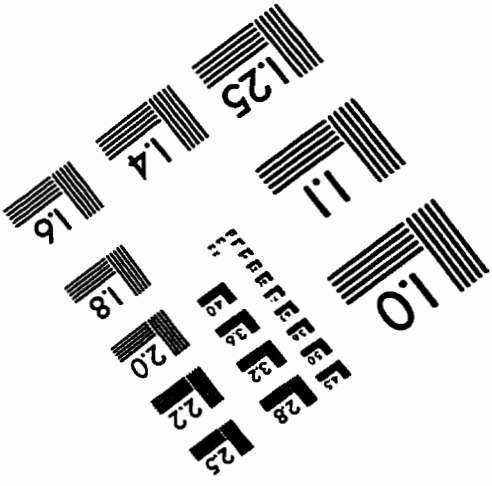

APPLIED IMAGE, Inc
1653 East Main Street
Rochester, NY 14609 USA
Phone: 716/482-0300
Fax: 716/288-5989